JAGIELLONIAN UNIVERSITY
Marian Smoluchowski Institute of Physics
The Faculty of Physics, Astronomy and Applied Computer Science
Kraków, Reymonta 4

Aleksandra Orzechowska

Investigations of the electron transfer in photosynthetic reaction centers of type Q

Kraków 2009

To my late Father

This Ph. D. thesis was prepared under the supervision of

dr hab Květoslava Burda

prof. AGH, University of Science and Technology

Faculty of Physics and Applied Computer Science, Kraków

The sample preparation described in this dissertation was carried out

in the Department of Plant Physiology and Biochemistry,

Faculty of Biochemistry, Biophysics and Biotechnology,

Jagiellonian University, Kraków

Acknowledgements

I would like to thank Prof. Květoslava Burda for her guidance, continuous support and encouragement throughout this work. I am deeply grateful for her kindness and help in organizing my work. I acknowledge many fruitful discussions which I have had with her. I am very grateful to her for providing a warm and friendly working atmosphere throughout my studies. Under the supervision of Prof. Burda I took my first steps in the fascinating field of photosynthesis.

I am also grateful to Prof. Kazimierz Strzałka for the opportunity to work in the laboratory of the Faculty of Biochemistry, Biophysics and Biotechnology at the Jagiellonian University.

I express my thanks to Prof. Ralph Bock for inviting me to work in his laboratory in the Max Planck Institute, for the concern and hospitality I experienced during my stay in Potsdam (Golm).

I am grateful to dr Joanna Fiedor for her help in bacteria culturing, the isolation of photosynthetic complexes and introducing me to the practical aspects of various experimental techniques.

I would like to acknowledge Krzysztof Matlak for the technical assistance during Mössbauer spectroscopy measurements.

I would also like to thank Martin Trtilék from *Photon Systems Instruments Ltd.* Brno, Czech Republic, for introducing me into the thermoluminescence spectroscopy and for the opportunity to use thermoluminescence and fast fluorescence transient methods in this dissertation.

Finally, I would like to express my gratitude to my friends and family for the patience, understanding and moral support at times when, to say the the least, progress was difficult.

This work was partially supported by the Polish Ministry of Science and Education (KBN grant N N302 2225 33)

Contents

Abbreviations

ATP	adenosine 5'- (tetrahydrogen triphosphate)
Bchl	bacteriochlorophyll
cyt	cytochrome
Chl	chlorophyll *a*
DBMiB	2,5- dibromo-3-methyl-6-isopropyl-p-benzoquinone
DEAE	diethylaminoethyl
LDAO	lauryldimethylamine *N*- oxide
NADP	nicitin- amide- adenosine diphosphate
NADPH	reduced form of NADP
OEC	oxygen evolving complex
o- phe	1,10-phenanthroline
P	primary donor
Pheo	pheophytin *a*
PC	plastocyanin
PSI	photosystem I
PSII	photosystem II
Q_A	primary quinone electron acceptor
Q_B	secondary quionone electron acceptor
Rb. sphaeroides	*Rhodobacter sphaeroides*
RC	reaction centre
TRIS	tris(hydroxymethyl)aminomethane
TL	thermoluminescence
Tyr_Z or Y_Z	tyrosine Z (D1- Tyr 161) of PSII
Tyr_D or Y_D	tyrosine D (D2- Tyr 160) of PSII

1 Introduction

1.1 Evolution of photosynthesis

Photosynthesis is the physico-chemical process by which plants, algae and photosynthetic bacteria use light energy to drive the synthesis of organic compounds. It provides the energy to reduce the carbon required for the survival of all life on the Earth, as well as the molecular oxygen necessary for all living organisms. In plants and algae, light driven photosynthetic reactions occur in chloroplasts, in their internal systems of membranes which are known as thylakoids. The total photosynthetic activity in the biosphere consumes 2 - 4 × 10^{18} kJ/ year of light energy. This is only 0.1% of the total light energy which reaches the surface of the Earth. From this energy input about 200 billion tons of biomass are produced by photosynthetic organisms fixing more than 10% of the total atmospheric CO_2 per year. The photosynthetic process results in the production of carbohydrates, lipids and proteins which are the source of food for all living creatures [1].

Oxygenic photosynthesis appeared about 2 billions years ago. Cyanobacteria already possessed a photosynthetic apparatus which allowed them to extract electrons from water. As a byproduct O_2 was produced. The existence of oxygen in the atmosphere changed the direction of the evolution of life on Earth. Oxygen is essential for respiration. During this process the organic compounds are oxidized back to carbon dioxide and water and the energy necessary for living organisms is generated. However, the first photosynthetic organisms appeared on Earth about 3.5 milliard years ago. They used reduced forms of sulfur as a source of electrons. Photosynthesis using electron donors other than water was carried out in photosynthetic bacteria. This process generally operated under anaerobic conditions.

Photosynthetic organisms can be classified by the type of their ultimate electron acceptor (Figure 1). One group is the Q- type (non-haem iron- type), and the other is the FeS cluster- type. Q- type organisms use quinone molecules, whereas the FeS- type iron-sulfur clusters, as terminal electron acceptors. Purple bacteria and green non sulfur bacteria, which are classified as Q-type organisms, contain type II reaction centres (RC), whereas green sulfur bacteria and heliobacteria (FeS- cluster type organisms) show a type I RC. Higher plants and cyanobacteria contain both type I RC (photosystem I, PSI) and type II RC (photosystem II, PSII). The main distinction between these two types of reaction centre is the midpoint redox potential (E_M) of their special pair of chlorophylls in the RC. Photosystem II is able to use electron donors with a very positive midpoint redox potential but it does not generate strong reductants, whereas photosystem I generates strong reductants and uses electron donors with lower redox potential than PSII. In photosystem II, water serves as the electron and proton donor. Its midpoint redox potential, E_M, which is the highest among all photosynthetic reaction centers (Figure 1) allows them to extract electrons from water. In the case of oxygenic photosynthesis, PSII and PSI cooperate in linear electron transfer via the cytochrome b6/f complex. However, only PSI reaction centers are able to reduce nicotinamide adenine dinucleotide (NAD) or

nicotinamide adenine dinucleotide phosphate (NADP) and produce NADH and NADPH, respectively. The reduced forms are further used in the dark reactions of photosynthesis.

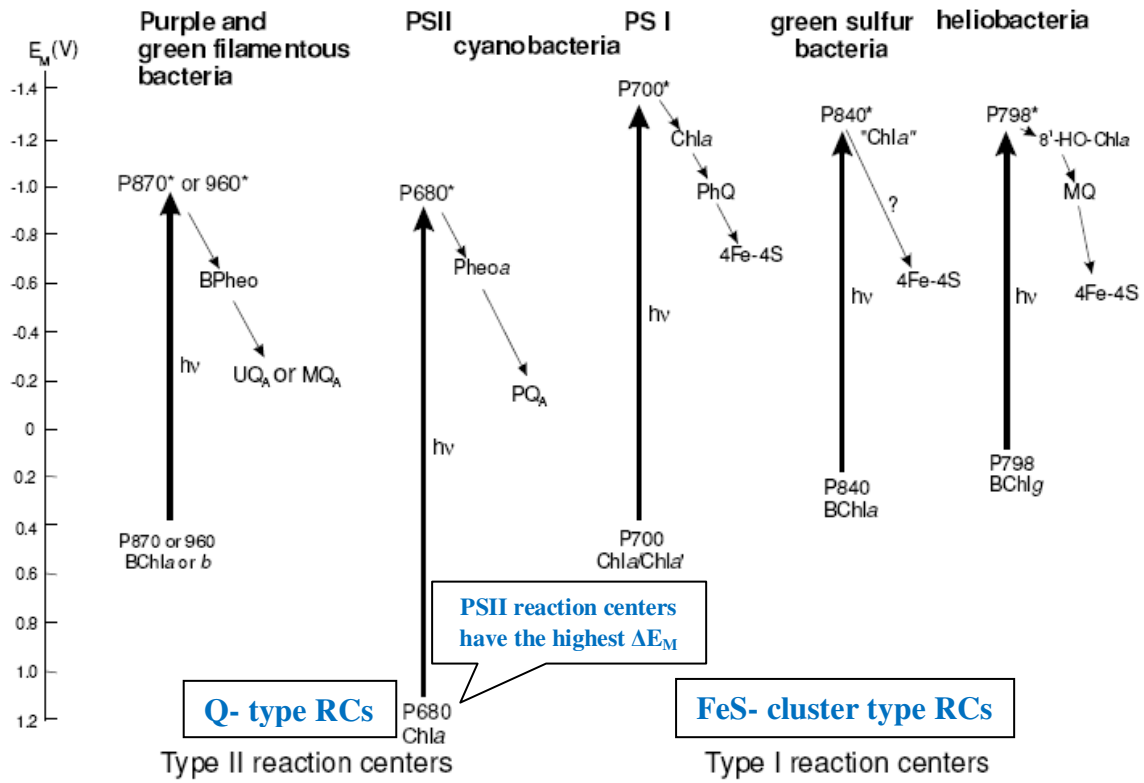

Figure 1. Reaction centers of photosynthetic organisms. The primary electron donors are shown, and the primary and secondary electron acceptors for the various reaction centers. In addition, their midpoint potentials are indicated. UQ: ubiquinone; MQ: menaquinone; PhQ: phylloquinone; PQ: plastoquinone.In the case of *Rb.sphaeroides*, the midpoint redox potential, E_M= 470 mV. PSII reaction centers have the highest midpoint redox potential equal 1.2 V The scheme is modified in line with: [1] and [2].

1.2 Architecture of photosynthetic apparatus

All photosynthetic systems have a fundamentally common structure [3], [4]. They are composed of an intergral membrane protein complex to which pigments (carotenoids and chlorophylls), lipids, and redox- active cofactors (such as chlorophylls, quinones and tyrosines) are bound [5]. Light energy is absorbed by antenna pigments (chlorophylls, phycobilins, carotenoids), which transfer it to their reaction centres. Carotenoids also have photoprotective and structural functions [6], [7]. Antenna pigments are either in the reaction centre complex (core antenna) or in separate protein complexes (peripheral antenna).

1.2.1 Photosynthetic reaction centers of purple bacteria

The photosynthetic reaction centres of purple bacteria, which belong to Q-type systems, are the best recognized photosynthetic structures and therefore they serve as a model system in studies of intramolecular electron transfer within proteins. Bacterial reaction centre complexes are composed of a cytoplasmic protein H, of cytochrome c on

the periplasm side and transmembrane protein chains L and M, which form a core of two- fold symmetry [4].

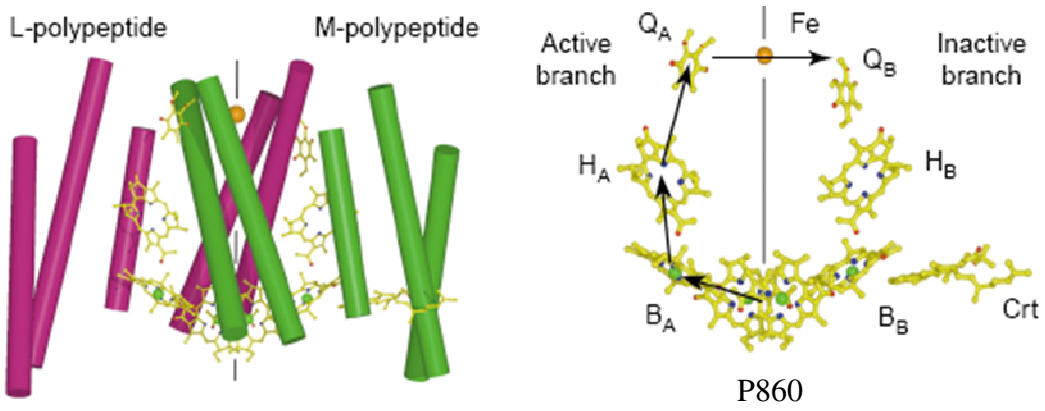

Figure 2. Structure of the *Rhodobacter sphaeroides* reaction centre (according to [4]): *Crt* represents a single carotenoid.

Each of the RC complexes has eleven membrane- spanning helices, five in L, five in M and one in the H subunit. The subsequent cofactors active in the subsequent electron transfer steps are found on the two core peptides L and M: a special pair of bacteriochlorophyll (P860) serving as a primary electron donor, two bacteriochlorophyll monomers (B_A and B_B), two bacteriopheophytins (H_A and H_B), a non- haem iron (Fe) and two molecules of quinone (in the case of *Rb. sphaeroides*- ubiquinone 10) ,Q_A and Q_B, which are the final electron acceptors. Despite the symmetry only one branch is used in wild type reaction centres in light- driven electron transfer. This branch is associated with the L subunit and is called the A (active)- branch, whereas the inactive one is called the B- branch. The inactive branch can be forced into operation with modification of amino acid side chains on the active branch [8]. Light activated electron transfer proceeds from the special pair to H_A via the monomeric accessory bacteriochlorophyll B_A. The primary quinone acceptor bound at site Q_A (localized on subunit M) accepts an electron from H_A, localized on subunit L, and delivers it to the secondary quinone acceptor at the Q_B site, with ubiquinone bound to the subunit L. The ubiquinone at the Q_A site can only accept one electron whereas ubiquinone Q_B can be doubly reduced. Ubiquinone Q_B, after binding two protons forms ubiquinol Q_BH_2, and leaves its binding site. It is further oxidized by the cytochrome bc_1 complex. The photo- oxidized special pair $P860^+$ is re- reduced by cytochrome c_2 in the cyclic electron flow.

1.2.2 Photosystem II

Photosystem II (PS II) is a specialized protein complex that uses light energy to extract electrons from water and create oxygene molecules (O_2) as a byproduct . It is embedded in the thylakoid membrane. The core of photosystem II is formed by a heterodimer protein complex composed of the D1 (39 kDa protein, PsbA) and D2 (39 kDa protein, PsbD) polipeptydes, which contain redox- active cofactors in photosynthetic electron transport. Each of these subunits consists of five transmembrane α- helices

organized in a manner almost identical to that of the L and M subunits of the reaction centre of photosynthetic purple bacteria . D1 and D2 are flanked by two internal antenna subunits CP43 (PsbC) and CP47 (PsbB), respectively. They are composed of six transmembrane α- helices and their cofactors capture light energy and transfer the excitons to the reaction centre. All photosystem II complexes contain cytochrome b_{559}, which is a heterodomer containing two subunits α (PsbE protein, 9 kDa) and β (PsbF protein, 4 kDa) connected via a haem iron.

In cytochrome b_{559} two histidines, each from separate transmembrane helices of the α and β subunits, respectively, serves as an axial ligand of the haem iron. Cytochrome b_{559} is known to potentially exist in various forms ranging from a high potential form (HP) which is characterized by a potential of 30- 400 mV to an intermediate potential (IP) to a low potential form (LP) of 20- 80 mV [9]. Independently of the potential form of cyt b_{559}, the haem iron can be in an oxidized or in a reduced state. Although the molecular mechanism responsible for the transformation between its different potential forms has not been established, it is suspected that this ability of the cytochrome is crucial for its possible role in the protection of PSII against photoinhibition [10]. It may participate in cyclic electron flow or in a side path of electron transport through PSII [10], [11], [12]. It may also scavenge photogenerated free radicals [13]. Moreover, cyt b_{559} is predicted to stabilize the oxygen evolving complex (OEC) during its photoactivation [14], [15] and to accept protons during the S- state turnover of the manganese cluster [16]. Thus, there are strong indications that cyt b_{559} has an important regulatory function in the oxidizing and reducing sides of PSII and has a structural function in PSII assembly and stability.

Although the photosynthetic apparatus found in higher plants and procaryoatic organisms has a common structure and acts in a similar way, the molecular mass membrane intrinsic and extrinsic subunits of plant PSII differ from those in cyanobacteria. There are a number of subunits which appear in plants but not in cyanobacteria (PsbR, PsbS, PsbT, PsbW) [17]. Plants also contain 23 kDa and 17 kDa extrinsic proteins [18] instead of cytochrome c_{550} (psbV, 12 kDa) and the 10 kDa PsbU protein which are inherent in cyanobacteria.

The arrangement of redox active cofactors attached to the D1 and D2 polypeptides is shown in Figure 3.

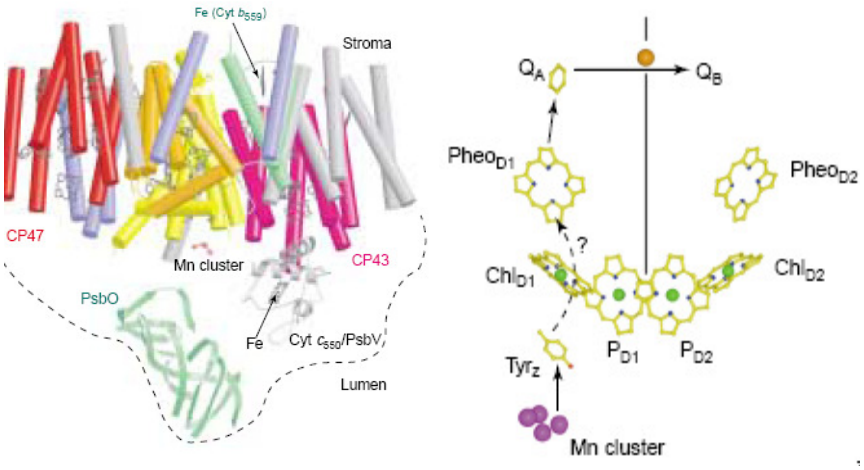

Figure 3. Structure of photosystem II from *Synechococcus elongatus* with assignment of protein subunits (left) and cofactors (right) [4], [19].

The polypeptides D1 and D2 form a symmetrical central structure which appears to provide two potential electron transport pathways through the reaction centre. However, as shown in Figure 3, only one (left, located mainly on the D1 peptide) pathway is active. The light activated electron transport is initiated by the ejection of an electron from the excited primary donor P680, a dimer of two chlorophylls *a*, having an absorption maximum at 680 nm. This leads to the formation of the cationic radical $P680^{\bullet+}$ and to a reduction of the nearest pheophytin, $Pheo_{D1}$. In this step the monomeric chlorophyll Chl_{D1} takes part in the electron transfer. Then the reduced $Pheo_{D1}^{-}$ passes the electron to the primary quinone acceptor Q_A, which is bound at the stromal (extrinsic side of thylakoid membrane) side of the subunit D2. Finally, reduced $Q^{\bullet-}_A$ transfers the electron to a secondary quinone acceptor, a plastoquinone localized at the Q_B site on the D1 subunit. The charge separation between the reaction center $P680^{+}$ and the PSII acceptor side results in the formation of plastoquinol Q_BH_2 after the uptake of two protons from the stroma by the Q_B plastoqionone doubly reduced. This mobile molecule Q_BH_2 is released from PSII and migrates to cytochrome b_6f, where it is oxidized. This results in the release of two protons into the lumen and the electron is transferred to the plastocyanin (a copper protein, PC) in higher plants or to the cytochrome c_6 in algae and cyanobacteria. These soluble electron carriers act as electron donors to the photosystem I (PSI).

The formed cationic radical $P680^{\bullet+}$ is reduced by the primary donor, a tyrosine residue Tyr_Z localised on the D1 protein. The tyrosine abstracts one electron from a manganese cluster forming the oxygen evolving complex. After four flashes, four positive charges are accumulated on the manganese cluster, which oxidizes two water molecules. This process is coupled with the release of one O_2 and four H^{+}.

The subsequent steps of the electron flow between the redox active components which take part in the whole chain of linear electron transfer in oxygenic photosynthesis are shown in Figure 4. This includes the role of PSII as the electron and proton donor in its light phase. This is called the Z- scheme of oxygenic photosynthesis.

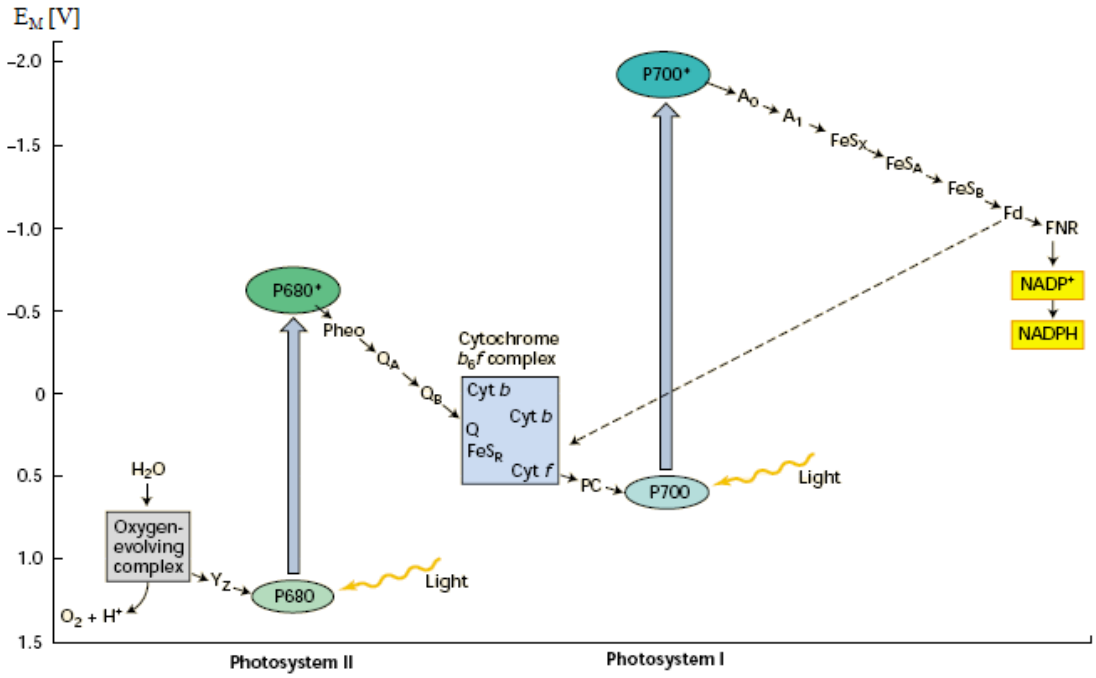

Figure 4. The Z- scheme of the pathway of oxygenic photosynthetic electron transport. The redox carriers are placed at their midpoint potentials (E_M). The dashed line indicates cyclic electron flow around PSI (modified in line with [20]). In PSI the primary donor P700 becomes oxidized upon light excitation, and the electron is transferred via an immediate acceptor A_0, a chlorophyll *a*, and the secondary acceptor A_1, a phylloquinone, to the first $[Fe_4S_4]$ iron sulfur cluster FeS_X located at the stromal side of the membrane. From FeS_X the electron can be further transferred to FeS_A and FeS_B, two $[Fe_4S_4]$ iron sulfur clusters. The formed $P700^{\bullet+}$, located on the lumenal side of PSI, becomes rereduced by an electron donation from a reduced PC or cytochrome c_6. On the stromal side the electron is further transferred from the reduced iron sulfur cluster FeS_A or FeS_B to the soluble electron carrier ferredoxin (Fd) containing a $[Fe_2S_2]$ iron sulfur cluster. Finally, by the action of Fd and flavoprotein FNR a chemical free energy (NADPH) is produced. Additionally,a proton concentration difference across the thylakoid membrane is generated. The resulting electrochemical trans membrane potential in turn is used to generate ATP.

The strong reductant NADPH and high energetic compound ATP are utilized in the dark phase of photosynthesis, called the Calvin cycle and used to produce carbohydrates.

Mn- cluster and water oxidation

The oxygen evolving complex (OEC) is localized on the lumenal side of PSII, close to the D1 protein. In higher plants it is protected by three extrinsic polypeptides, which are comprised of the 27- kDa protein (PsbO) known as the manganese- stabilizing protein, the 20- kDa protein (PsbP) and the 17-kDa protein (PsbQ) [17].

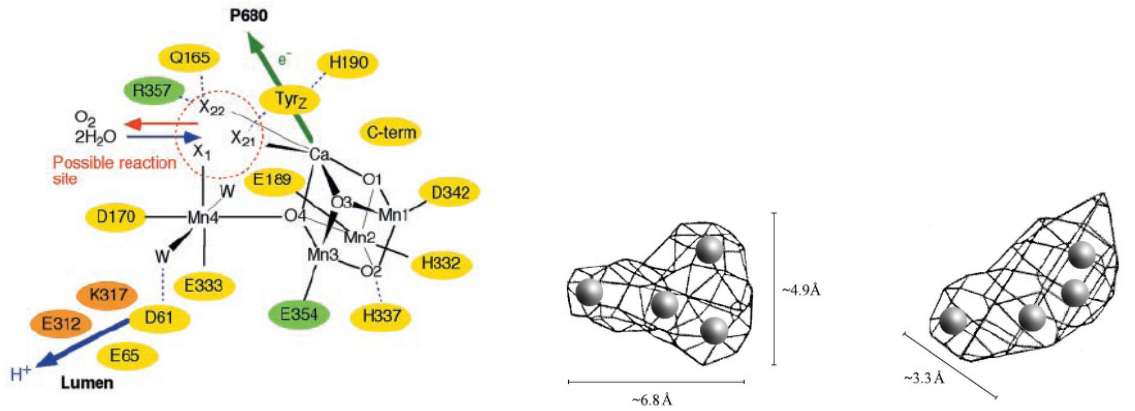

Figure 5. Schematic view of the OEC *(left)*. Residues in D1, D2 and CP43 subunits are shown in yellow, orange and green, respectively. X_1, X_{21} and X_{22} are possible substrate water binding positions to Mn^4 (X_1) and to Ca^{2+} (X_{21}, X_{22}) although one of the Ca^{2+} ligands can represent a Cl^-. Dark dotted lines indicate possible hydrogen bonds (in line with [21]). There is a view of the electron density of the manganese cluster *(in the middle)* and along the membrane (*right)* with the luminal side on top (90° rotated around the horizontal axis). (Modified from [19] and [22]).

The OEC is composed of 4 manganese ions, a calcium ion [23] and most probably chloride and bicarbonate ions [24]. The 4MnCa cluster acts as a storage device, accumulating redox equivalents of four consecutive light- driven charge separations and links this to the process of electron and proton extraction from water molecules. The oxidation of two water molecules results in the release of one oxygen molecule, of four protons into the lumen, and of four electrons. These are transfered to the PSII acceptor side, Q_A and Q_B.

A large step forward in the understanding of the water splitting enzyme activity was Joliot's observation that oxygen evolution stimulated by short saturating flashes has a periodicity of four [25]. The damped O_2 oscillations were described by Kok et al. [26], who proposed a linear four- step model for the water oxidizing cycle.

$$S_0^0 \xrightarrow{h\nu} S_1^{1+} \xrightarrow{h\nu} S_2^{2+} \xrightarrow{h\nu} S_3^{3+} \xrightarrow{h\nu} (S_4^{4+}) \longrightarrow S_0^0 + O_2 + 4H^+ + 4e^- \qquad (1.2.2.)$$

The state S_i is assigned to a certain arrangement and oxidation state of the Mn complex, where the superscript describes the number of accumulated charges and i = 0, 1, 2, 3, 4. Water oxidation is supposed to occur only after formation of the S_4 state. The parentheses around S_4 are to signal that the S_4 state is not detectable because of its very short lifetime. The amount of oxygen evolved at the *n*- th flash is a measure of the concentration of the centers, which were in the S_3 state before the flash. In order to explain the first maximum of the oxygen yield under the third flash, Kok and coworkers suggested that the Mn-complex is mainly stabilized in the S_1 state (about 75%), rather than in the S_0 one (25%) in dark- adapted chloroplasts and that the S_0 state is formed exclusively by the reaction $S_3 + h\nu \rightarrow (S_4) \rightarrow S_0 + O_2$. Later it was postulated that in

prolonged darkness, the OEC tends to put itself in the S_1 due to the oxidation of the S_0 to S_1 state by the tyrosine D (Tyr D) on the D2 polypeptide [27]. The Kok model also assumes the probability of the transition between $S_i \rightarrow S_{i+1}$ to be ≤ 1 as well as the existence of double hits, $S_i \rightarrow S_{i+2}$. This could explain the loss of oxygen pattern periodicity with an increasing number of flashes. The progressive damping in the O_2 oscillations observed in experiments reflects the random redistribution of the OEC among the S states.

Research Topic

The aim the work was to study the role of non-haem iron and cytochrome b_{559} in the process of energy and electron transfer within photosystem II (PSII). It has been suggested that cytochrome b_{559} participates in cyclic electron flow around PSII, can dissipate energy under light stress conditions, may oxidize plastoquinol molecules or stabilize the manganese complex. Most probably the function of cytochrome b_{559} is related to the fact that it may have different redox potential and haem iron can change its valence state. Protonation and deprotonation events are the triggering mechanisms most probably resposnsible for the functions of cytochrome b_{559}. However, where and how these processes occur still remains to be elucidated. Non-haem iron is an even more enigmatic component of the photosynthetic reaction centers of type Q because it is conserved in primitive photosynthetic bacterial organisms. But up to now the valence changes of non- haem iron have not been observed, which excludes its direct participation in electron transfer within the iron-quinone complex. On the other hand, two different spin states of non -haem iron were detected in an algae PSI^- mutant. This could have an important implication for the regulatory role of non-haem iron in the stabilization of the iron-quinone complex.

In our studies we used a wild type tobacco and mutant with a point mutation on the β-chain of cytochrome b_{559}. These systems allow us to investigate the influence of cytochrome b_{559} on the stabilization of the acceptor and donor PSII side and the kinetics of the electron transport processes, as well as to check the possible role of cytochrome b_{559} in the regulation of the quinone-iron complex. The additional measurements of the wild and mutated types of tobacco in the presence of copper cations give us an opportunity to gain an insight into the protonation and deprotonation mechanisms activated in photosynthetic systems, because copper is known to be a protonophore. Its highly specific interaction with non-haem iron and cytochrome b_{559} has been already recognized. Studies on the bacterial reaction centers isolated from *Rb. sphaeroides* provide us with an opportunity to use unique methods such as Mössbauer spectroscopy and nuclear resonant inelastic X-ray scattering of synchrotron radiation in the investigations of the dynamical properties of non-haem iron in the iron-quinone complex, which is similar in its organization to that in photosystem II. Here we also present the first thermoluminescence experiments on the bacterial reaction centers, which provide information on the free energy of the charge stabilization process between the special bacteriochlorophyll pair and the acceptor side of the reaction center and especially the iron-quinone complex. The measurements of the variable fluorescence of the bacterial photosystem and of photosystem II as well as photobleaching experiments and studies of oxygen evolution by the fast polarographic method completed the complex investigations of energy and electron transfer within Q-type photosystems. From the results we were able to draw conclusions which cast new light on the connectedness of the acceptor and donor side of these photosystems. In the case of photosystem II we were able to indicate a special role for cytochrome b_{559} in the regulation of the Q_B quinone binding site and the cyclic electron flow around PSII.

2 Materials

2.1 Isolation of photosystem II

2.1.1 *Nicotiana tobacco* plant raising

Nicotiana tobacco plants grew under moderate insolation conditions at 25°C in a green house. Only young tobacco leaves were harvested and used in preparations.
Investigations were performed on wild type and mutated tobacco with modified cytochrome b_{559}. In the cytochrome b_{559} mutant, known to be active in oxygen evolution, the highly conserved phenylalanine 26 residue that is present in the β subunit (PsbF protein) was changed to serine [28]. This point mutation caused an unusual flexibility of the haem group of cyt b_{559} and altered the activity of the electron flow within PSII and oxygen evolution.

2.1.2 Isolation of thylakoids membranes enriched in photosystem II

Thylakoids enriched in photosystem II obtained from *N. tobacco* were isolated according to the method decribed in [29]. The tobacco leaves were washed, dried and left in a dark cool room for an hour. After homogenization in a washing buffer (pH 7.8) the suspension was centrifuged (Sigma 6K15, 5500×g, 15 min, 4°C). The pellet was washed twice in a HEPES I buffer (pH 6.5) and then once again in a HEPES II buffer and resuspended at concentration of 1 mg/ ml. After that, a 20% TRITON solution was added. The suspension was kept stirring at 4°C for 25 minutes and centrifuged (Sigma 6K15, 4500×g, 6 min, 4°C). The pellet was discarded and the supernatant was centrifuged again (Beckman J2- MC, 43700×g, 30 min, 4°C) and if necessary, was again suspended in the HEPES II buffer, and centrifuged (usually four times). The resulting pellet was resuspended in the same buffer at a final concentration of 1mg/ml and stored at - 80°C .

Table 1. Buffers used for thylakoids membranes isolation.

Compound	Concentration [mol/l]
HEPES I	
NaCl	1.5×10^{-2}
$MgCl_2\,(6H_2O)$	5.0×10^{-3}
Hepes	2.0×10^{-2}
HEPES II	
NaCl	1.5×10^{-2}
$MgCl_2\,(6H_2O)$	5.0×10^{-3}
Hepes	2.0×10^{-2}
Sucrose	0.4
WASHING BUFFER	
NaCl	1.0×10^{-2}
$MgCl_2\,(6H_2O)$	5.0×10^{-3}
Sucrose	0.4
TRIS	5.0×10^{-2}

Chlorophyll determination

The amount of chlorophyll in prepared samples was estimated using a formula described in [30]:

$$\frac{\left(E_{663}\times 45.6 - E_{645}\times 9.25\right)\times 1.16\times 3}{3585\times 0.03} = chla\left[\frac{mg}{ml}\right] \qquad (2.1.2.1)$$

$$\frac{\left(E_{645}\times 82.04 - E_{663}\times 16.75\right)\times 1.07\times 3}{3585\times 0.03} = chlb\left[\frac{mg}{ml}\right] \qquad (2.1.2.2),$$

where E_{663} and E_{645} are the values of absorption for wavelenghts equal to 663 nm and 645 nm respectively. The suspension included 2.7 ml of 90% MeOH, 270 µl of water, and 30µl of the sample was mixed (biomix, BVX- 10) and centrifuged (MPW- 52, 5000×g , 5 min, 20 ° C). The absorption of the supernatant was measured at the two wavelengths given above using a spectrophotometer (Meterek SP- 830).

2.2 Preparation of photosynthetic bacterial reaction centers

2.2.1 Cell culture of photosynthetic bacteria

A strain of *Rb. sphaeroides 2.4.1* was grown in anaerobic heterotrophic conditions at 27°C in a modified Hutner medium [31]. For Mössbauer measurements the medium was supplemented with ^{57}Fe. After inoculation, the bacteria were kept in darkness for 12 hours. The cells were harvested after 7 days of illumination in white light (55µmol·m^{-2}·s^{-1}) by centrifugation (Sigma 6K15, 5500×g, 15 min, 15 ° C), and washed twice with 20 mM TRIS- HCl buffer (pH 7.8).

Table 2. Medium used for bacteria cultivation (pH 6.9).

Compound	Concentration [mol/l]
KH_2PO_4	3.67×10^{-3}
$MgSO_4\times7H_2O$	1.62×10^{-3}
NaCl	6.84×10^{-3}
$(NH_4)_2SO4$	3.25×10^{-3}
$CaCl_2$	4.50×10^{-3}
Succinid acid ($C_4H_6O_4$)	1.48×10^{-3}
Yeast powder	1g/l
Microelements	1.0 ml/l
Citric acid solution of ferrous ion	6.0 ml/l

Microelements:

Compound	Concentration [mol/l]
$ZnSO_4\times7H_2O$	3.47×10^{-4}
$MnCl_2\times4H_2O$	1.51×10^{-4}
H_3BO_3	4.85×10^{-3}
$CoCl_2\times6H_2O$	8.40×10^{-4}
$CuCl_2\times2H_2O$	5.86×10^{-5}
$NiCl_2\times6H_2O$	8.41×10^{-5}
$NaMoO_4\times2H_2O$	1.37×10^{-4}

Citric acid solution of ferrous ion (pH 6.5):

Compound	Concentration [mol/l]
$FeSO_4$	4.0×10^{-4}
$(NH_4)_2SO_4$	4.0×10^{-3}
Citric acid ($C_6H_8O_7\times7H_2O$)	8.0×10^{-3}

2.2.2 Isolation of chromatophores

The cells were suspended in a 20 mM TRIS-HCl buffer (pH 7.8) containing sodium ascorbate and a small amount of DNase I to digest the long DNA strands. The cells were disrupted by a twofold passage through French Pressure Cell (SLM- Aminco FA-031, 12.000 psi). After that, the suspension was centrifuged (Sigma 3K30, 18000×g, 30 min, 4°C) to remove cell debris. If necessary, the pellet was again suspended in the buffer and centrifuged.

2.2.3 Purification of reaction centers

The chromatophore pellet was resuspended in a 20 mM TRIS- HCl buffer , 100 mM NaCl in the presence of sodium ascorbate. This was diluted to an absorbance of 50 (A_{850} ~50) with a salt buffer, being adjusted at the same time to a concentration of 0.25 % LDAO and left stirring for 30 min. at room temperature. After centrifugation (Sigma 3K30, 20000×g, 30 min., 4 ° C) the supernatant contained mostly reaction centre proteins. Devoiding a part of antenna chlorophyll was followed by 20%- 26% amonium sulphate precipitation and then centrifuged. The supernatant was further dialyzed against a 20 mM TRIS- HCl buffer (pH 7.8) containing 0.08% LDAO and purified by ion-exchange chromatography on DEAE52- cellulose (DE-52, Watman). The column was washed with a 20 mM TRIS- HCl buffer and then at least 2 vol. of 20 mM TRIS- HCl (pH 7.8) with 0.08% LDAO. Reaction centers were eluted using an NaCl gradient changing from 100 mM to 300 mM in a 20 mM TRIS-HCl buffer and 0.08% LDAO. The best purified reaction centers were achieved using 160 mM NaCl. The obtained fractions were collected separately and further dialysed against a 20 mM TRIS-HCl buffer pH 7.8 and 0.08% LDAO. Reaction centers of higher purity were obtained by a second DEAE chromatography step. Final purification was achieved by a density- gradient centrifugation (0.2- 0.8 M sucrose in a 20 mM TRIS- HCl buffer, pH 7.8, containing 0.08% LDAO, 200000×g, 20 h). Reaction centers were located in the 0.6 M region.
They were withdrawn, dialyzed against a TRIS- HCl buffer (20 mM, pH 7.8, containing 0.08% LDAO). After isolation the reaction centers were concentrated in a pressure cell (Amicon) and stored at -40 ° C. All purification steps were protected from strong illumination.

From 20 liters of the liquid medium 100 g of cells were harvested. This produced 80 g of chromatophores and 170 mg of photosynthetic reaction centers. Using ASA (atomic spectroscopy absorption) and Mössbauer spectroscopy the enrichment of samples in ^{57}Fe was estimated to be 30-50%.

Bacteriochlorophyll determination

Pigment extraction was performed by adding acetone to a small volume of the isolated reaction centers.The suspension was sonificated on ice for 3 minutes and centrifuged (Sigma 3K30, 7000×g, 8 min, 15°C). The supernatant was collected. The pellet was suspended in methanol, sonificated for 3 minutes on ice and centrifuged (Sigma 3K30, 7000×g, 8 min, 15°C). Both supernatants were mixed and the absorption

spectrum was taken immediately using a Cary 50 Bio (Varian, Australia) spectrophotometer. Bacteriochlorophyll (Bchl) absorbance measured at 760 nm (A_{760} ~ 0.2) and an extinction coefficient of 6×10^4 $cm^{-1} \cdot M^{-1}$ was used for the calculation of its concentration. The amount of Bchl was estimated using the Beer- Lambert law:

$$A = \varepsilon \cdot l \cdot c \qquad (2.2.3),$$

where A is absorbance, ε is the molar extinction coefficient [$M^{-1} \cdot cm^{-1}$], l is the path length of the cuvette in which the sample is contained [cm], and c is the molar concentration of the compound in solution [M].

3 Methods

3.1 UV/ VIS spectroscopy

The steady state absorption spectra and kinetics of RC photobleaching were recorded at room temperature on a Cary 50 Bio (Varian, Australia) spectrophotometer using 1 cm path length quartz cells. Absorption spectra were recorded in the 250- 1000 nm range. For kinetic studies RCs (A_{860}~0.2) were suspended in a 20 mM Tris- HCl buffer (pH 7.8) containing 0.08% LDAO and the desired amount of salt. As a light source a flash lamp (Unomat 20*Bauto*, Germany) was used. All samples were exposed to 2-3 flashes fired at 60 s intervals. The photobleaching of RCs was monitored at 860 nm.

3.2 Fluorescence

Fluorescence is a very valuable tool for investigating photosynthesis . The fluorescence yield (the number of photons emitted relative to the photons absorbed) is usually on the level of a few percent in photosynthetic systems and it is sufficient to investigate them using fluorescence methods. Fluorescence activity can be schematically illustrated with a classical Jabloński diagram to describe the absorption and emission of light (Figure 6).

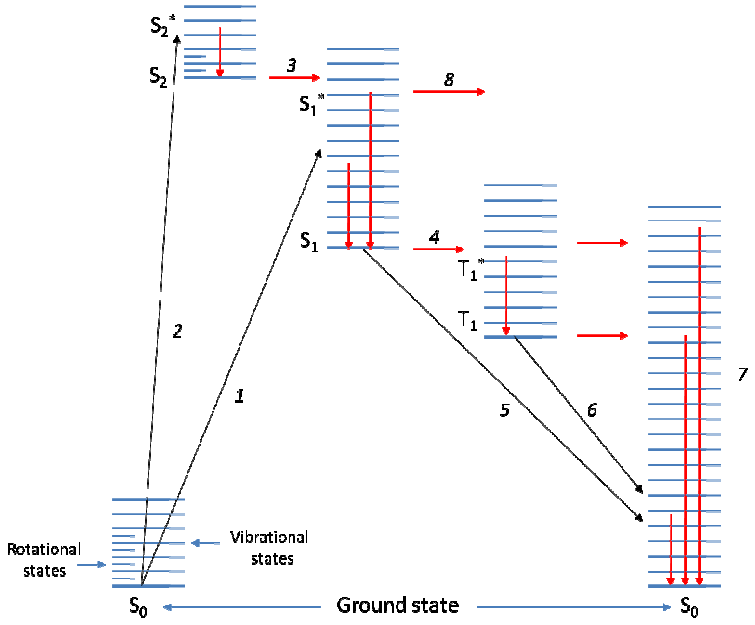

Figure 6. Jabłoński diagram. Black arrows represent absorption and emission of light, red arrows represent non- radiative transitions. A photon is absorbed by a molecule, according to the law $\Delta E = h \cdot \nu = h \cdot (c/\lambda)$, where ΔE is the difference between the energy levels of the ground and excited states, ν and λ are the frequency and the wavelenght of the light, respectively, c is the velocity of the light, and h - Planck's constant. The absorbed photon promotes the electron from the ground singlet state S_0 to the excited singlet state S_1 or S_2 (steps 1 and 2, respectively). A molecule brought to an upper excited state usually returns to

the first excited state in 10^{-14}– 10^{-15} s by "internal conversion" (step 3). By this pathway a portion of the energy of the higher excited state is dissipated as heat to the surroundings by a sequence of small transitions through the vibrational sublevels of the electronically excited state. An excited molecule in a singlet state usually has maximum lifetime of ~ 10^{-8} s and can undergo various modes of a nonradiative as well as a radiative decay, the latter generally termed *luminescence*. The excited molecule can return to one of the lower vibrational sublevels of the first excited singlet state. It is also likely to return to one of the lower vibrational sublevels of the ground state by emitting a photon as *fluorescence* (step 5). Another important energy pathway is called „intersystem crossing" (step 4) , which refers to the conversion of an excited singlet state to an excited triplet state, followed by radiative or nonradiative decay of the excited triplet state to the ground singlet state. The light emitted by the radiative, triplet- to- ground state transition is called *phosphorescence* (step 6). As well as, returning to the ground state S_0 from the S_1 state by emission, the S_1 state may alternatively go to S_0 by radiadiationless deactivation (step 4, but from S_1 to S_0, followed by step 7). As the name implies, no radiation is emitted and the electronic excitation energy is converted into a vibrational excitation of S_0 , which is then transferred to the adjacent solvent. For certain excited molecules the most useful decay pathway is "energy transfer" (step 8), which eventually leads to what is known as a charge- separated state, and which is of vital importance to photosynthesis (modified in line with [1]).

3.2.1 Steady- state fluorescence measurements

In the steady- state fluorescence measurements the sample is illuminated with a continuous beam of light, and the intensity of the emission spectrum is recorded. The steady- state intensity *(I_{ss})* is given by:

$$I_{SS} = \int_0^\infty I_0 e^{\frac{-t}{\tau}} dt = I_0 \tau \qquad (3.2.1),$$

where, I_0 is the intensity at time $t=0$,which is considered to be a parameter that depends on the fluorophore concentration and a number of instrumental parameters, and τ is the measured lifetime.

The steady state fluorescence spectra were recorded at 77 K. The measurements were performed on a Jasco FP- 6500 spectrofluorometer at the Max Planck Institute of Molecular Plant Physiology, Potsdam- Golm. The emission spectra were recorded in a range of 655- 800 nm. The fluorescence excitation was 430 nm and the scanning speed 200 nm/min. Samples of thylakoids enriched in PSII were suspended in a 30 mM Hepes buffer (pH 7.6). The chlorophyll content in the samples was 10 µg/ml.

3.2.2 Kautsky effect

Changes in the yield of chlorophyll fluorescence were first observed in 1931 by Kautsky and Hirsch. They found that upon transferring photosynthetic material from dark to light conditions an increase in the yield of chlorophyll fluorescence occurred over a time period of around 1s [32]. This rise has been explained as a consequence of the efficiency of energy transfer to the reaction center and the later efficiency of its use for driving the linear and cyclic electron flow in photosynthetic systems. In particular, variable fluorescence is sensitive to the redox states (reduced or oxidized) of the quinone electron acceptors in photosystems of type II, in present instance, and especially of

quinone bound at the Q_A side. Once the RC absorbs light and Q_A is reduced, it is not able to accept another electron until it has passed the first one onto a subsequent electron carrier Q_B . During this period the reaction centre is said to be "closed". When plant material is transferred from darkness into light, the PSII reaction centres are progressively closed. During illumination one can observe two characteristic plateaus (Figure 18 and Figure 19 chapter 4.1.1). The first increase in the yield of chlorophyll fluorescence appears in a time scale from hundreds of microseconds to miliseconds while the second plateau, from tens of miliseconds to a few seconds, depending on the state of the donor and acceptor side of the sample. The decrease in fluorescence at longer times is caused by damage to the photosynthetic systems. This phenomenon, termed fluorescence quenching, is explained in two ways. Firstly, there is an increase in the rate at which electrons are transported away from the reaction centre. Such quenching is referred to as "photochemical quenching". At the same time, there is an increase in the efficiency with which energy is converted to heat. This latter process is termed "non- photochemical quenching" (NPQ) and it exists to protect the photosynthetic apparatus from photodamage [33].

The Kautsky effect was measured during a period of 250 s. The actinic light interval was 150 s, the actinic light voltage and measuring flash voltage were 100% and 50%, respectively.

The fast fluorescence transient (known as a type of protocol called PEA) was measured on 1s time scale (up to 2 ms-every 2 μs and starting from 3 ms- every 1 ms). In this case the actinic light voltage was 40%.

The measurements were performed using a double modulation fluorometer FL 3300 (Photon Systems Instruments, Czech Republic) as described in [34], with a high time resolution of 2 μs for a fast rise in fluorescence kinetics and 1ms for a slow rise. For measurement of the Kautsky effect thylakoids enriched in PSII were suspended in a Hepes (pH 6.5) buffer and then copper salts was added. Each sample contained 10-12 μg chlorophyll/ml (~12 μM) in the case of the PSII BBY preparation and 40 μg chlorophyll/ml for thylakoids.

In the case of bacterial RCs, for fast kinetic measurements (PEA), the reaction centers were suspended in a 20 mM Tris-HCl buffer (pH 7.8) containing 0.08% LDAO and a given amount of salt. The sample concentration was ~ 0.7 μM.

In all cases samples were incubated for 10 minutes in darkness.

The fluorescence spectra of the Kautsky effect and the PEA were evaluated using the following function:

$$F_{KE}(t) = y_0 + \sum_{i=1}^{n} A_i (1 - e^{-\frac{t-t_0}{t_i}}) \qquad (3.2.2),$$

where n is the minimal number of components necessary for fitting the experimental data, y_0 is the value of the dark signal (in normalized curves it is equal 0), A_i is the contribution of each of the components and t_i is a characteristic life time.

3.2.3 QA- reoxydation kinetics

Measurements of Q_A reoxidation can give information complementary to that obtained from the Kautsky effect. The differences between the two types of process lies in the time of illumination of the sample as well as the conditions of measurement. For the Kautsky effect one uses continuous light and the measurement is performed under light conditions. In the case of Q_A reoxidation, the sample is treated with one single saturated flash but the measurement is carried out in darkness.

The dark- relaxation kinetics of the photosynthetic apparatus indicate several pathways of Q_A- reoxidation in darkness, namely by electron transport $Q_A^{\bullet-} \rightarrow Q_B$ ($Q_B^{\bullet-}$) (Figure 7). There are also possible back reactions $Q_B^{\bullet-} \rightarrow P680^{+\bullet}$ [35], [36] to a special chlorophyll pair via different intermediate carriers, for example pheophytin.

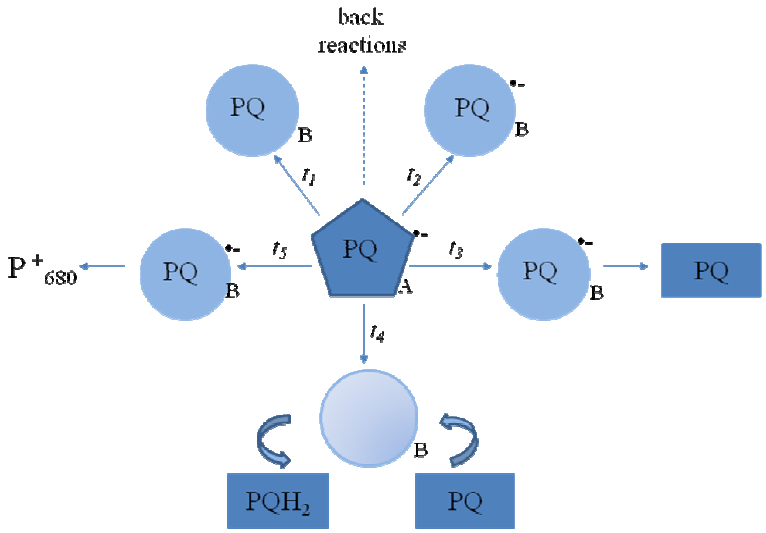

Figure 7. Scheme of possible ways of $Q_A^{\bullet-}$ reoxidation. Circle- plastoquinone bound at the Q_B site, squares- plastoquinone from the external pool. The time constants t_1 (t_2) are correlated with the exchange between PQ_A and PQ_B ($PQ_B^{\bullet-}$).The time constant t_4 is correlated with the time rate of PQ diffusion and its exchange at the Q_B site, whereas- t_3 is correlated with a direct electron exchange between $PQ_B^{\bullet-}$ and the PQ pool. The longest time constant t_5 is in the order of the equilibrium processes occuring within the iron- quinon complex result in a back reaction $PQ_B^{\bullet-} \rightarrow P_{680}^+$.

Transients yielded by flash- induced chlorophyll fluorescence were measured using a double modulation fluorometer FL 3300 (Photon Systems Instruments, Czech Republic) in a 60 s time range to determine the kinetics of the Q_A reoxidation [37]. The actinic flash voltage and the measuring flash voltage was 100 and 50%, respectively. The actinic flash duration was 20 µs. The chlorophyll content in the samples was the same as in the Kautsky effect measurements. The dark adaptation time was always 10 minutes.

The fluorescence spectra of Q_A reoxidation were evaluated using the following function:

$$F_{Q_A-reoxy}(t) = y_0 + \sum_{i=1}^{n} A_i e^{\frac{-t-t_0}{t_i}} \qquad (3.2.3),$$

where n is the minimal number of components necessary for fitting the experimental data, y_0 is the value of the dark signal , A_i is the contribution of each of the components and t_i is a characteristic life time.

3.3 Thermoluminescence

Thermoluminescence (TL) is a phenomenon which can be briefly described as an emission of light at characteristic temperatures from samples that have been exposed to electromagnetic or particle radiation prior to their warming up in the darkness [38]. TL can be observed in many biological systems, for example in the photosynthetic apparatus. The basic idea of the TL phenomenon is the storage of radiant energy in metastable trap states, which can be released via thermally stimulated radiative detrapping.

After light absorption by chlorophylls primary photoreaction produces charge separation between P680, or P860 in the case of plants and bacteria, respectively, and pheophytin (or bacteriopheophytin) (Figure 8). The separated charges are stabilized on the secondary donors (D), and acceptors (A). For (D), for example, there are the charge storage states of the water- oxidizing complex, or the redox active tyrosines (in the case of reaction centers containing PSII). For (A) we may quote the quinone acceptors, Q_A and Q_B. The charge separation process is reversible. This leads to charge recombination and results in a temperature dependent reexcitation of P680 or P860, and antenna chlorophylls. The observed light emission due to their de- excitation gives the TL signal. The stabilization energy of the separated charge pair, ΔG_{Stab} ,is given by the difference between photon energy and the energy stored by the system, ΔG_{Stored} .

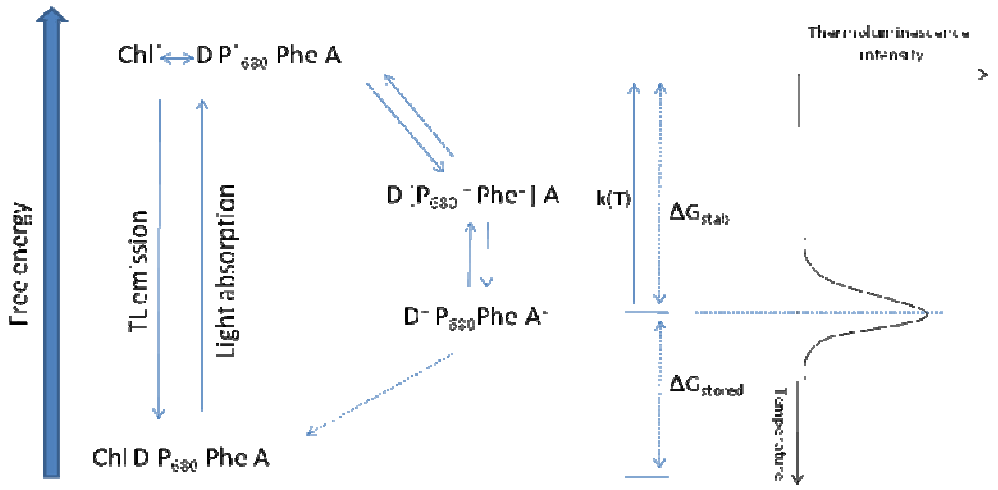

Figure 8. A scheme of the thermoluminescence (TL) emission arising from charge recombination in photosystem II, as an example. The dashed arrows indicate non- radiative charge recombination pathways. The peak position of the TL band is determined byΔG_{stab} (modified in line with to [39]).

Thermoluminescence measurements were done using thermoluminescence system TL- 200/PMT (Photon Systems Instruments, Czech Republic) in a linearly increasing range up to 100°C with a heating rate of 0.5- 1.1 °C/s . The samples kept before the measurements in darkness, were additionally incubated 120 s in darkness at 0°C and then 10 s before the heating flashed with a single actinic flash (a duration of 100 μs) having the intensity of about 200 000 μmol photons× $m^{-2}s^{-1}$. The experiments were performed with a single turnover flash or with a series of flashes 1, 2, 3 or 4 separated by 200 ms dark periods. In the flash studies a new sample was taken for each of the experiments. The spectral response of the photomultiplier was 300- 900 nm. The amount of chlorophyll in the samples was 0.7 μM. Native bacterial RCs and others treated with various concentrations of copper salt were measured.
For an evaluation of the experimental data the following Gaussian function was applied:

$$F_{TL} = y_0 + \sum_i A_i e^{-2\left(\frac{x-x_i}{w_i}\right)^2} \qquad (3.3),$$

where y_0 is the backgroud of the spectrum, A_i is the amplitude of the peak, x- x_i is the central position, and w_i is the width of the peak, respectively.

3.4 Fast polarography method

Fast polarography method (three electrode system) is used for oxygen evolution from photosystem II. The modus operandi is based on an electrochemical reduction of O_2 at a negatively polarized electrode. A platinum cathode and a concentric silver anode are linked by an electrolyte solution (KCl). They are set in an epoxy resin disc, the cathode at the centre and the silver anode in a circular groove called the well or electrolyte reservoir, surrounding the cathode (Figure 9). When the potential of the electrode has settled at -680 mV, oxygen can be efficiently reduced at the platinum surface forming H_2O_2 . During measurement of oxygen evolution the polarity changes. The voltage difference is proportional to the amount of O_2 reduced on the electrode.

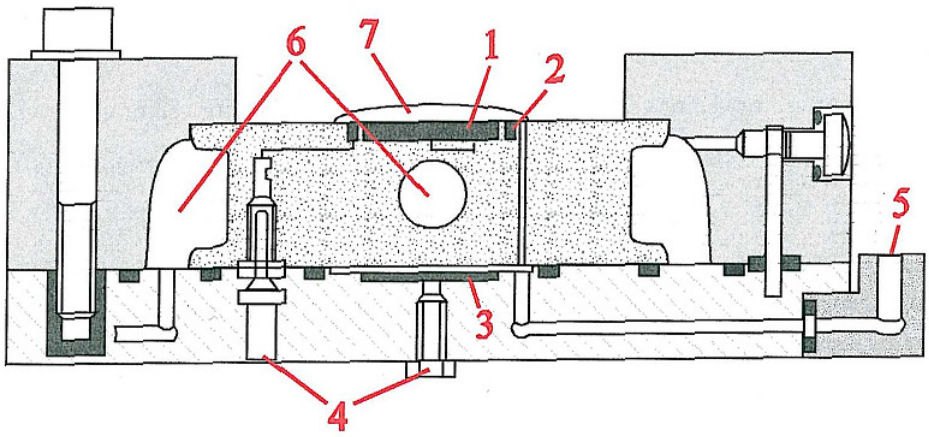

Figure 9. The scheme of the three- electrode system described in [40]. 1: Pt electrode, 2: Ag/AgCl electrode, 3: Ag electrode, 4: electric connections, 5: inlet for KCl, 6: thermostatic coat, 7: sample position.

The following reactions take place on the platinum electrode :

$O_2 + 2H_2O + 2e^- = H_2O_2 + 2OH^-$

$H_2O_2 + 2e^- = 2OH^-$,

whereas on the silver electrode following reactions occure:

$4Ag = 4Ag^+ + 4e^-$

$4Ag^+ + 4Cl^- = 4AgCl.$

Amperometric measurements of oxygen evolution under short saturating flashes were carried out with a three- electrode system as described in [40]. The polarization voltage was -680 mV. Flashes were provided by a Stroboscope 1539A from General Radio (xenon flash lamp) with a flash duration of 5 μs at half intensity. Usually, 15 flashes spaced 300 ms apart were given. The samples were suspended in a Hepes buffer (pH 6.5) with the desired amount of copper salt. In the samples prepared from *N.tobacco,*

containing thylakoids enriched in PSII the amount of chlorophyll was 40 µg (4×10^{-8} M). The total volume of the sample was 500 µl.

The data were analyzed using the (S_0, S_1, S_1, S_3, (S_4)) model assuming heterogenity of oxygen evolution [41]. The 5S- state model is shown in Figure 10. Parameter *d* corresponds to the fraction of the fast transition via the S_4 state: $S_3\ (S_4) = S_0 + O_2$ whereas *1-d* is the fraction of the O_2 yield due to the slower transition via a metastable S_4 state.

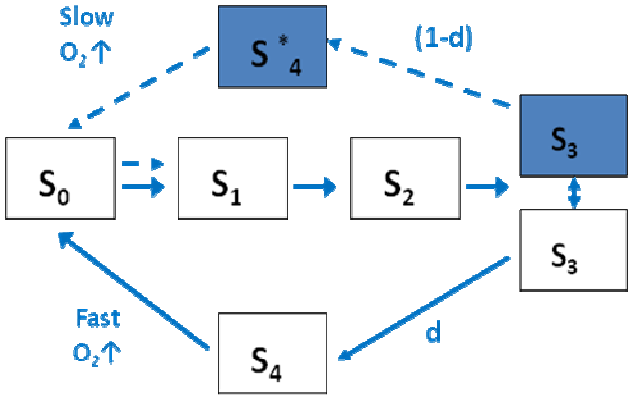

Figure 10. A scheme of two paths of oxygen evolution. *d*, fraction of the fast channel of O_2 yield; *(1-d),* fraction of the slow channel of O_2 yield.

3.5 Mössbauer spectroscopy

3.5.1 Fundamental principles

Mössbauer spectroscopy is a technique which gives very precise information about the chemical, structural, magnetic and time-dependent properties of a probing atom binding site. There are many isotopes that can be used in Mössbauer spectroscopy, [42], [43]. However, in biological samples, for example in photosynthetic systems, the most popular one is ^{57}Fe [44], [45]. The standard Mössbauer source for ^{57}Fe is ^{57}Co (Figure 11). The Mössbauer effect relies on the recoilless emission of a gamma ray by an excited nucleus with subsequent recoilless absorption by another nucleus.

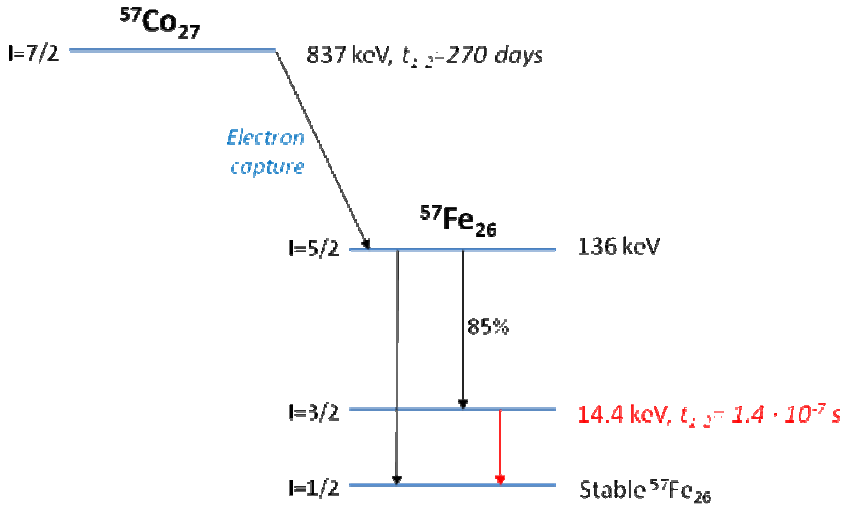

Figure 11. A nuclear decay scheme for ^{57}Fe Mössbauer resonance. ^{57}Co decays by electron capture and initially populates the 136 keV nuclear level of ^{57}Fe with nuclear spin quantum number I = 5/2. This excited state decays after about 10 ns and populates, with 85 % probability the intermediate excited level by emitting 122 keV gamma quanta and with 15 % probability the ground state of ^{57}Fe by emitting 136 keV gamma quanta. The deactivation of the intermediate excited state of ^{57}Fe (I=3/2) deactivates to the ground by emitting gamma quanta of 14.4 keV energy , the most suitable radiation for the Mössbauer spectroscopy.

From conservation of momentum and energy, the recoil energy E_R of a system with mass M due to the emission or absorption of a photon having E_γ is equal to:

$$|E_R| = \frac{E_\gamma^2}{2Mc^2} \qquad (3.5.1.1),$$

where c is the light velocity.

Due to the nuclear recoil, the emission and absorption spectra of free nuclei will be shifted with respect to each other by the amount of E_{abs}-E_{em}=2E_R , and one has to remember that $E_R >> \Gamma_0$ (Γ_0= 4.6×10^{-9} eV is the natural linewidth of the nuclear transition, E_R = 1.96×10^{-3} eV). The overlapping of the emission and absorption line, and therefore recoiless resonance absorption, is possible only when the recoil energy can be

neglected. This is fulfilled for bound emitter and absorber nuclei in a rigid net. The momentum of the recoil is here absorbed by the whole crystal as its mass is considerably larger than that of the free nucleus. That is why in these studies a biological sample has to be frozen or liofilized.

The recoilless absorption fraction measured as a function of temperature allows one to investigate the dynamic properties of the probing atom binding site. The logarithm of the area under the absorption curve is proportional to the Lamb – Mössbauer factor, which is given by:

$$f = A\exp\left(-k^2\left\langle x^2\right\rangle\right) \qquad (3.5.1.2),$$

where $k=1/0.137\ \text{Å}^{-1}$ is the wave number of the 14.4 keV gamma ray for ^{57}Fe, A is the proportional constant and $\langle x^2\rangle$ is the mean square displacement of the iron atom.
Using the Debye model the recoilless fraction, can be expressed by [46]:

$$f = \exp\left\{-\frac{3E_R}{2k_B\theta_D}\left[1+4\left(\frac{T}{\theta_D}\right)^2\int_0^{\frac{\theta_D}{T}}\frac{x}{e^x-1}dx\right]\right\} \qquad (3.5.1.3),$$

where T is the absolute temperature, θ_D is a characteristic Debye temperature defined as $\hbar\omega_D/k_B$ (k_B being the Boltzmann constant, and $\hbar$ is a Planck constant divided by to 2π).

For a given resonant nuclear transition energy, the recoil-free fraction increases with the Debye temperature. This means that the Lamb – Mössbauer factor rapidly decreases above a characteristic temperature. For biological samples the temperature is typically around θ_D = 200 (± 30) K. According to the Debye model, at high temperatures ($T \geq \theta_D$) the mean square displacement of the Mössbauer atom should be proportional to temperature T (eq. 3.5.1.4.a)

$$f = \exp\left(-\frac{6E_RT}{k_B\theta_D^2}\right) \quad T > \theta_D \qquad (3.5.1.4.a)$$

$$f = \exp\left(-\frac{3E_R}{2k_B\theta_D}\right), \quad T < \theta_D \qquad (3.5.1.4.b).$$

From the equation (3.5.1.4a and 3.5.1.4b) one can then get information on the mean square displacement of the probe atom (in our case ^{57}Fe). For biomolecules one usually observes that $\langle x^2\rangle$ deviates from linear behaviour. These deviations arise from anharmonic vibrations of the lattice [47]. Below θ_D, the mean square displacement of iron indicates a solid –like (lattice) behaviour, whereas above that temperature it is influenced by additional molecular fluctuations. Slow collective motions additionally cause a broadening of absorption lines.

3.5.2 Hyperfine interactions

The differences in Mössbauer spectra stem from interactions between the nucleus and the electric and magnetic fields. These hyperfine interactions give rise to isomer shift (I.S.), quadrupole splitting (Q.S.) and magnetic Zeeman splitting.

3.5.2.1 The isomer shift

The isomer shift results from the electrostatic (Coulomb) interaction of the nuclear- charge distribution over a finite nuclear radius *R* in the excited and ground states and the electron- charge density at the nucleus (mainly from the s electrons). This interaction leads to a slight shift of Mössbauer energy levels in a compound relative to those in the free atom (Figure 12).

The nucleus is assumed to be a uniformly charged sphere of radius *R*, and the s- electron density at the nucleus, $[\Psi(0)_S]^2$, is assumed to be constant over the nuclear dimensions. One computes the difference between the electrostatic interaction of a point nucleus with $[\Psi(0)_S]^2$, and the interaction of a nucleus having a radius *R* with $[\Psi(0)_S]^2$. The difference in energy is given by:

$$\delta E = [\Psi(0)_S]^2 R^2 \qquad (3.5.2.1).$$

Since *R* is generally different for ground and excited nuclear states, δE will be different for both, and:

$$\delta E_e - \delta E_g = K[\Psi(0)_S]^2 (R_e^2 - R_g^2) \qquad (3.5.2.2),$$

where *K* is a nuclear constant, and the indexes *e* and *g* refer to the excited and ground states respectively. The isomer shift is given by the difference of eq. (3.5.2.2) for source and absorber:

$$I.S. = K(R_e^2 - R_g^2)\{[\Psi(0)_S]_a^2 - [\Psi(0)_S]_s^2\} \qquad (3.5.2.3),$$

where the subscripts *a* and *s* refer to the absorber and source, respectively. Since the change in radius R_e- R_g is very small, the isomer shift can then be written in its usual form:

$$I.S. = 2KR^2 \frac{\delta R}{R}\{[\Psi(0)_S]_a^2 - C\} \qquad (3.5.2.4),$$

where $\delta R = R_e - R_g$ and *C* is a constant characteristic of the probing atom used.

3.5.2.2 Quadrupole interaction

Electric quadropole interaction occurs if at least one of the nuclear states (ground or excited) of the Mössbauer probe possesses a quadrupole moment *eQ*, ie. for *I>1/2* , and if the electric field at the nucleus is unhomogeneous. In the case of the ^{57}Fe nucleus, in the presence of an electric field gradient (EFG) the excited state with *I=3/2* splits into

two substates with the magnetic spin quantum numbers $m_I = \pm 3/2$ and $\pm 1/2$ (they are still doubly degenerated) The ground state with $I=1/2$ level remains unsplit ($Q=0$) and also doubly degenerated. Due to the selection rule $\Delta m_I = 0, \pm 1 \ldots \pm$ I-1, $\pm$ I, two characteristic lines in the Mössbauer spectrum are observed for ^{57}Fe (Figure 12).

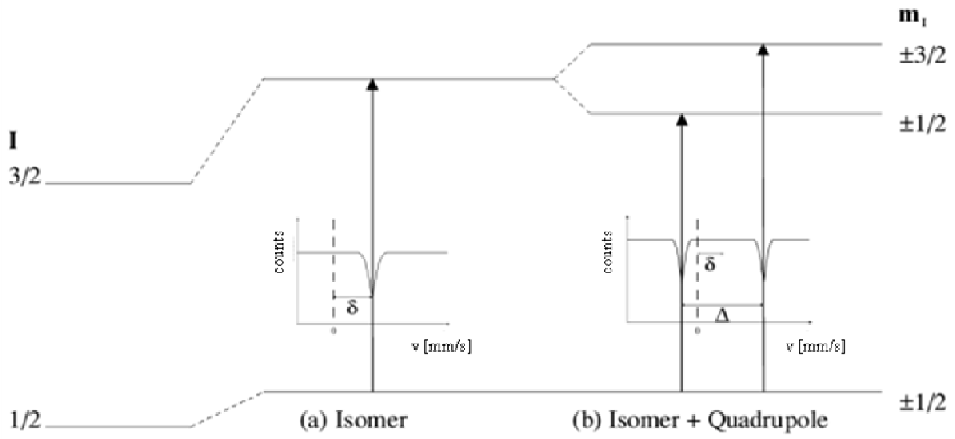

Figure 12. Effect of isomer shift (a) and quadrupole splitting (b) on Mössbauer spectra (adapted from: http://www.cmp.liv.ac.uk).

The separation energy of the peaks is called quadrupole splitting (*Q.S).* The quadrupolar interaction energies E_Q derived from perturbation theory (for axial symmetry) can be expressed as:

$$E_Q(I, m_I) = \frac{eQV_{zz}}{4I(2I-1)}[3m_I^2 - I(I+1)]\left(1+\frac{\eta^2}{3}\right)^{\frac{1}{2}} \qquad (3.5.2.5).$$

The electric field E at the nucleus is the negative gradient of the potential V and the electric field gradient (EFG) is given by the nine components:

$$EFG = \nabla E = -\begin{bmatrix} V_{xx} & V_{xy} & V_{xz} \\ V_{yx} & V_{yy} & V_{yz} \\ V_{zx} & V_{zy} & V_{zz} \end{bmatrix} \qquad (3.5.2.6),$$

$$\text{where} \quad V_{ij} = \frac{\partial V_{ij}}{\partial_i \partial_j}.$$

For axial symmetry the EFG is solely given by the tensor component V_{zz} ,while for non-axial symmetry the asymmetry parameter η is defined:

$$\eta = \frac{V_{xx} - V_{yy}}{V_{zz}} \qquad (3.5.2.7).$$

3.5.2.3 Magnetic interaction

A nucleus with a non- zero spin has a magnetic dipole moment μ_N, given by the equation:

$$\mu_N = g_N \beta_N I \qquad (3.5.2.8),$$

where: g_N is the nuclear Landé factor, and β_N, the nuclear Bohr magneton given by:

$$\beta_N = \frac{e\hbar}{2mc} \qquad (3.5.2.9),$$

where e and m are the charge and mass of the proton, and c is the velocity of light.

In the presence of a magnetic field H (which can be an external or a local internal field), there is an interaction between the field and the magnetic moment μ_N leading to the splitting of the energy level with I into $2I+1$ energy levels formed with energies described by the equation:

$$E_m(m_I) = -g_N \beta_N H m_I \qquad (3.5.2.10),$$

where: magnetic spin quantum number $m_I = 0, \pm 1 \ldots \pm I-1, \pm I$ (Figure 13).

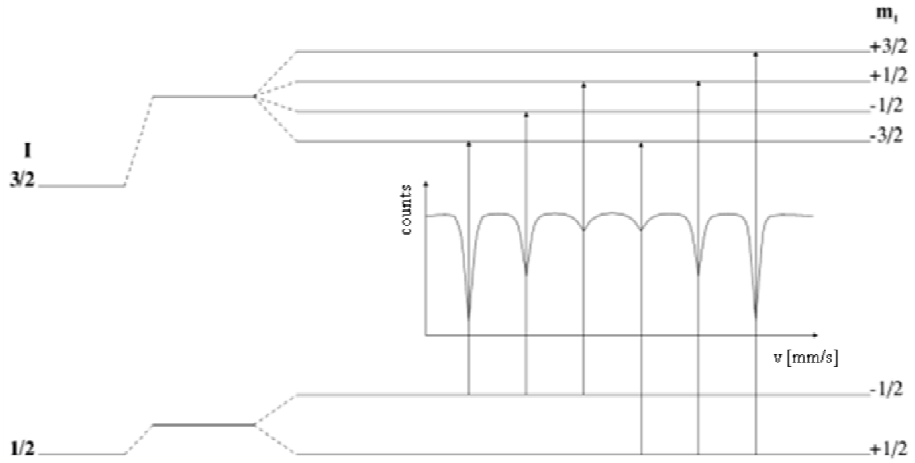

Figure 13. The effect of magnetic splitting on nuclear energy levels in ^{57}Fe. A nuclear state with spin $I \geq 1/2$ possesses a magnetic dipole moment μ_N which interacts with local or applied magnetic fields at the nucleus.This is the case for both the ground state with $I = 1/2$ and the first excited state with $I = 3/2$ of ^{57}Fe. The magnetic dipole interaction with the magnetic field leads to the splitting of the states $|I, m_I\rangle$ into $2I+1$ substates characterised by the magnetic spin quantum numbers m_I. Thus the excited state with $I = 3/2$ is split into four, and the ground state with $I = 1/2$ into two substates. These substates are no longer degenerate. The energies of the sublevels are given from eq. (3.4.2.10). For magnetic dipole radiation only transitions with $\Delta I=1$, $\Delta m=0, \pm 1$ are allowed, giving six possible transitions in ^{57}Fe. (adapted from: http://www.cmp.liv.ac.uk).

The line positions are related to the splitting of the energy levels, but the line intensities are related to the angle between the Mössbauer gamma- ray and the nuclear spin moment. The intensities are given by:

$$I_1 = I_6 = 3(1+\cos^2\theta)$$

$$I_2 = I_5 = 4\sin^2\theta$$

$$I_3 = I_4 = 1+\cos^2\theta \qquad (3.5.2.11),$$

where θ is the angle between the effective H and the direction of propagation of the radiation.
In polycrystalline samples the ratio of the subsequent lines I_1:I_2:I_3 is: 1:2:3.

3.5.3 Mössbauer Spectroscopy Instrumentation

Most commonly in order to vary the energy of the probing nucleus between source and absorber levels, the source is moved toward and away from the absorber, the velocity varying linearly with time (the first order Doppler effect is applied). It is also possible to leave the source stationary and oscillate the sample. The location of the detector relative to the source and the sample defines the geometry of the experiment (Figure 14).

a)

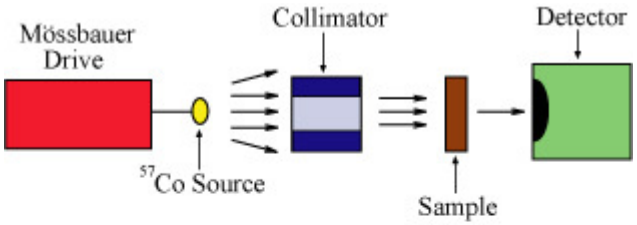

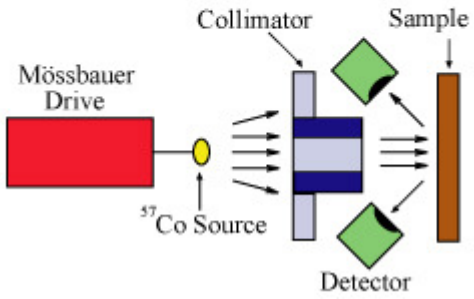

b)

Figure 14. Block diagram of Mössbauer spectrometer, (a) transmission geometry (b) backscattering geometry (adapted from: http://serc.carleton.edu).

Mössbauer spectra of the non-haem iron were recorded in a home made cryostat. Samples were measured in the range of 83- 265 K in the case of *Rb.sphaeroides*.

Temperature stabilization was within 0.1 K. The source of 50 mCi Co/Rh was kept at room temperature. A proportional counter was used for detection the 14. 4 keV γ radiation in the transmission mode.The isomer shifts were given vs. metallic Fe at room temperature. The spectra were fitted using a professional program *Recoil*.

3.6 Inelastic synchrotron radiation

The issue of nuclear inelastic scattering (NIS) may be resolved by measuring the energy spectra of the inelastic absorption of X- rays by nuclei. It is applied in the case of what are known as "Mössbauer" isotopes, which have low- energy nuclear transitions in a range 6- 30 keV [48]. When the energy of incident X rays coincides exactly with the energy of the nuclear transition (in the case of ^{57}Fe, the energy equals 14.4 keV), a peak of elastic nuclear absorption occurs. Nuclear absorption may also proceed inelastically, with the creation or annihilation of lattice vibrations (Figure 15). These processes cause inelastic sidebands in the energy spectra of nuclear absorption around a central elastic peak. From the energy spectrum of nuclear inelastic absorption, the density of the phonon states of ^{57}Fe can be determined.

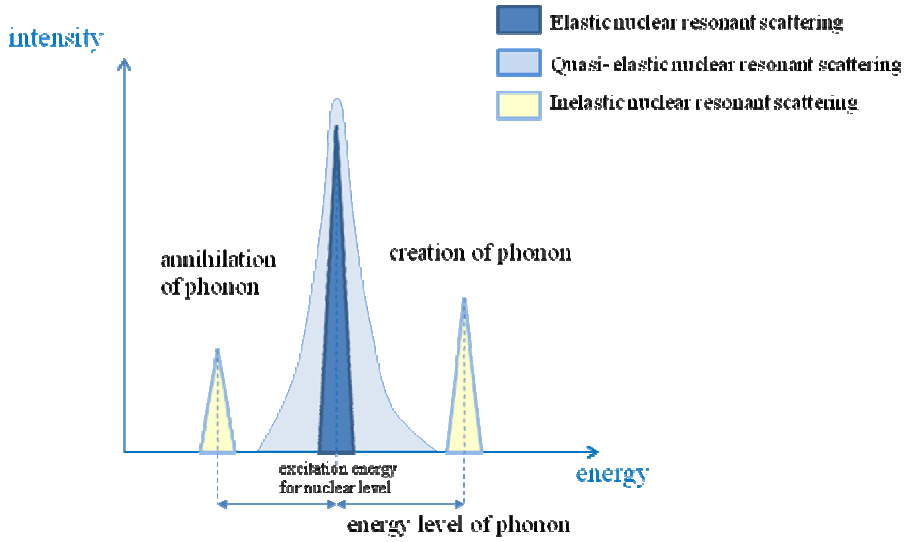

Figure 15. A conceptual scheme for inelastic nuclear resonant scattering. The incident x-ray photon changes its energy slightly due to the influence of the vibration of the lattice in the target material. Therefore, if one is measuring the intensity of inelastic nuclear resonant scattering with an energy scan near the resonant energy of the specific atom, the measured spectra show the peak intensity or the line broadening according to phonon annihilation or creation. These spectra provide us with information on the vibration of the lattice of a specific atom in the material.

In an inelastic scattering of synchrotron radiation a high- resolution monochromator selects a narrow (~ meV) band from the spectrum of the incident synchrotron radiation (Figure 16). By tuning monochromator crystals, the energy of the selected radiation is varied in the vicinity of the energy of the nuclear transition. The energy dependence of the nuclear absorption is measured by the first detector, which

counts the products of nuclear absorption- atomic fluorescence radiation. The second detector monitors coherent nuclear forward scattering. Since this is an elastic process, the data from the second detector also provide, at one and the same time the instrumental function of the spectrometer. The instrumental function of the nuclear inelastic spectrometer does not vary with energy because of the small relative energy transfer (< 10^{-5}). In order to distinguish the products of nuclear interaction from alternative channels of electronic absorption or scattering , the readings of both detectors are gated in time, and data is taken only between the pulses of synchrotron radiation. Nuclear interaction is delayed in time due to the finite lifetime of narrow nuclear levels (~ 100 ns), whereas electronic interaction is essentially instantaneous on this time scale.

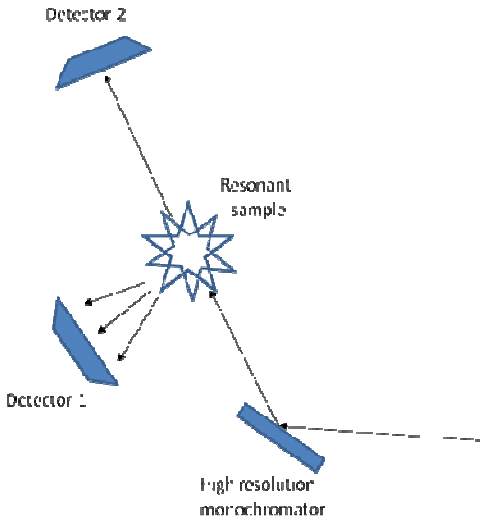

Figure 16. Experimental setup for nuclear inelastic absorption measurements.

Nuclear inelastic absorption of synchrotron radiation measurements were performed at the Nuclear Resonance Beamline, ID 18 at the European Synchrotron Radiation Facility in Grenoble. The storage ring was run in a 16- bunch mode, providing pulses of radiation energy every 176 ns. The average ring current was about mA. The energy resolution was 0.5 meV. The energy of radiation was tuned in a range from -40 meV to 100 meV around the transition energy of ^{57}Fe (14.413 keV) for measurements at T= 60 K and from -80 meV to 100 meV for measurements at T= 240 K. The flux on the sample was about 2×10^{8} photons/ s within a band width of 0.6 meV [49]. The intensity of nuclear absorption was measured by counting the delayed 6.4 keV K- line of Fe fluorescence using a large area fast avalanche photodiode (ADP) [50]. It was possible to obtain a statistically reasonable spectrum in the 16- band mode during 10- 12 hours depending on the ^{57}Fe iron concentration.

The plots were normalized using a procedure based on Lipkin's sum rule:

$$\int_{-\infty}^{\infty} W(E)EdE = E_R \qquad (3.6.1),$$

where $E_R = \frac{\hbar^2 k^2}{2m_R} = 1.96meV$ is the recoil energy of a free nucleus (*k*- a wave vector of *x*- ray quantum, m_R- the mass of the resonant nucleus, in this case that of an iron atom.

The normalized spectrum *W(E)* corresponds to the density probability of nuclear inelastic absorption, which can be expressed by a sum of the elastic fraction of nuclear absorption, f_{LM}, and a multiphonon term:

$$W(E) = f_{LM}(\delta(E) + \sum_{n=1}^{\infty} S_n(E)) \qquad (3.6.2),$$

where $S_n(E)$ is an inelastic absorption accompanied by the creation or anihilation of *n* photons, and the Dirac δ- function $\delta(E)$ describes the elastic part of the absorption (zero-phonon term). For a single photon event:

$$S_1(E) = \frac{E_R g(E)}{E(1 - e^{\frac{E}{k_B T}})} \qquad (3.6.3)$$

and for $n \geq 2$ in a harmonic approximation:

$$S_n(E) = \frac{1}{n} \int_{-\infty}^{\infty} S_1(E') S_{n-1}(E - E') dE' \qquad (3.6.4).$$

Here k_B is the Boltzmann constant and *T* is temperature.

For randomly oriented samples, be they in the form of liquid, glass or powder, the function *g(E)* is the normalized partial density of vibrational states (DOS). The *g(E)* function assumes average values in all crystallographic directions and using the same parameters, may be derived from equations (3.6.2 - 3.6.4):

$$g(E) = V_0 \sum_j \int \frac{dg}{(2\pi)^3} \delta[E - \hbar\omega_j(q)] \qquad (3.6.5),$$

where V_0 is the volume of the unit cell and $\vec{q}$ is the phonon momentum.

4 Results and discussion

4.1 Photosynthetic reaction centers of higher plants

In order to investigate the role of cytochrome b_{559} in photosynthesis, comparative studies of energy and electron transfer in the wild type tobacco (WT) and mutant (MT) with modified cyt b_{559} were carried out. In addition, we followed changes on the acceptor side of PSII using the Kautsky effect and Q_A^- reoxidation measurements and on the donor PSII side applying the fast polarography method under the action of copper ions. It has been found that photosystem II (PSII) is very sensitive to Cu^{2+} [51]. Copper inhibits either the acceptor or donor side of PSII. It has been shown that Cu^{2+} may induce conformational and redox changes of the iron- quinone complex in the vicinity of both binding sites of quinone acceptors (of the primary quinone acceptor Q_A and the secondary quinone acceptor Q_B) [12], [52]. Copper ions can modify the redox properties of the non-haem iron as well as the haem iron of cytochrome b_{559} [12], [52], [53]. Knowing that inhibitory action of Cu^{2+} on PSII strongly depends on the ratio of copper ions per reaction center, [54], [55], [56] the studies of the dependence of the efficiency of electron transfer within PSII on the various concentrations of Cu^{2+} ($CuCl_2$ and $CuSO_4$) were performed.

4.1.1 Kautsky effect

Studies of the fluorescence transient were carried on the reaction centers isolated from thylakoids enriched in PSII according to the method described in *Materials,* (chapter 2.1). We did not use any external acceptors. Samples were treated with different concentrations of copper (from 0.6 Cu^{2+}/PSII - 1260 Cu^{2+}/PSII). The samples were always incubated for 10 minutes in darkness before the measurement. The experiemnts were performed under dim light conditions. The state of the samples were checked using fluorescence measurements at 77 K. The spectra of thylakoids and thylakoids enriched in PSII (BBY PSII) are presented in Figure 17.

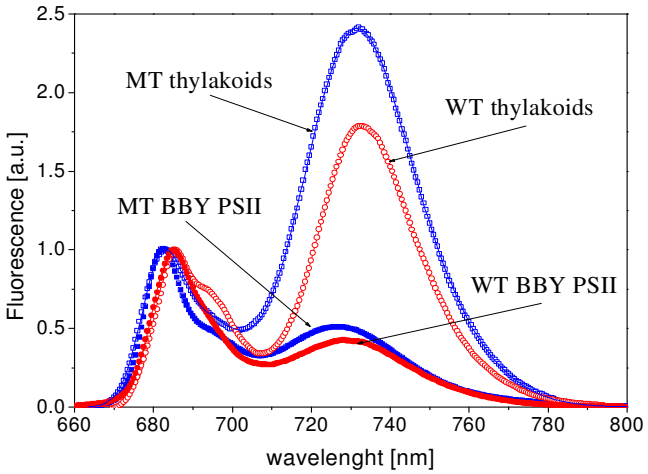

Figure 17. The steady state fluorescence spectra of thylakoids and thylakoids enriched in photosystem II (BBY PSII) measured at 77 K. The peaks at around 686 nm are characteristic for PSII and those at around 730 nm for PSI.

One can see that in the samples of thylakoids enriched in PSII (WT BBY PSII and MT BBY PSII) the amount of photosystem I is significally reduced. Both samples have comparable intensities and the amounts of the contamination of the PSI system.

The Kautsky effect observed in thylakoids membranes enriched in BBY PSII prepared from WT and MT is presented in Figure 18.

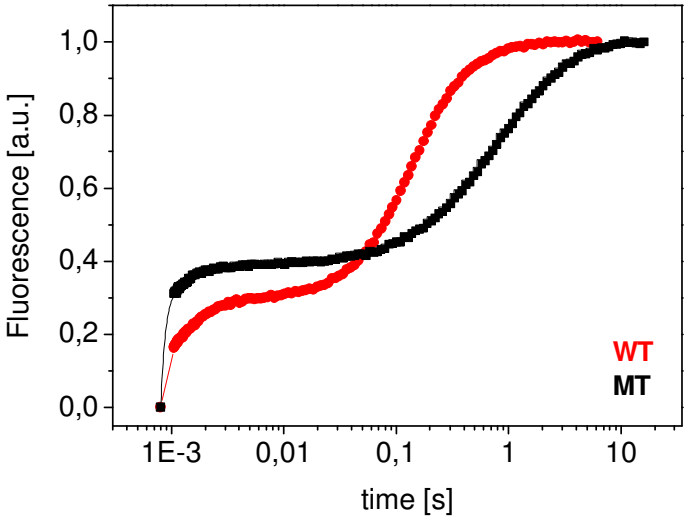

Figure 18. The semilogarithmic plot of the fluorescence spectra of thylakoids enriched in PSII (red: WT; black: MT). Spectra are normalized to F_M , the maximum of the fluorescence. The solid lines represent theoretical curves.

The experimental data normalized to the maximum value of the fluorescence, F_M were analyzed by applying eq. (3.2.2.) (Figure 18 and Figure 19.).

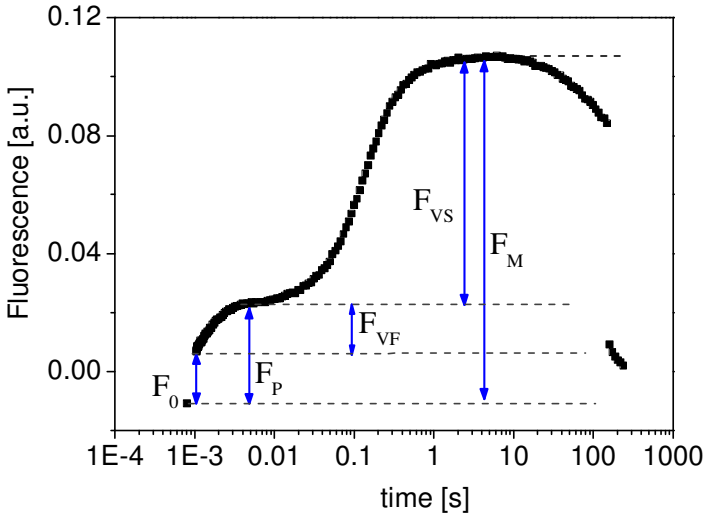

Figure 19. An example of the variable fluorescence spectrum of WT BBY PSII shown in semilogarithmic plot. The parameters F_0, F_P, F_{VF}, F_{VS}, can be elucidated from the fitted A_i amplitudes according to the eq. 3.2.2.

In Figure 20 the dependence of the F_M values on the copper salt concentrations are presented.

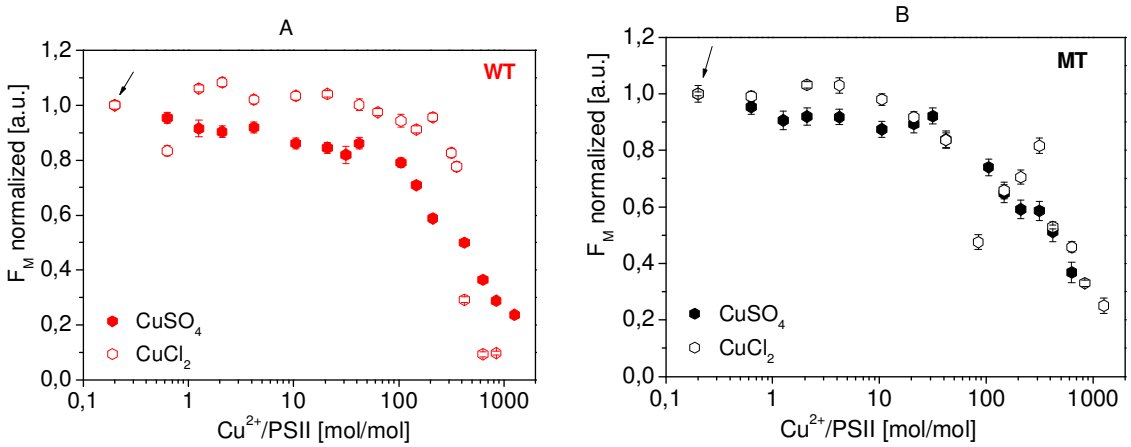

Figure 20. The semilogarithmic plots of the F_M normalized to the control sample for (A) WT BBY PSII and (B) MT BBY PSII.

One can see from Figure 20 that in the WT BBY PSII the maximum of the fluorescence decreases significantly for $CuCl_2$/PSII > 300 and $CuSO_4$/PSII >100 whereas in the MT BBY PSII at Cu^{2+}/PSII >30 for both copper salts, although the F_M decrease starts in the presence of the Cl^- ions already at about 4 $CuCl_2$/PSII. For WT the F_M parameter has higher values for $CuCl_2$ than $CuSO_4$ (even a 10% stimulation is observed for 1< $CuCl_2$/PSII < 4 in comparison to the control sample) within the range of the applied copper concentrations up to about 400 Cu^{2+}/PSII but at larger than 400 Cu^{2+}/PSII concentrations the fluorescence inhibition is stronger in the case of $CuCl_2$. For MT the F_M values are higher in the case of $CuCl_2$ than $CuSO_4$ up to about 20 Cu^{2+}/PSII concentration. With the further increase of the copper ions concentration the maximum of the fluorescence is comparable with the range of 20-40 and 400 – 1260 Cu^{2+}/PSII concentrations. The most striking difference of the F_M values detected for $CuCl_2$ and $CuSO_4$ in the case of MT BBY PSII is observed for the 80-400 Cu^{2+}/PSII concentrations when the F_M increase occurs for $CuCl_2$ but decrease for $CuSO_4$. This effect is obviously related to the point mutation of the cytochrome b_{559}.

One can see some additional characteristic changes of the F_M values at 0.6, 1, 2, 4, 10, 20, 200, 400 and 600 $CuCl_2$/PSII and 1, 4, 40, 100 and 400 $CuSO_4$/PSII for WT BBY PSII. In the case of MT BBY PSII, additionally, one can point the following $CuCl_2$/PSII concentrations: 0.6, 2, 4, 40, 80 and 600 and $CuSO_4$/PSII concentrations: 1, 4, 10, 30, 100, 200, 300 and 600. The more detailed analysis of the experimental data and discussion of the results presented below allowed us to indicate some processes responsible for the observed variations of the maximal fluorescence within the two studied tobacco types, depending on the $CuSO_4$ and $CuCl_2$.

The amplitude A_1 related to the fast initial increase of the fluorescence curve corresponds to F_0 whereas the amplitude A_2 to the fast variable fluorescence, F_{VF} (Figure 21). Amplitudes A_i, for i=3,4, are related to the slow variable fluorescence, F_{VS} (Figure

22.).Usually, the F_0 parameter is taken directly from the experimental data, as the first experimental point measured after the light switching on, here we call it F_{0exp}. Its value is systematically higher than that one obtained from the fits of the experimental data using eq. 3.2.2 (chapter 3.2.2), F_0. This is because the theoretical approach allows one to estimate the F_0 value with a higher time resolution, even at the level of the experimental setup, i.e. about 20 µs. In Figure 21 A and B, we compare the fitted F_0/F_M values to the experimental F_{0exp}/F_M values. In Figure 21 C and D we show the fast variable fluorescence, F_{VF}. This parameter can be obtained in two ways: (i) as the difference between the amplitude of the first plateau F_P and of the F_{0exp} value; $F_{VFexp} = F_p - F_{0exp}$, or (ii) as the amplitude A_2 from the theoretical fits of the experimental data; then $F_P = A_1 + A_2$. The dependences of the parameter F_{0exp} and F_{VFexp} on the $CuCl_2$ and $CuSO_4$ concentrations do not vary from the dependences of the corresponding theoretical parameters obtained from the fits of the experimental data (Figure 21 A-D). Therefore for the further discussion we will concentrate on the theoretically estimated parameters F_0 and F_{VF} and their contributions to the fluorescence spectrum, i.e. their values normalized to the F_M value.

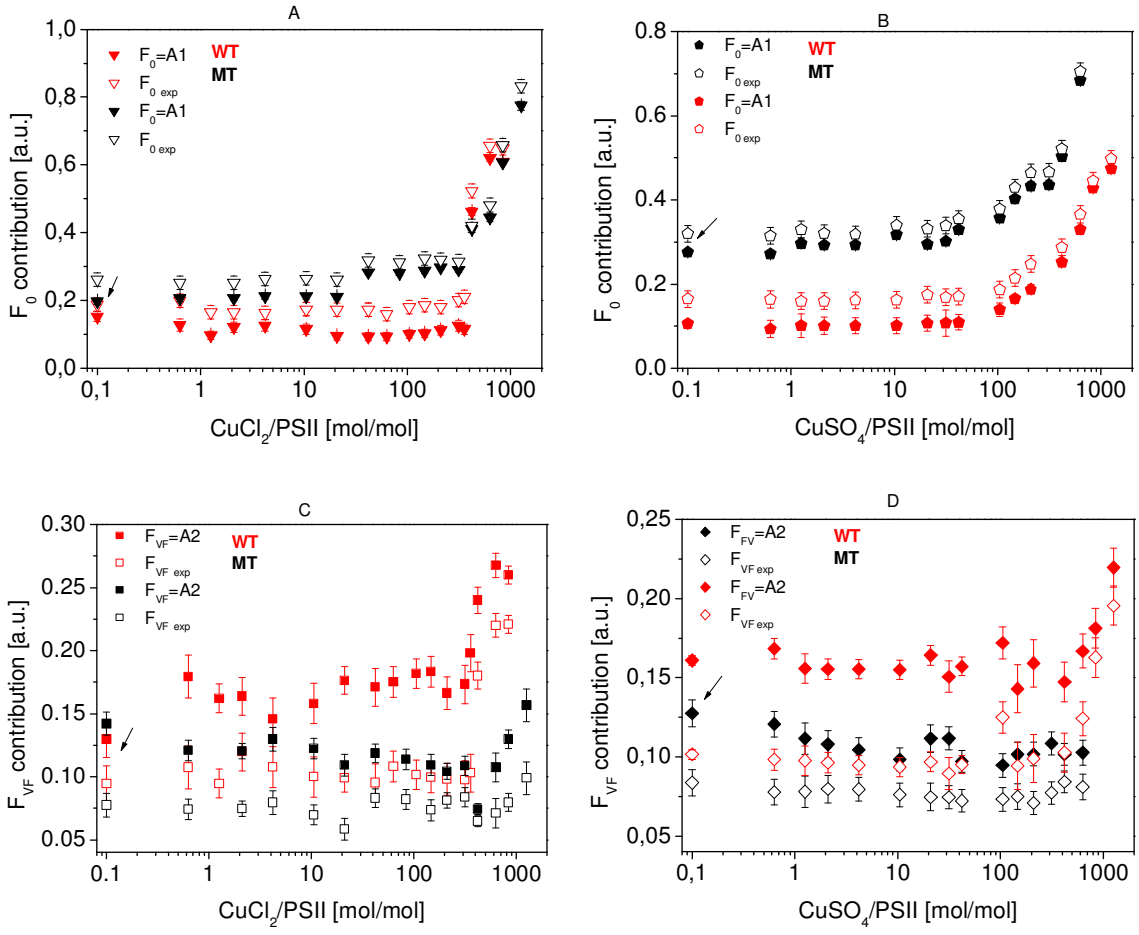

Figure 21. The semilogarithmic plots of the parameters F_0 (A,B) and F_{VF} (C,D) normalized to F_M value shown as a function of copper concentrations (the left panel, A, C- $CuCl_2$ and the right panel, B, D- $CuSO_4$). The arrows indicate the F_0 and F_{VF} values for the control samples.

In the case of WT BBY PSII, one can observe a discontinuity of the initial fluorescence F_0/F_M at around 1 $CuCl_2$/PSII. This discontinuity is not present in WT treated with $CuSO_4$ and in MT treated with $CuCl_2$. For MT BBY a small jump of the F_0 contribution is visible at $CuCl_2$/PSII > 20 and at $CuSO_4$ > 4. These effects are not observed in WT preparations. The most pronounced change of the normalized F_0 parameter is its increase at around 400 $CuCl_2$/PSII for MT and WT and at around 30 and 40 $CuSO_4$/PSII for MT and WT, respectively. In the case of sulfate copper one can distinguish two additional transitions of F_0/F_M at 200 $CuSO_4$/PSII and 400 $CuSO_4$/PSII for MT but only the second one is present in WT. For MT one more transition of the F_0 contribution is detected at 800 $CuCl_2$/PSII.

The F_{VF} contribution exhibits also some characteristic discontinuities. In MT samples treated with $CuSO_4$ the following $CuSO_4$/PSII concentrations can be pointed: 10, 20, 40, 100 and 300, whereas in the WT samples: 1, 10, 30, 100, 200 and 400 $CuSO_4$/PSII concentrations. Much more pronounced changes of F_{VF}/F_M are detected for WT and MT BBY PSII treated with $CuCl_2$, and especially at 150-200 and 300-400 $CuCl_2$/PSII, respectively. For both tobacco types one can distinguish four other characteristic discontinuities at 4, 10, 20 and 40 $CuCl_2$/PSII concentrations. It is important to note that the most pronounced changes of the F_0 and F_{VF} contributions occur at the similar $CuCl_2$/PSII concentrations, namely at around 200- 400 $CuCl_2$/PSII for MT and WT whereas the steep increase of the F_{VF} contribution is observed for 10 times higher concentrations of $CuSO_4$ than for the F_0 contribution in the case of WT. For MT a such increase of the F_{VF} contribution is not detected at all within the range of the applied $CuSO_4$ concentrations.

In Figure 22 we present the parameter F_p (first plateau) which is the sum of F_0 and F_{VF} and the slow variable fluorescence, F_{VS}. The first parameter corresponds to the reactions which kinetics are faster than 1.5 ms and the second one is related to the energy and electron transport processes slower than a few miliseconds.

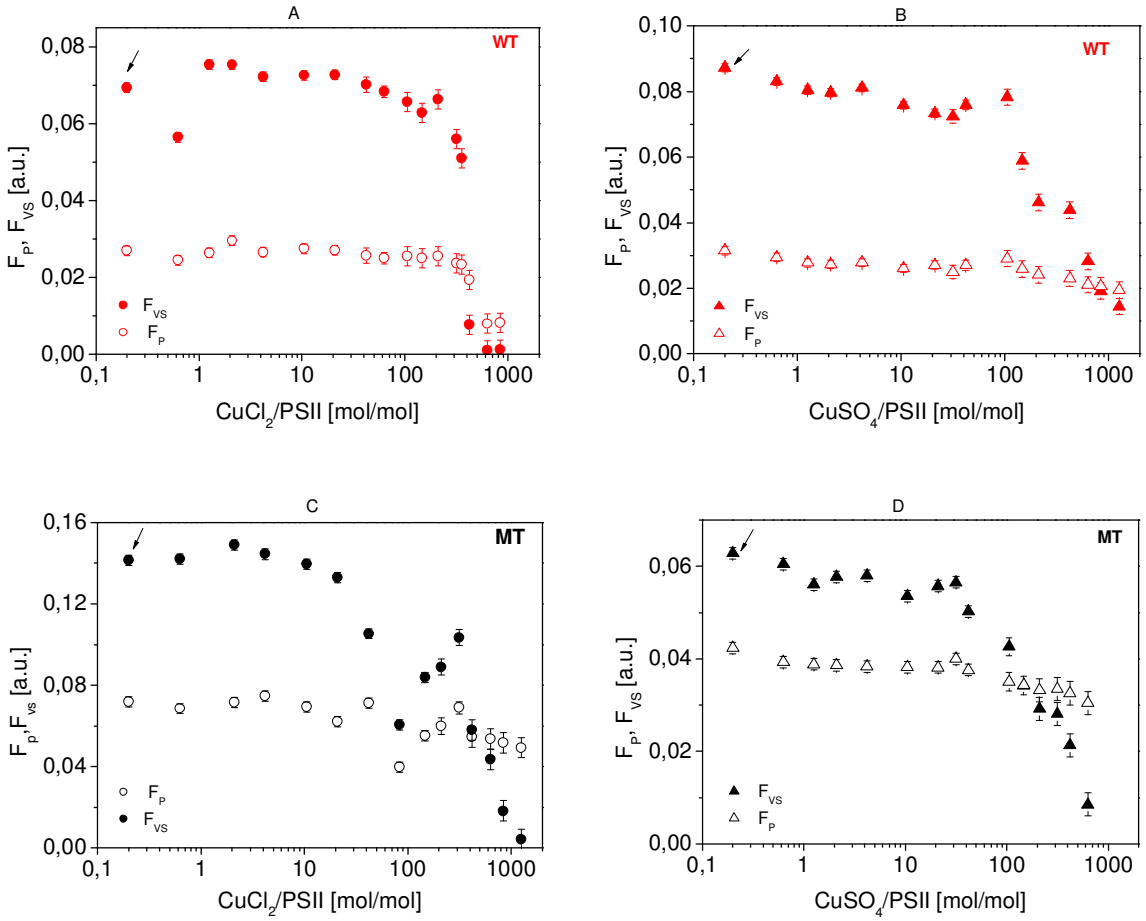

Figure 22. The semilogarithmic plots of the parameters F_p and F_{VS} shown as a function of copper concentrations (the left panel, A, C- $CuCl_2$ and the right panel, B, D- $CuSO_4$). The arrows indicate the values for control samples.

The value of F_{VS} is about 2.6 ± 0.1 times higher than the F_P value in WT BBY PSII within the low range of the copper salt concentrations, up to about 200 $CuCl_2$/PSII and 100 $CuSO_4$/PSII. This shift toward lower $CuSO_4$ concentrations is caused by the fact that the steep decrease of F_{VS} occurs at 2 times lower $CuSO_4$ concentrations than it takes place for $CuCl_2$. (Figure 22 A, B). Another striking difference of the Fvs dependence on the two various copper salts is that the slow variable fluorescence decreases and is close to 0 at $CuCl_2$/PSII > 600 whereas the F_{VS} fluorescence is still observed at the level of 10% of the control value at as high as 1260 $CuSO_4$/PSII concentration. Within the same ranges of these copper salts the F_P value decreases ~3 times for $CuCl_2$ and only by about 30% for $CuSO_4$. These observations give an evidence that WT preparations are more resistant to the action of copper ions in the presence of SO^{2-}_4 ions. There are some other F_{VS} changes observed for the increasing concentration of copper chloride. The F_{VS} value decreases at 0.6 $CuCl_2$/PSII by about 20% and then it increases to the value which is higher by about 8% at 1 $CuCl_2$/PSII in comparison to the control sample. At the copper chloride concentrations between 2 - 20 $CuCl_2$/PSII the slow variable fluorescence has again the same value as the control sample. Then the F_{VS} parameter starts to decrease up

to 200 $CuCl_2$/PSII, when a jump is observed, its value icreases by about 10%. Within the concentrations of 200-400 $CuCl_2$/PSII the F_{VS} value decreases ~5 times. A similar to F_{VS} behaviour of F_P is detected for the increasing $CuCl_2$ concentrations but the F_{VS} changes discussed above are observed at 2 times higher copper chloride concentrations in the case of the F_P parameter. In the WT samples treated with the copper sulfate the discontinuities of F_{VS} and F_P parameters appear at the same $CuSO_4$/PSII concentrations, namely at: 4, 20, 100, 200 and 400. The only difference is observed at 1 $CuSO_4$/PSII when a drop of the F_{VS} value is visible but not of the F_P one.

The comparison of the F_{VS} and F_P changes with increasing copper concentrations between WT BBY PSII and MT BBY PSII show that the mutant is less resistant against the Cu^{2+} action, but in contrary to the WT tobacco it is more sensitive to Cu^{2+} action in the presence of Cl^- ions. An increase of F_{VS} by about 7% is visible at 2 $CuCl_2$/PSII and then its monotonously decrease up to 20 $CuCl_2$/PSII concentration. The most interesting behaviour of the F_{VS} and F_P parameters distinguishing MT BBY PSII from WT BBY PSII is the steep decrease of these two parameters within the range of 40-80 $CuCl_2$/PSII and then their increase for the $CuCl_2$/PSII concentrations from 80 to 400. Within these copper concentrations the F_{VS} value changes by the factor of 1.6 and the values of F_P by a factor of 1.8. These transitions are not observed in MT BBY PSII treated with $CuSO_4$. The enhancement of F_{VS} at 200 $CuCl_2$/PSII and at 100 $CuSO_4$/PSII in the WT BBY PSII preparations could be related to the same effect observed for MT treated with $CuCl_2$ but its scale is much smaller. Generally, for MT the same discontinuities of the F_P parameter are observed as for the F_{VS} one but with two exceptions: (ii) there is an additional transition of the F_{VS} parameter at 600 $CuCl_2$/PSII and (ii) the F_P value change shows a small maximum at 4 $CuCl_2$/PSII, which occurs at two times higher copper concentration in the F_{VS} case.

The value of the F_P parameter for MT is lowered by the salt concentaration of 0.6 $CuSO_4$/PSII in comparison to control sample and it slightly decreases with increasing salt concentrations up to 20 $CuSO_4$/PSII. Then it increases and again starts to decrease showing the discontinuities at 40 and 200 $CuSO_4$/PSII. The value of the parameter F_{VS} shows additional changes at: 2, 4, 30 and 100 $CuSO_4$/PSII, but not at 20 $CuSO_4$/PSII. The F_{VS} value is at the level of 10% of the control value for the copper concentrations of 600 $CuSO_4$/PSII and 800 $CuCl_2$/PSII, what suggests a higher sensitivity of the mutant to the Cu^{2+} action at its high concentrations in the presence of the SO_4^{2-} anions.

The measurements of MT BBY PSII treated with sulfate copper and WT BBY PSII treated with both copper salts give evidence that the characteristic transition observed for the mutant incubated with 100-400 $CuCl_2$/PSII concentrations is unique for the photosystem II containing the modified cytochrome b_{559}. The specific action of copper ions on the MT PSII is completely diminished in the presence of the SO_4^{2-} ions.

All the changes of the F_P and F_{VS} parameters discussed above are related to: (i) the changes of F_M as well as (ii) the variable contribution of the fast and slow events in the fluorescence spectrum. In order to distinguish the influences of these two effects on the F_P and F_{VS} fluorescence parameters, the F_P and F_{VS} contributions (their normalized values: F_{VS}/F_M and F_P/F_M)) are discussed below (Figure 23 A and B).

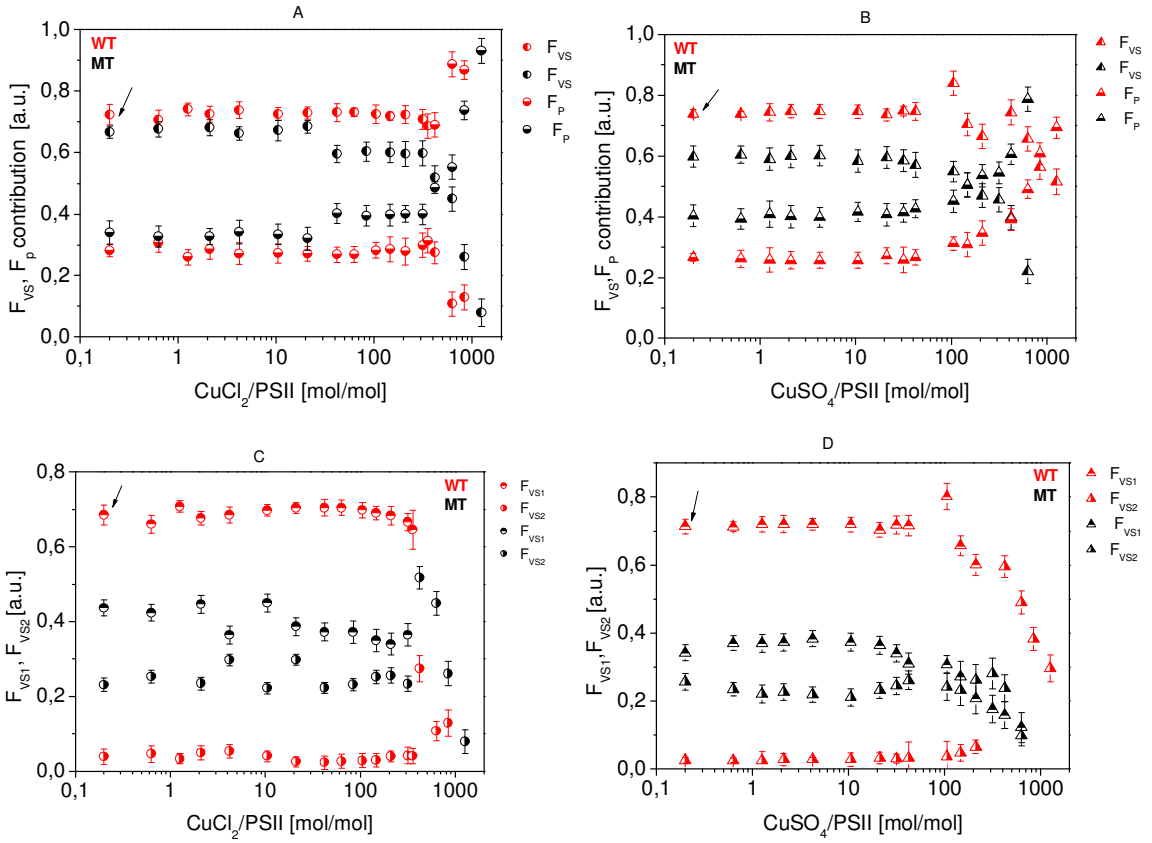

Figure 23. The semilogarithmic plots of the parameters F_P and F_{VS} normalized to F_M corresponding to their contribution in the fluorescence spectra (given in a.u.) as a function of copper concentrations (A-$CuCl_2$ and B-$CuSO_4$). In (C-the dependence on $CuCl_2$ concentrations) and (D-the dependence on $CuSO_4$ concentrations) the contributions of the fast, F_{VS1}, and slow, F_{VS2}, subcomponets in the slow variable fluorescence, F_{VS}, are shown. The arrows indicate the control measurements.

In the case of WT BBY PSII treated with $CuCl_2$ one can see characteristic discontinuities of the F_{VS} and F_P contributions at the following $CuCl_2$/PSII concentrations higher than: 0.6, 1, 200 400 and 600. In MT BBY PSII, besides these observed for WT, additional transitions are present, one at the $CuCl_2$/PSII concentration higher than 2, and a more pronounced one, at $CuCl_2$/PSII higher than 20. There are not detected any changes of the F_{VS} and F_P contributions up to 40 $CuSO_4$/PSII for WT BBY PSII and up to 20 $CuSO_4$/PSII for MT BBY PSII. At the higher copper concentrations one can distinguish some changes of these parameters at 100, 200 and 400 $CuSO_4$/PSII for WT and at 100, 200 and 300 $CuSO_4$/PSII for MT. One should notice that the increase of the F_P contribution accompanies the decrease of the F_{VS} contribution. It is especially pronounced at the higher copper concentrations (300 and 400 $CuCl_2$/PSII for MT BBY PSII and WT BBY PSII, respectively; 40 and 100 $CuSO_4$/PSII for MT BBY PSII and WT BBY PSII, respectively). At these high copper concentrations the fluorescence spectra starts to be dominated by the F_P contribution and especially by the F_0

fluorescence which contribution increases significantly because one does not observe so strong changes of the fast variable fluorescence contribution, F_{VF} (Figure 21).

It was interesting to see which one of the subcomponents of F_{VS} is responsible for its variations with the increasing concentrations of the copper salts. Looking at the Figure 23 C and D one can find that for MT the contribution of the fast component F_{VS1} is about 2 times higher in the fluorescence spectrum in the presence of $CuCl_2$ and about 1,5 in the presence of $CuSO_4$ for the copper concentrations < 40 Cu^{2+}/PSII. In WT the F_{VS} is dominated by the faster component, F_{VS1} which is > 15 times more intensive than the slow component, F_{VS2} (up to 100 Cu^{2+}/PSII) independently on the copper salt.

In the case of WT BBY PSII the F_{VS}/F_M changes for the low $CuCl_2$ concentrations (at 1, 2 and 4 $CuCl_2$/PSII) are caused by both components, F_{VS1}, and $F_{VS2.}$ The normalized F_{VS1} and F_{VS2} values show also a complementary variation at a round 10-20 $CuCl_2$/PSII and therefore this change is not visible in the case of the F_{VS} parameter. At the concentrations higher than 400 $CuCl_2$/PSII and 200 $CuSO_4$/PSII a complete inhibition of F_{VS1} (its contribution is equal 0) is observed. At the 400 $CuCl_2$/PSII and 200 $CuSO_4$/PSII concentrations an increase of the slower component F_{VS2} contribution by a factor of 6 and of 10 is observed, respectively, but with the further increase of $CuCl_2$ and $CuSO_4$ concentrations the F_{VS2} contribution decreases. The changes of the normalized F_{VS1} and F_{VS2} parameters are observed only at higher copper sulfate concentrations and they are present at 40, 100 and 200 $CuSO_4$/PSII and for the lower component additionally at 400 $CuSO_4$/PSII. In WT BBY PSII the enhancement of the F_{VS} contribution at 100 $CuSO_4$/PSII is due to the higher contribution of the faster component, F_{VS1}, whereas at 400 CuSO4/PSII and 400 $CuCl_2$/PSII due to the increase of the slower component contribution, F_{VS2}, (Figure 23).

In MT BBY PSII the discontinuities of the F_{VS1} and F_{VS2} contributions are detected at: 0.6, 2, 4, 10, 20, 40, 100 and 300 $CuCl_2$/PSII and at the following concentrations of $CuSO_4$/PSII: ~1, 10, 40,100, 200 and 300. The F_{VS1} component disappears in the fluorescence spectrum at the concentrations higher than 300 $CuCl_2$/PSII, whereas it is still present at the highest applied concentrations of $CuSO_4$ (630 $CuSO_4$/PSII) at which the variable fluorescence is still detectable. At this concentration the F_{VS1} contribution decreases by a factor of 1.3 and the F_{VS2} one by a factor of 2.5 in comparison to the control sample. Comparing the contributions of the slower and faster component one can see that the decrease of the F_{VS} contribution in the fluorescence spectrum at about 40 $CuCl_2$/PSII is caused by the faster one.

To get more deep insight into the processes responsible for the equilibration the photochemical events within PSII under light conditions one should compare also the kinetic parameters of the components, related to the fast variable fluorescence, F_{VF}, and of the subcomponents of the slow variable fluorescence, F_{VS} (F_{VS1} and F_{VS2}). The saturation time constant of the initial fluorescence, F_0 obtained from the fits of the experimental data is of order of 50 ± 20 μs. It is at the level of the time resolution of the fluorometer and therefore this parameter will not be discussed here but it is worth to mention that it was stable within the whole range of the applied copper salt

concentrations. However, the time constant obtained for the fast variable fluorescence, t_{VF} changes with the increasing concentration of the copper salts (Figure 24).

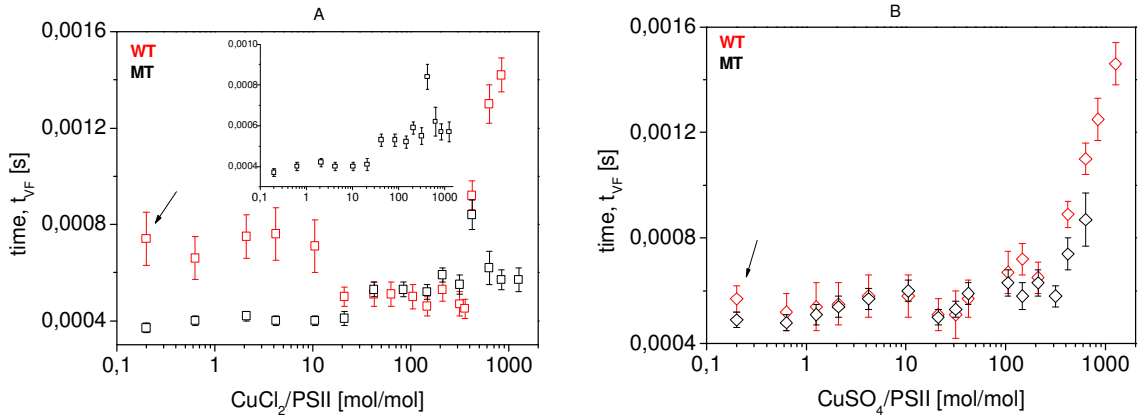

Figure 24. The semilogarithmic plots of the time constants related to the fast variable fluorescence F_{VF}, called t_{VF} (for the samples treated with $CuCl_2$ (A) and $CuSO_4$ (B)). The arrows indicate values of t_{VF} obtained for the control samples.

In the case of samples treated with $CuCl_2$ it is almost 2 times higher for WT than for MT BBY PSII within the copper concentrations up 10 $CuCl_2$/PSII. Then it decreases in the WT preparations treated with 20 $CuCl_2$/PSII whereas it increases in the MT preparations treated with 40 $CuCl_2$/PSII. The parameter t_{VF} is equal within the error bars at $40 \leq CuCl_2/PSII \geq 400$ and the same its behaviour is observed for both types of tobacco within this range of the $CuCl_2$ concentration. There are three t_{VF} discontinuities visible for the higher copper concentrations at about: 200 , 400 and 600 $CuCl_2$/PSII. Starting from the 600 $CuCl_2$/PSII concentration the t_{VF} value decreases down to about 550 µs in MT BBY PSII whereas it increases 1.5 times in WT BBY PSII up to about 1.4 ms. At low copper chloride concentrations for MT one can point an additional discontinuity of the time constant at 2 $CuCl_2$/PSII.

The time constant t_{VF} has the same values (about 500 µs) and shows the same behaviours (one transition at $CuSO_4$/PSII > 10) within the range of the applied $CuSO_4$/PSII concentrations up to 100. The t_{VF} shows a discontinuity at 150 $CuSO_4$/PSII for WT whereas at 100, 200 and 400 $CuSO_4$/PSII for MT. At the higher applied concentrations of $CuSO_4$ the increase of this parameter is not so pronounced in MT as it is observed in WT BBY PSII.

The dependence of the two time constants, t_{VS1} and t_{VS2}, on the copper salts concentrations for both tobacco types are presented in Figure 25 and Figure 26.

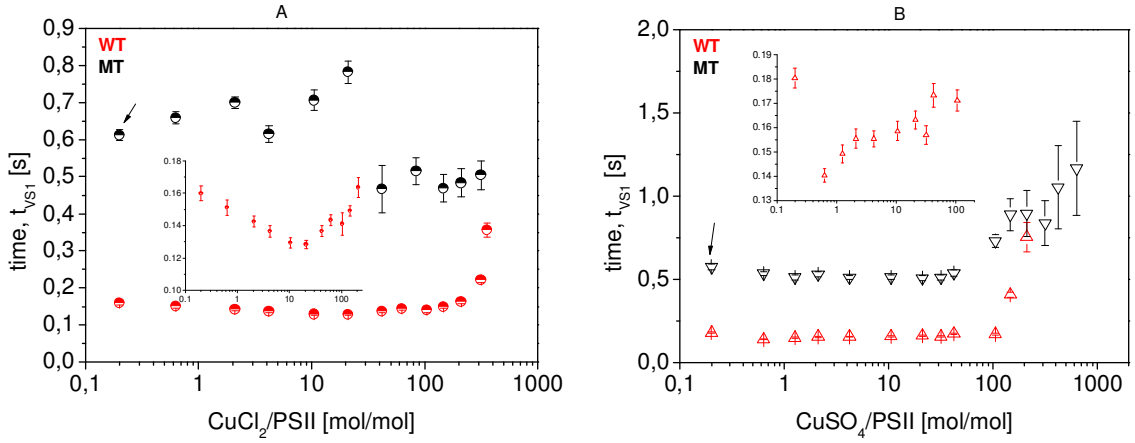

Figure 25. The semilogarithmic plots of the fast time constant t_{VS1} related to the faster component of the slow variable fluorescence F_{VS1} for MT and WT BBY PSII treated with $CuCl_2$ (A) and $CuSO_4$ (B). The arrows represent the values obtained for the control samples.

The time constant t_{VS1} changes at 10, 20, 60, 100 and 200 $CuCl_2$/PSII for WT. In the case of MT this parameter shows discontinuities at 2, 6, 20, 40, 80 and 150 $CuCl_2$/PSII. The component F_{VS1} was not detected for $CuCl_2$/PSII ≥ 400 and $CuCl_2$/PSII > 300 for WT and MT BBY PSII, respectively. In the MT sample treated with $CuSO_4$ the t_{VS1} exhibits discontinuities at around 1, 10, 40, 150 and 300 $CuSO_4$/PSII. The most pronounced changes are detected at the copper concentrations higher than 40 $CuSO_4$/PSII, when t_{VS1} increases 2 times. For WT one can distinguish the following characteristic $CuSO_4$/PSII concentrations at which the t_{VS1} time constant changes significantly: 2, 20, 40, 100 and 200. Within the range of $CuSO_4$/PSII concentrations from 100 - 200, this parameter increases about 4.5 times. This component disappears again in the case of WT at $CuSO_4$/PSII > 200. One should notice that t_{VS1} is about 5 and 2.5 times higher for MT in comparison to WT for sample treated with $CuCl_2$/PSII < 200 and with $CuSO_4$/PSII < 50, respectively.

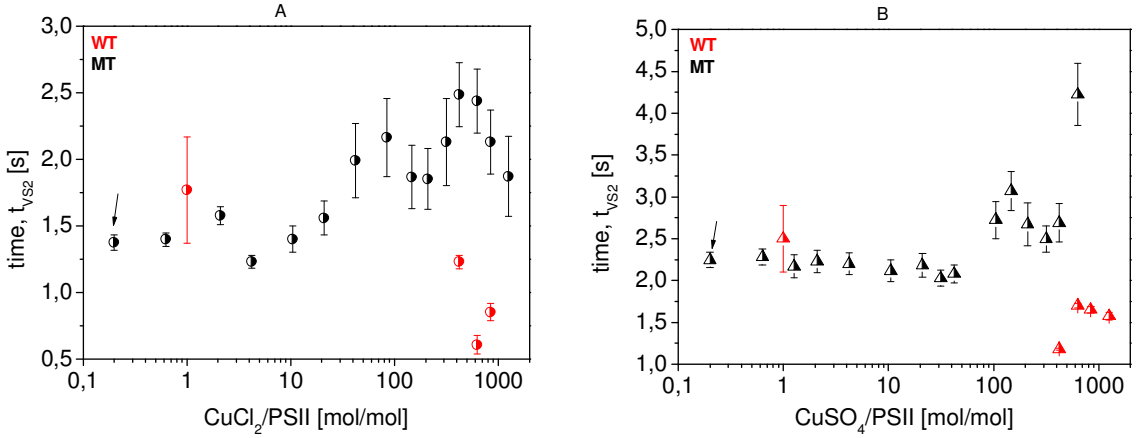

Figure 26. The semilogarithmic plots of the slow time constant t_{VS2} related to the slower component of the slow variable fluorescence, F_{VS2} for MT and WT BBY PSII treated with $CuCl_2$ (A) and $CuSO_4$ (B). The arrows represent the values obtained for the control samples. For WT sample the time constant t_{VS2} is constant in the whole range of $CuCl_2$ and $CuSO_4$ concentrations.

In the case of WT BBY PSII the time constant t_{VS2} is at the level of 1.7 ± 0.4 s and 2.5 ± 0.4 s for the copper concentrations up to about 300 Cu^{2+}/PSII for $CuCl_2$ and $CuSO_4$ respectively. At higher $CuCl_2$ concentrations the t_{VS2} parameter decreases by a factor of about 2 and starting from 600 $CuCl_2$/PSII it increases. In the WT samples treated with $CuSO_4$ this time constant decreases about 2 times at 400 $CuSO_4$/PSII, then it jumps to the value of about 1.75 s and starts to decrease at $CuSO_4$/PSII > 600.

In MT BBY PSII one can observe discontinuities of the time constant t_{VS2} at around 2, 100, 200 and 400 $CuCl_2$/PSII and at 20, 40, 150 and 400 $CuSO_4$/PSII. It increases significantly (by about 1.6 ± 0.2) at the $CuCl_2$/PSII concentrations > 20 showing two maxima at around 100 and 400 $CuCl_2$/PSII and at the $CuSO_4$/PSII concentrations > 40 having one maximum at around 150 $CuSO_4$/PSII. For the highest applied concentration of $CuSO_4$/PSII this parameter increases even 2 times in comparison to its value obtained for the low copper sulfate concentrations and for the control sample.

Summary.

The studies of the Kautsky effect in the wild type tobacco and in the mutant with modified cytochrome b_{559} treated with $CuCl_2$ and $CuSO_4$ have shown that the action of the copper ions is different in these two tobacco types and it depends on the presence of the chloride anions.

The maximal fluorescence is at the level of about 10% of the control value for $CuCl_2$/PSII ≥ 600 in WT BBY PSII. At the same $CuSO_4$ concentration the maximal fluorescence is at the level of 30% of the control sample and it remains to be still of about 20% at two times higher $CuSO_4$ concentrations. Thus, one can conclude that sulfate ions protect WT BBY PSII against the inhibitory action of copper cations. This is pronounced especially within the Cu^{2+}/PSII concentrations between 400 and 600, when a steep decrease of maximal fluorescence is observed for $CuCl_2$. However, at lower copper concentrations the chloride anions protect PSII against the copper inhibitory action but only at the $CuCl_2$/PSII concentration ≥ 1. Some characteristic changes of F_M were observed in the presence of the both copper salts but the most characteristic are shifted toward 5 times lower $CuSO_4$ concentrations than in the $CuCl_2$ case. The inhibition of MT BBY PSII in the presence of Cu^{2+}/PSII ≥ 400 is similar for Cl^- and SO_4^{2-} ions and comparable to WT BBY PSII incubated with $CuSO_4$. But at Cu^{2+}/PSII concentrations lower than 6, the F_M dependence is the same for MT and WT and very similar at higher $CuSO_4$ concentrations. However, F_M behaviour is completely different in MT BBY PSII treated with $CuCl_2$ and especially within the range of $CuCl_2$/PSII concentration between 4 and 400 from those observed in WT samples treated with both copper salts and MT with $CuSO_4$. The most striking difference is for 40 ≤ $CuCl_2$/PSII ≤ 80 and 80 ≤ $CuCl_2$/PSII ≤ 400 when a strong F_M decrease and increase occurs, respectively. These transitions are observed only in MT BBY PSII and only in the presence of chloride anions.

We have performed more detail analysis of the measured Kautsky curves and we have found that:

(i) the steep decrease of the fluorescence amplitude at Cu^{2+}/PSII concentrations ≥ 400 for $CuCl_2$ (MT and WT) and ≥ 300 for $CuSO_4$ (WT) is due to the inhibition of the variable fluorescence related to the processes characterized by kinetics longer than 1.5 ms and especially to its faster component with a time constant of order of hundreds milliseconds, which disappears at these concentrations; the only exception is MT treated with $CuSO_4$, when the faster variable fluorescence is still visible even at the highest applied $CuSO_4$ concentration but it is 3 times lower than in the corresponding control sample;

(ii) at these copper concentrations discussed above the fluorescence spectrum is dominated by the fluorescence related to processes faster than 1.5 ms, F_P component and especially by the initial fluorescence F_0, which contribution increases by a factor of about 4 (of 2.5 in the case of MT treated with $CuSO_4$) in comparison to the control sample.

(iii) the contribution increase of the F_{VF} and F_{VS2} components and the contribution decrease of the F_{VS1} component in the fluorescence spectra accompany the increase of their time constants usually by a factor of 2 at the Cu^{2+}/PSII concentration > 100;

(iv) the characteristic F_M dependence on $CuCl_2$ observed only in MT BBY PSII is caused by the changes of either the fast (F_{VF}) or slow processes (F_{VS}) but the steep F_M decrease at $CuCl_2$/PSII ≥ 40 is due to the faster component of the variable fluorescence F_{VS1}; at the same time the time constant t_{VS1} decreases almost 2 times;

(v) the F_M transition at 400 $CuCl_2$/PSII (its strong decrease) in MT is coupled with the time constant t_{VF} decrease and disappearance of the F_{VS1} component;

(vi) the slow F_M decrease observed in WT and MT treated with $CuSO_4$/PSII > 40 and >30, respectively, is related to the decrease of the F_{VS} contribution (in the case of WT at higher copper concentrations, to the F_{VS2} contribution because the F_{VS1} one disappears) with simultaneous increase of the F_P contribution in the fluorescence spectrum.

(vii) the increase of the F_{VS} contribution in the fluorescence spectrum in WT BBY PSII at around 80 and 400 $CuSO_4$/PSII is due to the rise of the contribution of the faster and slower subcomponent, respectively.

The most characteristic transitions of the parameters describing the subsequent fluorescence components are observed at: 1, 2, 10, 20, 30-40, 80 -100, 200 and 400 Cu^{2+}/PSII.

Finally we would like to note that the number of discontinuities observed within the whole range of applied copper salts and their different character in these two studied

tobacco types give a clear evidence that there are more high affinity binding sites of copper ions located in the vicinity of the cofactors important for the energy and electron transfer within PSII, which are regulated by the cytochrome b_{559} [57], [58]. One of them is the iron-quinone complex and especially the Q_B binding site, what is known from the measurements of the inhibitory effect of DCMU (data not shown here, see [59]). The other results presented in this dissertation indicate also the non-haem iron as the target of the copper action.

4.1.2 Q_A reoxydation measurements

The processes of the photochemical efficiency in WT and MT BBY PSII discussed above were related to the measurements stabilized under light conditions. One can expect that the kinetics of these processes can be different in systems treated only by short light flash and studied in darkness. Therefore the measurements of Q_A reoxydation give complementary information on the processes occuring in the photosynthetic apparatus under the action of copper in the wild type and mutated tobacco.

The fluorescence spectra of Q_A reoxidation are presented in Figure 27.

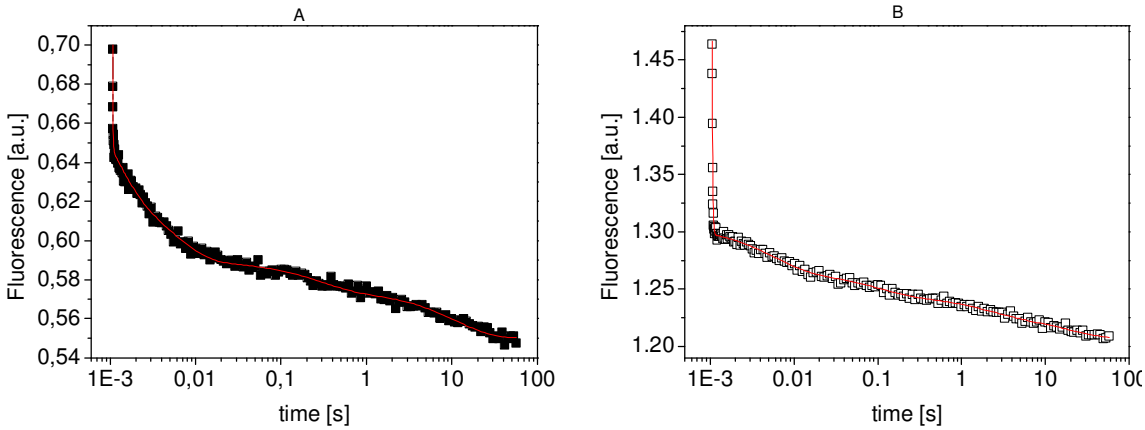

Figure 27. The fluorescence spectra of Q_A reoxidation measured for WT (A) and MT (B) BBY particles.The red lines represent theoretical curves.

The experimental data were evaluated using eq. 3.2.3 (chapter 3.2.3). Usually, five components were necessary to get reasonably good fits. The fastest component with the time constant of order of 50 µs is at the level of the time resolution of the spectrometer. The other five time constants characterize the process of Q_A reoxidation under dark conditions. Some of them have their counterparts among the time constants obtained from the evaluations of the Kautsky curves. In the WT and MT BBY PSII the time constants of order from hundreds microseconds to a few milliseconds and of order from hundreds milliseconds to a few seconds can be compared. The corresponding time constants for the two tobacco types are compared in Figure 28 and Figure 30.

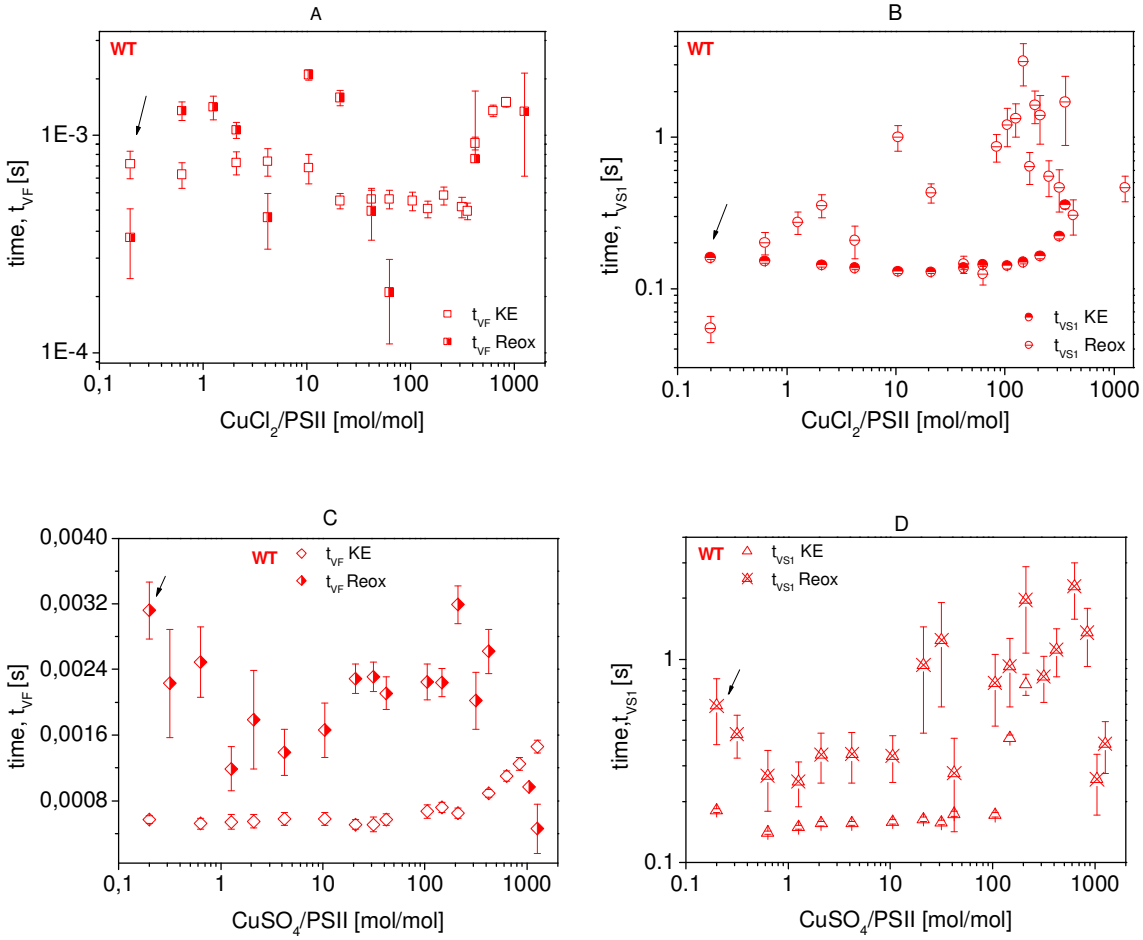

Figure 28. The semilogarithmic plots of the time constants obtained from the fits of the experimental data from the Q_A reoxydation measurements, t_{Reox}, and from the Kautsky effect measurements, t_{KE} for WT BBY PSII treated with $CuCl_2$ (A,B) and $CuSO_4$ (C,D).

For WT BBY PSII the time constant t_{VFReox} changing from 200 µs to 2 ms depends on the $CuCl_2$ concentrations. It can be compared to the t_{VFKE} time constant obtained from the Kautsky measurements but varies much stronger than the corresponding t_{VFKE} within the applied $CuCl_2$ concentrations up to 100 $CuCl_2$/PSII. These time constants have similar values for the higher copper chloride concentrations. The transitions of these two parameters occur at the same copper concentrations: 1, 2, 10, 20, 100, 200 and 400 $CuCl_2$/PSII. The same conclusion can be drawn from the results obtained for WT samples incubated with $CuSO_4$ but there are two differences: (i) within the range of copper concentration up to 200 $CuSO_4$/PSII the time constant obtained from the reoxidation measurements is, in average, about 3.5 times higher than those evaluated from Kautsky effect measurements, t_{VFKE} and (ii) it decreses at the $CuSO_4$/PSII concentrations > 400 when the time constant t_{VFKE} increases.

An opposite effect of the anions is observed for the time constant of order of hundreds milliseconds because a good agreement between the changes of this value and the corresponding t_{VS1} time constant is observed in the case of $CuSO_4$ whereas they differ

significantly when $CuCl_2$ is applied (Figure 28 B and D). In the case of copper sulfate the following characteristic $CuSO_4$/PSII concentrations can be pointed: 0.6, 2, 10, 30, 40, 100 and 200. In the Kaustky experiments the component characterized by t_{VS1} time constant disappears for $CuSO_4$ concentrations > 200 but for the $t_{VS1Reox}$ two additional copper sulfate concentrations one can indicate, 600 and 1000 $CuSO_4$/PSII. For WT samples incubated in $CuCl_2$ the time constant $t_{VS1Reox}$ shows discontinuities at 0.6, 2, 4, 10, 20, 40, 80, 100, 150, 200, 300, 400 and 600 $CuCl_2$/PSII. It reaches the maximum at around 150 $CuCl_2$/PSII (almost 10 times slower than for the low $CuCl_2$ concentrations).

For WT BBY PSII treated with copper salts there are three other time constants which can be derived from the Q_A reoxidation experiments and are not observed in the Kautsky effect measurements (Figure 29).

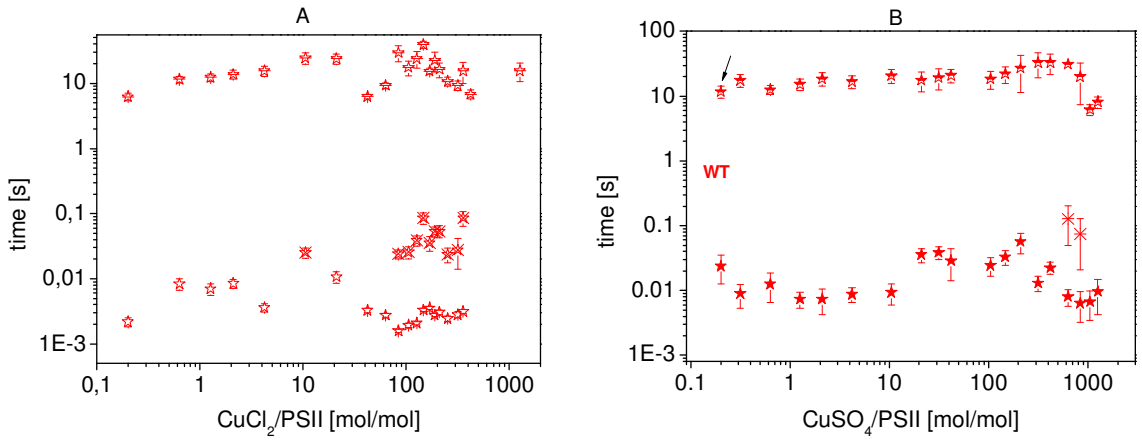

Figure 29. The semilogarithmic plots of the time constants obtained from the fits of the experimental data from Q_A reoxydation mesurements for WT BBY PSII treated with $CuCl_2$ (A) and $CuSO_4$ (B).

In the case of samples treated with $CuCl_2$ one can distinguish 3 time constants: (i) the first one with an average value of 5 ± 0.7 ms, which is not observed for the concentrations of $CuCl_2$> 400, (ii) the second one having an average value of 45 ± 10 ms, which is observed for the concentrations of 10 $CuCl_2$/PSII, 60 <$CuCl_2$/PSII < 400, and (iii) the longest one, which is equal to about 20 ± 6 s (Figure 29 A). From these three time constants the shortest one changes at the following $CuCl_2$/PSII concentrations: 0.6, 2, 4, 10, 40 60, 80, 150, 200 and 300, the middle one at 10, 80, 100, 150, 200 and 300 whereas the longest one at 0.6, 4, 10, 20, 40, 100, 150, 200, 300 and 400. For samples treated with $CuSO_4$, one can distinguish the following time constants having the average value (i) of 20 ± 6 ms, (ii) of 100 ± 60 ms detected only for the concentrations at 630 and 830 $CuSO_4$/PSII, and (iii) of 20 ± 6 s (Figure 29 B). From these three time constants the shortest one changes at the following $CuCl_2$/PSII concentrations: 0.6, ~1, 10, 40, 100, 200, 300 and 400 whereas the longest one at 0.6, 2, 100, 300, 400 and 1000. The time constant of order of 20 s originates probably from the PSII deactivation processes.

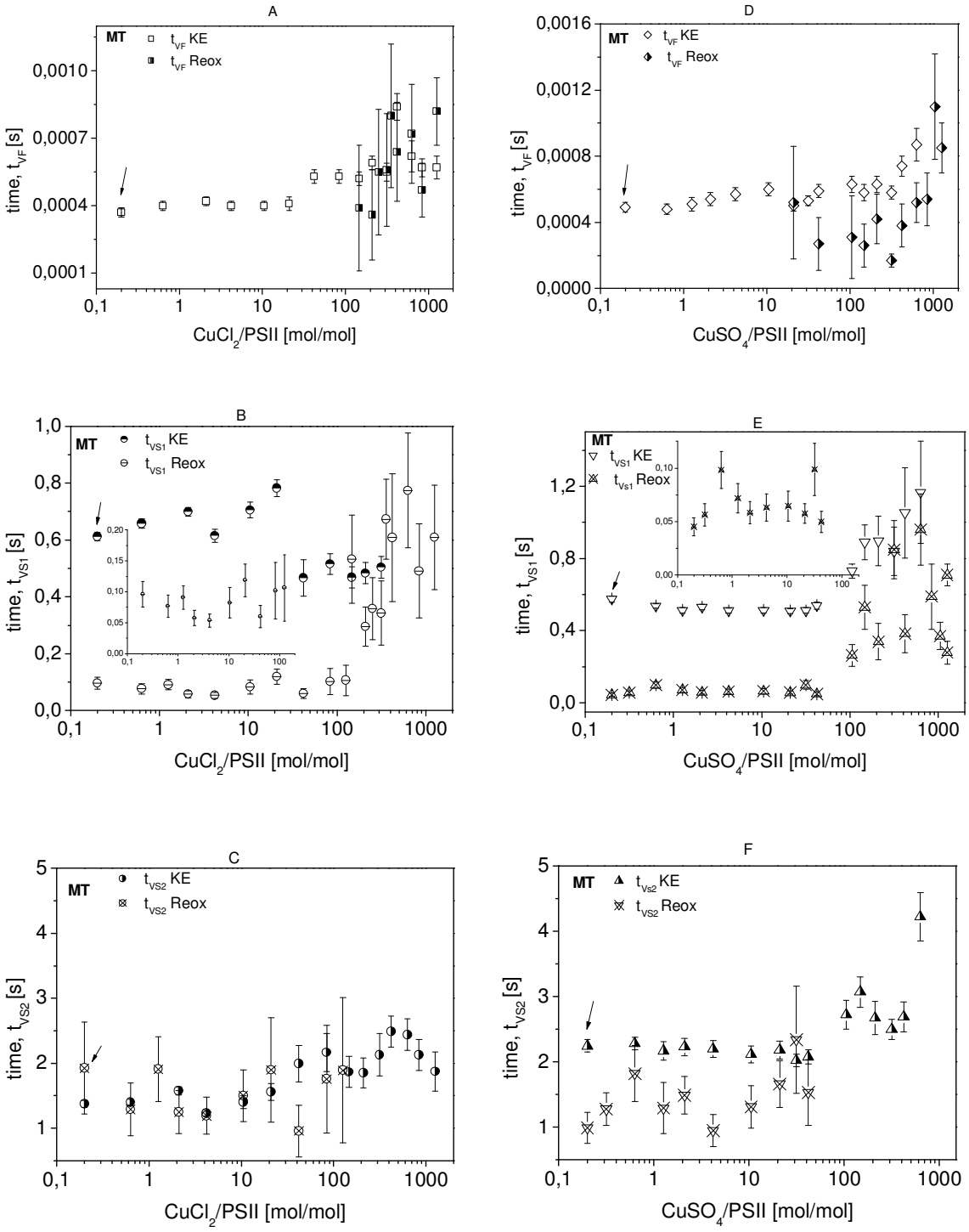

Figure 30. The semilogarithmic plots of the time constants obtained from the fits of the experimental data from the Q_A reoxidation measurements with those obtained from the Kautsky effect measurements for MT BBY PSII treated with $CuCl_2$ (A,B, C) and $CuSO_4$ (D, E, F).

For MT BBY PSII one can combine three time constants evaluated from the Q_A reoxidation experiments with the following time constants obtained from the Kautsky

effect measurements: t_{VF}, t_{VS1} and t_{VS2}, which are of order of hundreds microseconds, of hundreds milliseconds and of seconds, respectively (Figure 30). It is interesting to notice that the best agreement is observed for the time constant assign to t_{VFKE} and t_{VFReox} as well as t_{VS2KE} and $t_{VS2Reox}$. However, the component characterized by the t_{VFReox} time constant occurs only at the $CuCl_2$/PSII concentrations higher than 100 and at the $CuSO_4$/PSII concentrations higher than 10.

The almost parallel changes of the t_{VS1KE} and $t_{VS1Reox}$ constants are observed either for $CuCl_2$ (Figure 30 B) or $CuSO_4$ (Figure 30 E). The $t_{VS1Reox}$ value is in an average about 6 times lower than that one of t_{VS1KE} within the copper concentrations up to 100 $CuCl_2$/PSII and in the systems incubated with $CuSO_4$ it is almost 8-10 times lower up to 40 $CuSO_4$/PSII concentration and about 3 times lower at the copper sulfate concentrations > 40. These time constants have the same characteristic transitions at 2, 10, 40, 200 and 400 $CuCl_2$/PSII and at 0.6, 2, 10, 20, 40, 200, 400, 600 and 1200 $CuSO_4$/PSII.

A very good agreement is observed for the $t_{VS2\ KE}$ and the $t_{VS2Reox}$ parameters when MT BBY PSII was treated with $CuCl_2$ (Figure 30 C). In the case of $CuSO_4$ the variations of the $t_{VS2Reox}$ parameter are much stronger than those of t_{VS2KE} parameter (Figure 30 F). The $t_{VS2Reox}$ values oscillate at around an average value which is about 1.5 times lower than that one of t_{VS2KE} for the $CuSO_4$/PSII concentrations < 10. Another interesting experimental fact is the disappearance of the component characterized by the time constant $t_{VS2Reox}$ at $CuCl_2$/PSII > 150 and $CuSO_4$/PSII > 40. At the following $CuCl_2$/PSII and $CuSO_4$/PSII concentrations: 0.6, 1, 2, 4, 20, 40 and 150, characteristic $t_{VS2Reox}$ discontinuities are observed.

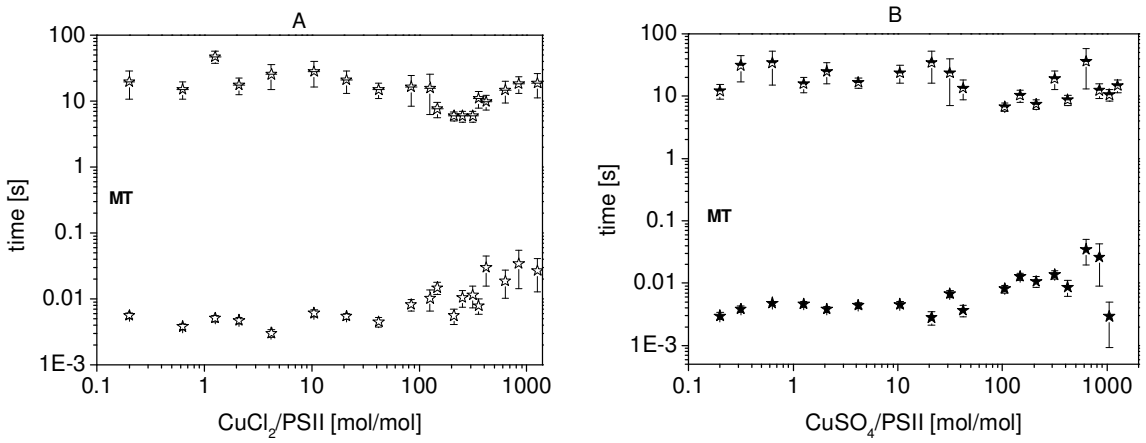

Figure 31. The semilogarithmic plots of the time constants obtained from the fits of the experimental data from Q_A reoxidation measurements for MT BBY PSII treated with $CuCl_2$ (A) and $CuSO_4$ (B).

In MT BBY PSII incubated with $CuCl_2$ and $CuSO_4$ there are two additional time constants observed in the Q_A reoxidation experiments. One can distinguish a component with an average value of 10 ± 0.4 ms, and the longest one of 18 ± 7 s. (Figure 31). All of

them change at the following Cu^{2+}/PSII concentrations 0.6, ~1, 2, 4, 10 150, 200, 300 and 400 and for $CuSO_4$ additionally at 20.

Summary.

The Q_A reoxidation measurements provide information on the efficiency of electron transfer from the reduced primary platoquinone acceptor Q_A^- to other redox active PSII components via forward or backward reactions (for example to Q_B plastoquinone or Pheo). These reactions activated by a short saturating flash result in the changes of the fluorescence decay. These reoxidation measurements give complementary information to those obtained from the Kautsky effect experiments.

The fluorescence decay curves could be reasonably well fitted using 5 components. The fastest processes described by the time constants called t_{VFReox} we assigned to the process of forward electron transfer from the plastoquinone Q_A to the bound plastoquinone acceptor at the Q_B site, being in the oxidized state, and to the back reactions (Figure 7, chapter 3.2.3). The slower time constant of order of hundreds milliseconds, called t_{VS1}, results from processes related to the exchange of the oxidized external plastoquinone with the doubly reduced and protonated plastoquinone at the Q_B site. These two time constants can be combined with the time constants detected in the Kautsky effect experiments. In the case of the wild type tobacco we find the correspondence only between these two time constants but in mutant additionally between the time constants of order of a few seconds, called t_{VS2}. It is interesting to note that a component with such a time constant in the reoxidation spectra is unique for MT BBY PSII (it is not observed in WT BBY PSII). This process most probably is related to the exchange mechanism of the oxidized and reduced plastoquinone at the Q_B site which is slowed down in the mutant due to the modified Q_B site. Such modified Q_B sites can occur also in WT BBY PSII and indeed in the Kautsky effect experiments we observe a component characterized by the time constant of seconds, t_{VS2}, but its contribution in the fluorescence spectra is on the level of 4-5% and that is why we cannot resolve it in the Q_A reoxidation spectra. The slowest time constant of order of tens seconds originates probably from the PSII deactivation processes and is present in the fluorescence spectra measured for these two tobacco types. There is another time constant of order of tens milliseconds which is not detected in the Kautsky effect measurements observed in the MT samples treated with the $CuCl_2$ and $CuSO_4$ and in the WT samples treated with $CuSO_4$ within the whole range of the applied concentrations of the salts and only at 10 $CuCl_2$/PSII and then $CuCl_2$/PSII ≥ 80 for WT. The mechanism characterized by this kinetic can be resolved only in darkness and can be assigned to electron transfer from Q_A to the single reduced Q_B^-. The appearance of this component in the reoxidation experiments and some discrepancies in the t_{VF} values obtained from the Q_A reoxidation and Kautsky effect measurements clearly show that the processes originated from the electron transfer between Q_A and Q_B plastoquinones stabilized under light conditions differ from those taken place in darkness. Another example is an extra

component of order of a few milliseconds observed in the WT preparations incubated in the presence of $CuCl_2$.

Generally, it is worth to notice that:

(i) the parameters obtained from the Q_A reoxidation measurements exhibit more oscillate character in comparison to those obtained from the Kautsky effect experiments;

(ii) in WT BBY PSII, the most pronounced changes of t_{Reox} parameters are observed for the following concentrations of $CuCl_2$/PSII: 1, 2, 4, 10, 20, 40, 80, 100, 200, 400 and of $CuSO_4$/PSII: 0.6, 2, 10, 30, 40, 100, 200, 600 and 1000;

(iii) in MT BBY PSII, the most pronounced changes of t_{Reox} parameters are observed for the following concentrations of $CuCl_2$/PSII: 1, 2, 10, 40, 200, 400 and of $CuSO_4$/PSII: 0.6, 2, 10, 20, 40, 200, 400, 600 and 1200.

The variation of the time constant values, t_{Reox} indicates the PSII acceptor side and especially the iron - quinone complex as the most sensitive target of copper ions. Detected discontinuities indicate the existence of various specific binding sites for the Cu^{2+} ions within PSII. The most interesting are the sites having the highest affinity for the copper cations. There are several binding sites of Cu^{2+}, which show different sensitivity dependent on the presence of Cl^- anions. The point mutation on the β-chain of cytochrome b_{559} also effects the kinetics of Q_A reoxidation.

4.1.3 Fast polarography measurements

The copper ions can influence both the donor and the acceptor sides of PSII. On the donor side the most sensitive site of Cu^{2+} action is oxygen evolving complex (OEC). We applied the fast polarography method to compare the functioning of the donor side in WT and MT BBY PSII to check how the point mutation in cyt b_{559} (in which highly conserved phenylalanine 26 residue that is present in the β subunit of this cytochrome b_{559} was replaced for serine [28]) can change the stabilization of the manganese complex redox potentials. We also applied the fast polarography to study the inhibitory action of the copper cations, Cu^{2+} on the oxygen evolution in WT and MT BBY PSII.

The details about the procedure of sample preparations are given in the chapter 2.1. Before the measurements samples were kept in darkness and after their transfer on the electrode they were additionally dark incubated for 10 minutes. Measurements were performed in the dim light conditions.

The polarography measurements of WT BBY PSII and MT BBY PSII in which we wanted to compare the activity of these two photosystems in oxygen evolution were peformed using fresh prepared samples (Figure 32). In the experiments in which we studied the dependence of oxygen evolution on the copper ions concentrations we used samples for one year stored at -80 ^{o}C in the freezer. They were not so active as the fresh BBY PSII (they lost about 30% of their activity) and from the damped oscillations in Figure 33 it is clear that the manganese complex was stabilized differently in the old preparations (most probably due to the lost of Ca^{2+} and some external proteins: PsbP and PsbQ) [60]. However, we still did not use any external acceptors and we did not increase calcium chloride concentration in the buffer.

In the case of fresh samples we could derive the information on the S- state transitions of the manganese complex in the OEC using the Kok model (Figure 32).

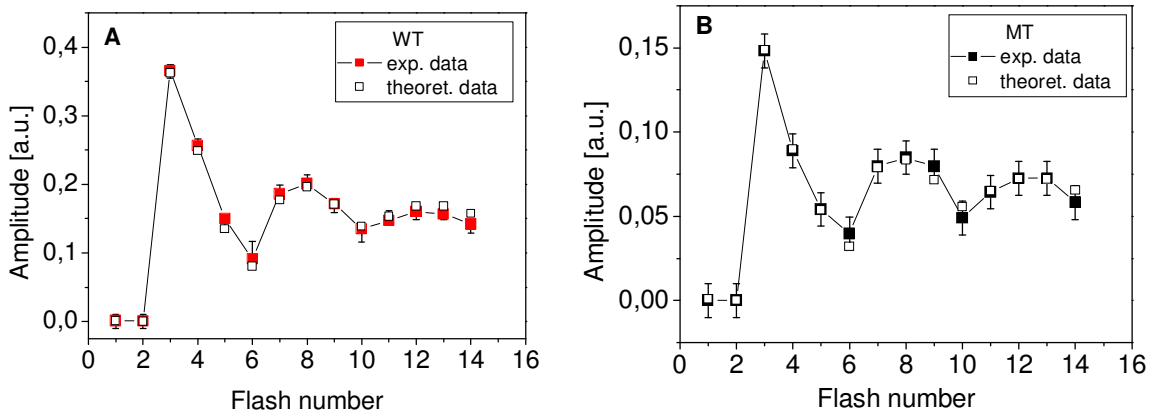

Figure 32. The flash induced oxygen yield pattern in tobacco PSII BBY isolated from WT (A) and MT (B). The empty squares are the theoretical values estimated using the extended 5S- state Kok model [41].

In Tab.3 we collected the S_i-state dark distributions and the probabilities of the unsuccessful transtions between the subsequent S_i states, α_i, (so called miss parameters) obtained from the fits of the experimental data (Figure 32) using the extended 5S –state Kok model (for more information see chapter 3.4).

Table 3. The parameters fitted to the O_2 pattern shown in Fig. 32 observed for WT and MT using the extended 5S-state Kok model

MT BBY PSII							
Flash separation [ms]	S_0	S_1	α_0	α_1	α_2	α_3	d
300	0.01	0.99	0.01	0.00	0.59	0.00	1.0
WT BBY PSII							
300	0.30	0.70	0.81	0.00	0.38	0.00	0.54

Using the 5S- state Kok model in which the metastable, S_4, state is taken into account [41], it is observed that for mutant, the S_1 state is occupied up to 99% in darkness and the only significant increase of a miss parameter occurs for the $S_2 \rightarrow S_3$ transition (to almost 0.6). All other miss parameters are close to 0. Thus, in the MT, the average miss parameter is about 0.15. For the WT, the S_1 state is occupied to 70% and the S_0 state to 30%. In the WT, the average miss parameter is almost 0.3, because of significant increase of the miss parameter for the $S_0 \rightarrow S_1$ transition occuring in addition to that one for $S_2 \rightarrow S_3$ transition. This analysis shows that the value of the total miss parameter decreases with the increase of the fraction of fast oxygen evolution. This fraction is equal 1 for the mutant but only 0.54 for the wild type. The mutant is able to evolve oxygen, although at a lower rate than WT. Measurements of the O_2 evolution under short saturating flashes show that MT yields about 2.4 ± 0.1 times less O_2 than WT. This is related to the concentration of PSII reaction center per chlorophyll, which is lower in the MT. The transitions between the S_i- states of the OEC have a higher efficiency in the MT than in the WT and the oxygen evolution proceeds exclusively (with probability 1) via the fast transition channel $S_3 \rightarrow (S_4) \rightarrow S_0 + O_2$ in MT, in contrast to WT, where the probability of this transition is about 0.54.

In the case of the oxygen yield patterns detected for the WT and MT BBY PSII treated with different $CuCl_2$ concentrations such analysis as above, using the Kok-model, was not so useful anymore because of the damped oscillations. However, these results are still valuable for evaluation of the OEC activity. The flash induced signal of the oxygen yield pattern for the native and treated with $CuCl_2$ WT BBY PSII are shown in Figure 33.

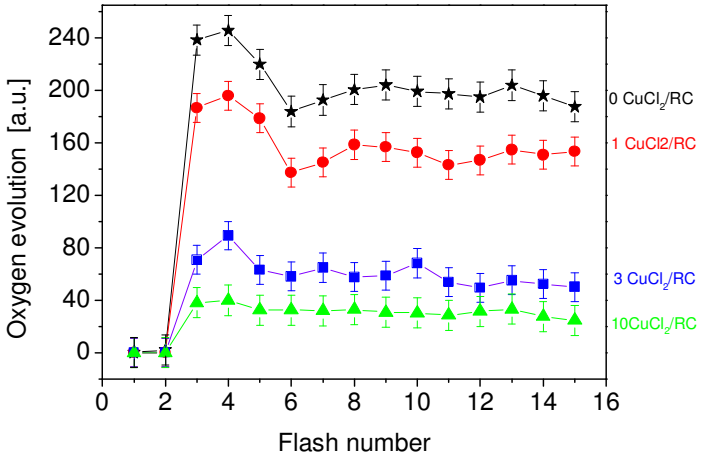

Figure 33. The effect of $CuCl_2$ on the flash-induced oxygen yield pattern in WT BBY PSII isolated from tobacco. Measurements of oxygen evolution under short saturating flashes show that with increasing concentration of copper salt the oscillations changed and the oxygen evolution is inhibited.

The sums of the amplitudes of oxygen yield obtained for different $CuCl_2$ concentrations were normalized to the sum obtained for the control sample and the results are presented in Figure 34 A as a function of Cu^{2+} concentration. The concentrations of the copper salt was chosen in a way to cover the ranges of $CuCl_2$ concentrations at which the characteristic changes of the variable fluorescence were observed (see chapter 4.1.1). There are less experimental data for MT BBY PSII because of the limited amount of the sample.

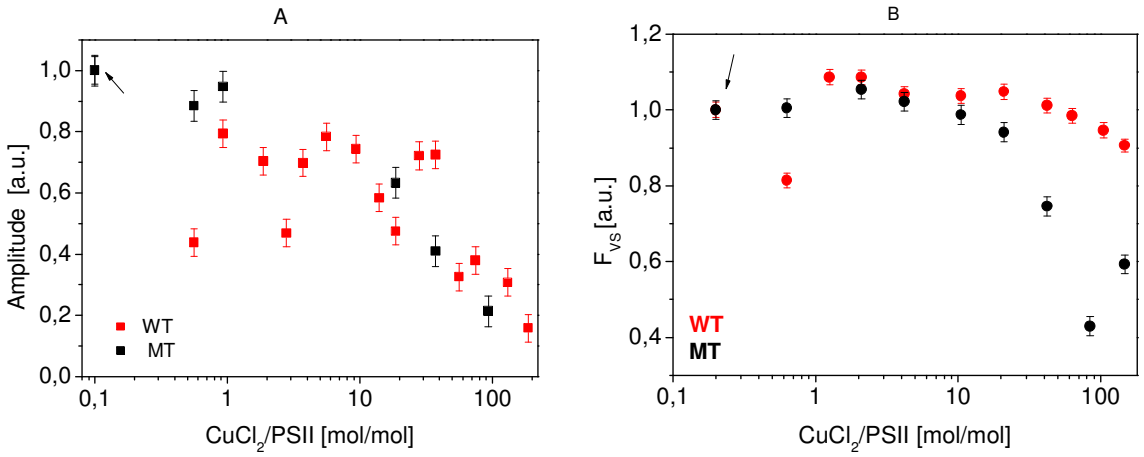

Figure 34. The sums of the amplitudes normalized to the control sample obtained from the fast polarography measurements WT BBY PSII –red symbols and MT BBY PSII – black symbols isolated from *N. tobacco* (A). In (B), for the comparison, we present the changes of the normalized F_{VS} which is related to the photochemical efficiency of the photosystem II. An arrow indicates measurement for control sample.

One can see that although the fast polarographic experiments were perfomed on weaker BBY PSII preparations whereas the fluorescence experiment (Figure 34 B) were done on fresh samples.There is a good correspondence between the inhibition of the oxygen yield and of the slow variable fluorescence caused by the copper ions. One can distinguish characteristic changes of the OEC efficiency in oxygen yield with different $CuCl_2$ concentrations which are also pronounced in the F_{VS} changes.
For example, in the case of WT BBY PSII one sees the oscillations of the sum of O_2 yield amplitudes in the range of $CuCl_2$/PSII concentrations from 0.6 to 20 and their increased inhibition of the oxygen evolution. This correlates well with the observed behaviour of the F_{VS} fluorescence.
In the case of MT BBY PSII the analysis is more difficult because of the limited amount of experimental points. However, an increase of the oxygen evolution at the lowest applied concentrations of $CuCl_2$ and the enhanced decrease of O_2 yield at the $CuCl_2$/PSII concentrations > 20 are visible. A similar dependence of the slow variable fluorescence for MT is observed.

Summary.

The fluorescence measurements have shown that the efficiency of the photochemical processes in wild type and mutated tobacco are different. The fast polarographic experiments allow to follow the activity of the PSII donor side, especially of the oxygen evolving complex. The MT BBY PSII preparations have lower activity in the amount of O_2 yield than WT BBY PSII because of the lower amount of active PSII but the electron transfer within the photosystem is more efficient. Applying the 5-S state model we could estimate that in MT PSII the oxygen is evolved only via the fast channel whereas in WT PSII this process proceed in about 50% via the channel with a metastable S_4-state. The lower average miss parameter, estimated for MT, by a factor of 2 in comparison to that one obtained for WT gives another independent evidence that the transition between the S-states of the manganese complex is more efficient in the case of MT what can also suggest a more efficient electron transfer within this PSII complex. It is also interesting to note that the Mn-cluster is stabilized mainly in the S_1-state in the darkness in MT whereas about 30% occupation of the S_0-state is observed in WT.

The effect of the point mutation in the β-chain of cytochrome b_{559} on the energy and electron transfer within PSII is especially pronounced in the results obtained from the fluorescence experiments on samples treated with different copper concentrations. Therefore such experiments were also carried out using the fast polarographic method in order to check the activity of the oxygen evolving complex in the presence of the copper ions. From the earlier studies it was known that Cu^{2+} can stimulate O_2 yield at low concentrations [54], whereas at higher concentrations they inhibit this process [12], [61]. This is due to the copper action either on the acceptor PSII side or its donor side. We compared the inhibitory effects of $CuCl_2$ on the oxygen evolution with the variable fluorescence related to the photochemical PSII efficiency at the chosen characteristic

copper concentrations. We found a very good correlation between the polarographic and fluorescence results. Some discrepancies can come from the fact that the samples used in these polarographic experiments were not any more as active as those used in the fluorescence measurements.

4.2 Photosynthetic reaction centers of purple bacteria

In order to check how the copper may interact with the quinone- iron complex and modify the electron transfer in the reaction centers of type Q we have extended our investigations on the bacterial reaction centers of *Rhodobacter sphaeroides.*

4.2.1 Absorption measurements

The absorption spectrum of the reaction centers isolated from *Rhodobacter sphaeroides* used in the photobleaching and fluorescence measurements is presented in Figure 35.

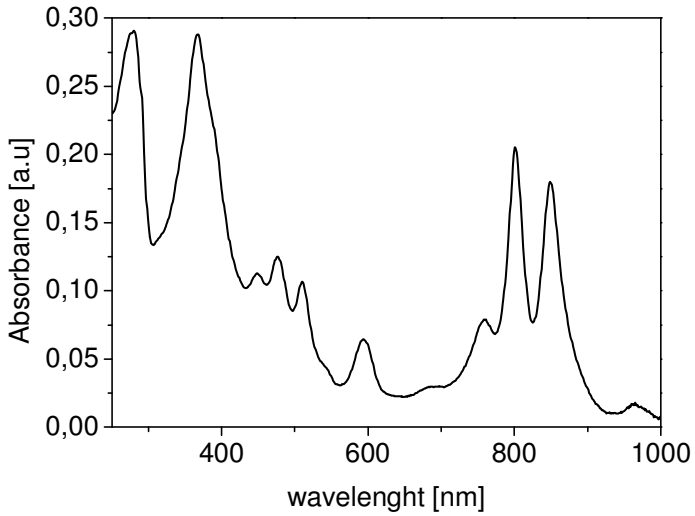

Figure 35. Absorption spectrum of the reaction centers isolated from *Rb. sphaeroides.*

The maximum at 860 nm in the plot corresponds to the bacteriochlorophyll special pair of the bacterial RCs, P860. In the light the peak at 860 nm disappears, when $P860^{\bullet+}$ is formed and it is recovered in the darkness while the special pair is rereduced [62], [63]. The photobleaching experiments give information on the rate of the charge recombination between $P860^{\bullet+}$ $BPheo^{-}\rightarrow$ P860BPheo, $P860^{\bullet+}Q_A^{\bullet-}\rightarrow P860Q_A$ and $P860^{\bullet+}Q_B^{\bullet-}\rightarrow P860Q_B$. The kinetics of the recovering of the signal at 860 nm for the control sample of the *Rb. sphaeroides* RCs is shown in Figure 36.

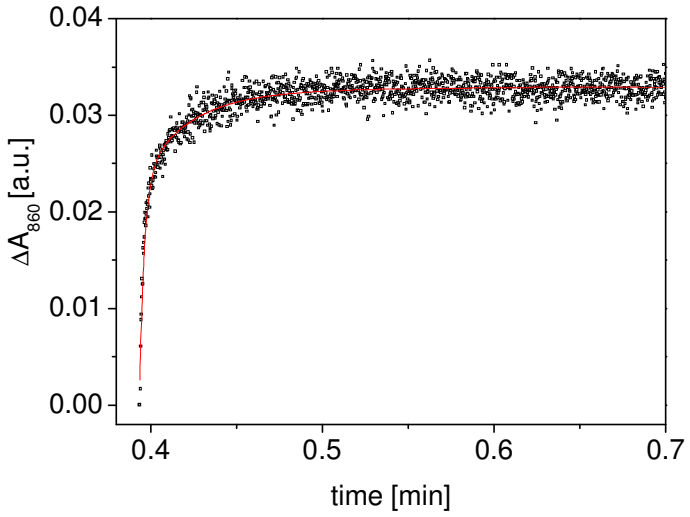

Figure 36. The time dependent changes of the absorption signal detected at 860 nm for *Rb. sphaeroides* RCs. The signal was stimulated by a short saturating flash. The red line represents the theoretical curve.

The experimental data for the control sample of *Rb. sphaeroides* was fitted using three exponents. The obtained time constant of 2.94 ± 0.1 ms corresponds to the rate of the charge recombination between $BPheo^-$ →$P860^{\bullet+}$ [62], [63]. The two slower components having the time constants of 26.8 ± 3.7 ms and 110 ± 39 ms are related to the $Q_A^{\bullet-}$ →$P860^{\bullet+}$ charge recombination. The two different kinetics of the $P860^{\bullet+}$ rereduction come most probably from two different states of the charge stabilization between the special pair and the primary quinone acceptor Q_A. We do not observe the component which could be ascribed to the charge recombination between $Q_B^{\bullet-}$→$P860^{\bullet+}$, because it is known that this process is of order of 1 s [63], [64].

In Figure 37 the experimental data of the photobleaching measurements for the bacterial reaction centers treated with $CuCl_2$ and $CuSO_4$ in the range from 1000 Cu^{2+}/RC to 8000 Cu^{2+}/RC are presented. We applied so high copper concentrations in order to check the resistance of the bacterial photosystems in the charge stabilization between the acceptor side and the special pair to the Cu^{2+} ions. In the case of photosystem II isolated from tobacco (see chapter 4.1) we observed almost complete inhibition of its function for as high copper concentrations as 1000 Cu^{2+}/RC.

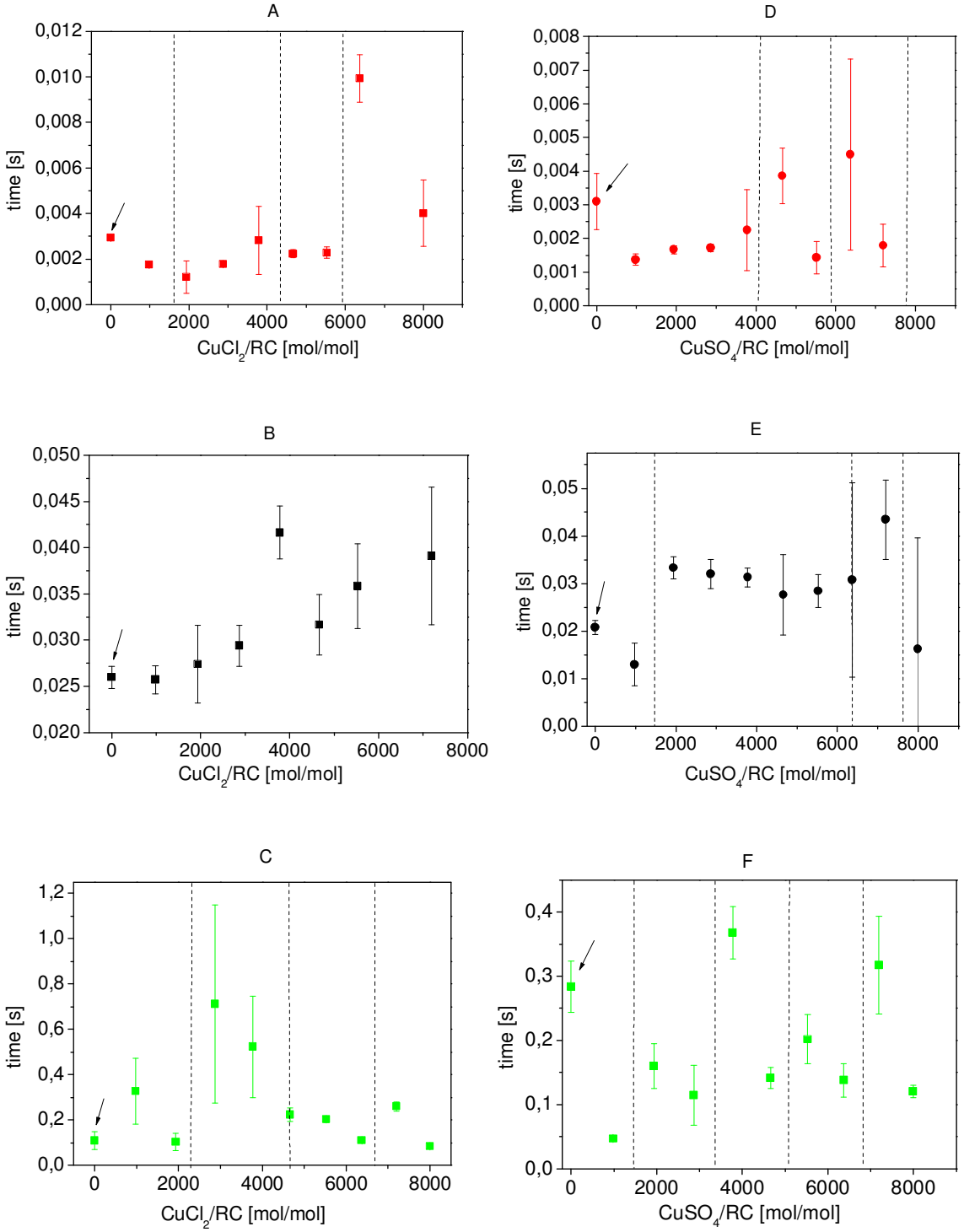

Figure 37. The semilogarithmic plots of the time constants obtained from the theoretical evaluation of the photobleaching curves detected for the bacterial reaction centers treated with the indicated concentrations of $CuCl_2$ (left panel; A, B, C) and $CuSO_4$ (right panel, D, E, F). In A and D the shortest time constants of order of a few ms are shown, related with charge recombination between $BPheo^-$ and $P860^{\bullet+}$. The time constants presented in B and C and E and F correspond to the kinetics of the charge recombination between $Q_A^{\bullet-}$ and $P860^{\bullet+}$ most probably characterized by different stabilization energy.

The fastest time constant of order of a few ms ($BPheo^- \rightarrow P860^{\bullet+}$) exhibits three characteristic ranges of the $CuCl_2$ concentration when it behaves in different ways. It decreases to the value of about 2 ms up to 2000 $CuCl_2$/RC, then it increases up to 3800 $CuCl_2$/RC. Further, it is constant and at the concentrations > 6000 $CuCl_2$/RC it shows a sharp transition, when it increases about 5 times and then steeply decreases. In the case of $CuSO_4$ the fastet time constatnt decreases about two times in comparison to the control value for 1000 $CuSO_4$/RC but then it only slowly increases. However, at the sulfate copper concentrations > 4000 $CuSO_4$/RC it increases 2 times and then steeply decreases showing again a discontinuity at the copper concentrations > 6000 $CuSO_4$/RC, when it increases almost 3.5 times. Finally, it again decreases. The time constant of order of tens ms ($Q_A^{\bullet-} \rightarrow P860^{\bullet+}$) increases slowly up to 3000 $CuCl_2$/RC and it shows discontinuity for 3800 $CuCl_2$/RC. Then it decreases back to the previous value at the concentration of about 4700 $CuCl_2$/RC and again increases for the higher copper concentrations. For $CuSO_4$ the behaviour of the intermediate time constant is completely different than in the case of $CuCl_2$. It is almost constant within the range of 2000 – 6000 $CuSO_4$/RC being about 1.5 times slower than for the control sample. It increases again about 1.5 times at concentrations of 7200 $CuSO_4$/RC and it is about 3 times slower than for the concentration of 1000 $CuSO_4$/RC. The slowest time constant of order of hundreds ms ($Q_B^{\bullet-} \rightarrow P860^{\bullet+}$) exhibits the dicontinuities within similar ranges of higher concentrations of both copper salts: ~4000-5000 Cu^{2+}/RC, 5000-7000 Cu^{2+}/RC and > 7000 Cu^{2+}/RC. At lower concentrations the transitions are down shifted by 1000 Cu^{2+} ions /RC in the case of $CuCl_2$. The sulfate ions shift the transitions toward higher concentrations and additionally decrease the jump of the time constant by a factor of 2 for ~4000 $CuSO_4$/RC in comparison to the transition observed at ~3000 $CuCl_2$/RC. The relative shift of the concentrations of these copper salts may explain why in the case of $CuSO_4$ one detects an additional discontinuity at 1000 $CuSO_4$/RC.

Summary.

The photobleaching measurements show that in the bacterial reaction centers isolated from *Rb. sphaeroides* the charge recombination between $Q_A^{\bullet-} \rightarrow P860^{\bullet+}$ dominates the rereduction process of $P860^{\bullet+}$. The studies of the kinetics of charge recombination between the acceptor side and the special pair in the RCs as a function of the concentrations of $CuSO_4$ and $CuCl_2$ show that:

(i) the bacterial reaction centers are much more resistant to the action of copper ions than photosystem II from higher plants (in our case isolated from tobacco) and even the highest applied concentrations of the copper salts (8000 Cu^{2+}/RC) could not inhibit the primary charge separation process;

(ii) the time constants characterizing the three processes of the charge recombination between the acceptor side of the reaction centers and the bacteriochlorophyll special pair show different sharp transitions within the studied ranges of copper

salts, what indicates a various binding sites of copper ions modifying in a different way the total free energy of the process of the charge stabilization;

(iii) the shifts of some discontinuities of the time constants toward higher Cu^{2+} concentrations for the applied concentrations of the copper salts caused by sulfate ions suggest a special sensitivity of the Cu^{2+} binding sites for the chloride anions.

These results show that the acceptor side of the bacterial reaction center of type Q , especially the iron-quionone complex, and the special pair of bacteriochlorophyll are very sensitive to the action of copper ions, which can modify the kinetics of the charge recombination. Therefore it was very interesting to study also the action of the copper cations on the forward electron transfer. Basing on the results obtained from the Kautsky effect and Q_A reoxidation measurements of the BBY PSII isolated from tobacco one may also expect a highly specific interaction of the copper ions with the iron-quinone complex in the bacterial reaction centers for low copper concentrations. Therefore, we have also perfomed the measurements of the variable fluorescence using the PEA mode of the fluorometer with a double modulation for the isolated bacterial reaction centers treated with various $CuCl_2$ concentrations. This method has enough high time resolution which allow us to follow the electron transfer within the iron- quinone complex.

4.2.2 Fast fluorescence transient

In order to show how the low copper concentrations influence the fast processes of the energy and electron transport within bacterial reaction centers, fast fluorescence method was used. Studies of fast fluorescence transient were performed on the reaction centers isolated from *Rb. sphaeroides* as it was described in *Materials*, chapter 2.2. Each sample was incubated for 10 minutes in darkness before the measurement. All experimental procedures were carried on under the dim light conditions.

An example of the normalized experimental spectrum of the induced fast fluorescence of the native *Rb. sphaeroides* RCs is shown in Figure 38.

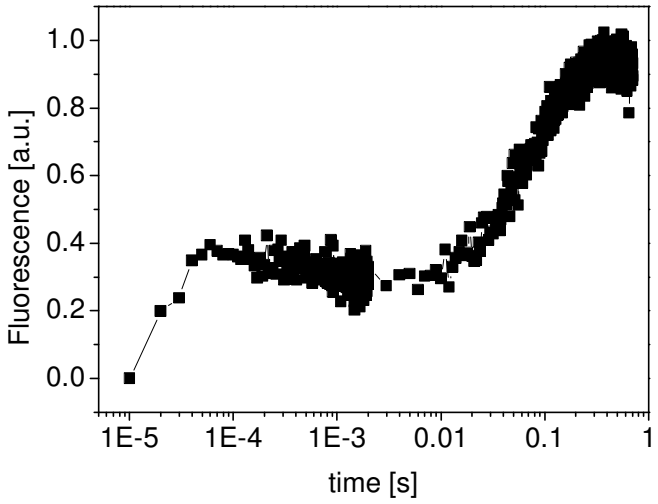

Figure 38. The semilogarithmic plot of the fast fluorescence transient spectrum of the native RCs isolated from *Rb. sphaeroides*.

In these measurements the first point corresponds to the F_0 initial fluorescence (the spectrum shown above is shifted to 0 for the easier evaluation of the contribution of the other components). The fluorescence spectra were fitted using function described by the eq. (3.2.2, chapter 3.2.2.). Three components were necessary to get a reasonable fit of the experimental spectra. The discussion of the dependence of the obtained parameters on the copper concentration is done basing on the linear plots but for clarity the experimental data is shown in the semilogarithmic plots.

In Figure 39 the dependence of the F_0 values, read from the fluorescence curves, on the applied $CuCl_2$ concentrations is shown.

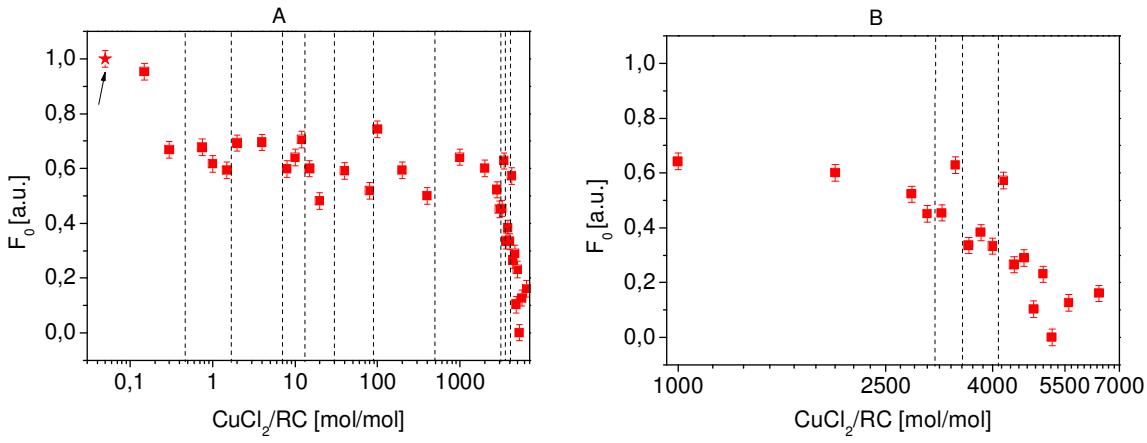

Figure 39. The semilogarithmic plots of the initial value of the fluorescence, F_0 normalized to the control value , as a function of $CuCl_2$ concentration (A). In (B) the experimental data are presented in a spread scale from 1000- 7000 $CuCl_2$/RC. The value obtained for the control sample is indicated by the arrow in the figure.

One can distinguish at least 8 characteristic ranges of the $CuCl_2$ concentrations up to 1000 $CuCl_2$/RC within which the monotonity of the F_0 behaviour is different or its discontinuities are observed. The transitions are visible for the following concentrations of $CuCl_2$/RC: 0.3, 0.7, 2.0, 8.0, 12, 20, 40, 100, 400, 1000. Within the range of 0.3-2000 $CuCl_2$/RC the value of F_0 varies at around 0.6 ± 0.1 of the control values, normalized to 1. Only as low concentration as 0.15 did not change significantly the F_0 value. At the concentrations higher than 3600 $CuCl_2$/RC the subsequent decrease of the F_0 amplitude is observed and it is only of about of 10% of the F_0 control value at the highest concentrations. For the copper concentrations > 1000 $CuCl_2$/RC (up to 6800 $CuCl_2$/RC) one sees at least next 8 transitions of F_0 values . The most striking discontinuities which we could detect appear at around 3400, 4200, 4600, 5000 and 5200 $CuCl_2$/RC.

The fluorescence amplitudes fitted to the normalized experimental curves as an example shown in Figure 38 are collected in Figure 40.

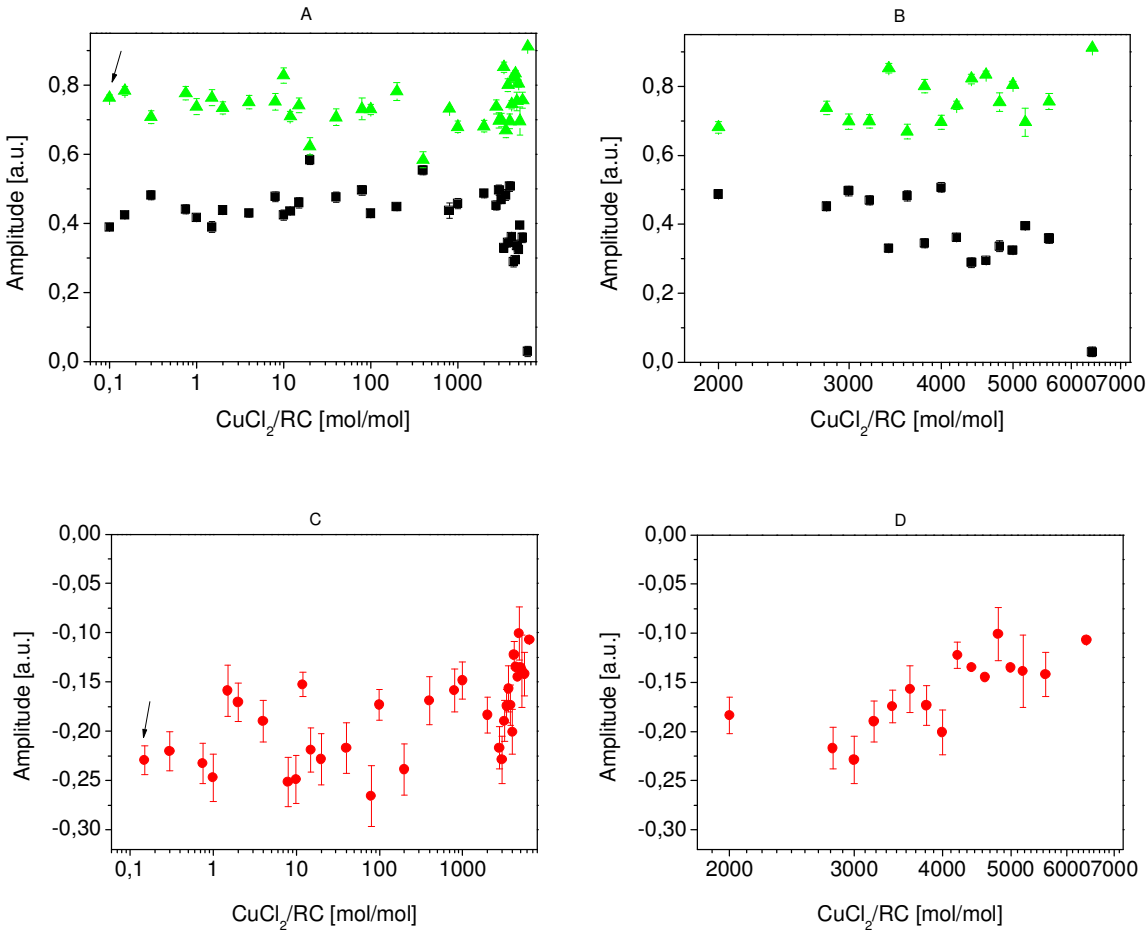

Figure 40. A semilogarithmic plots of the amplitudes: A_1,A_2,A_3- black, red, green, respectively, obtained from the fits of the experimental data. (A,C) - a whole range of applied $CuCl_2$/RC concentrations and (B,D)-a spread x scale for 2000-7000 $CuCl_2$/RC). The values obtained for the control sample are indicated by the arrows in the figure.

The aplitude A_1 which is a component with a time constant of the order of microseconds can be ascribed to the contribution of the fast variable fluorescence F_{VF}. The A_3 amplitude which is a component with a time constant of the order of tens miliseconds represents the contribution of the slow variable fluorescence F_{VS} in the spectra. The best fits, according to the (eq. 3.2.2, chapter 3.2.2.), were obtained when a component having a negative amplitude, A_2, was used. This evaluation way of the experimental data caused the increase of the slowest amplitude, A_3 but only by about 5%. That is why we increased the error of the A_3 amplitude up to 5% of its value.

One can distinguish a characteristic ranges of the copper concentrations, when the parameters A_1, A_2 and A_3 change in different ways. There are the following characteristic concentrations of $CuCl_2$/RC for the A_1 parameter: 0.3, 0.7, 1.5, 4, 10, 20, 40, 100, 400, 1000 and for the A_3 parameter: 0.3, 10, 20, 40, 200, 800 at the copper concentrations $\leq$ 1000 $CuCl_2$/RC. At the higher Cu^{2+} concentrations one can point dicontinuities of both parameters for a similar copper concentrations, namely: 2000, 2800, 3300, 3600, 4000, 4300, 4800, 5100 $CuCl_2$/RC. In the case of the A_2 parameter we can indicate the

following $CuCl_2$/RC concentrations: 0.3, 1.5, 8, 12, 20, 40 200, 400, 1000, 3000, 3600, 4200 and 4800. For the highest applied $CuCl_2$ concentrations per RC (6500) the $|A_2|$ and A_1 amplitudes decreases whereas the A_3 amplitude increases.

It is interesting to compare the concentrations of copper ions at which the discontinuities of the A_i parameters are observed and the behaviour of the corresponding t_i time constants changes. In Figure 41 we present only the the t_2 and t_3 time constants because the t_1 parameter is constant within the whole range of the copper concentrations applied and it is equal 20 ± 5 µs (it is at the level of the time resolution of the spectrometer).

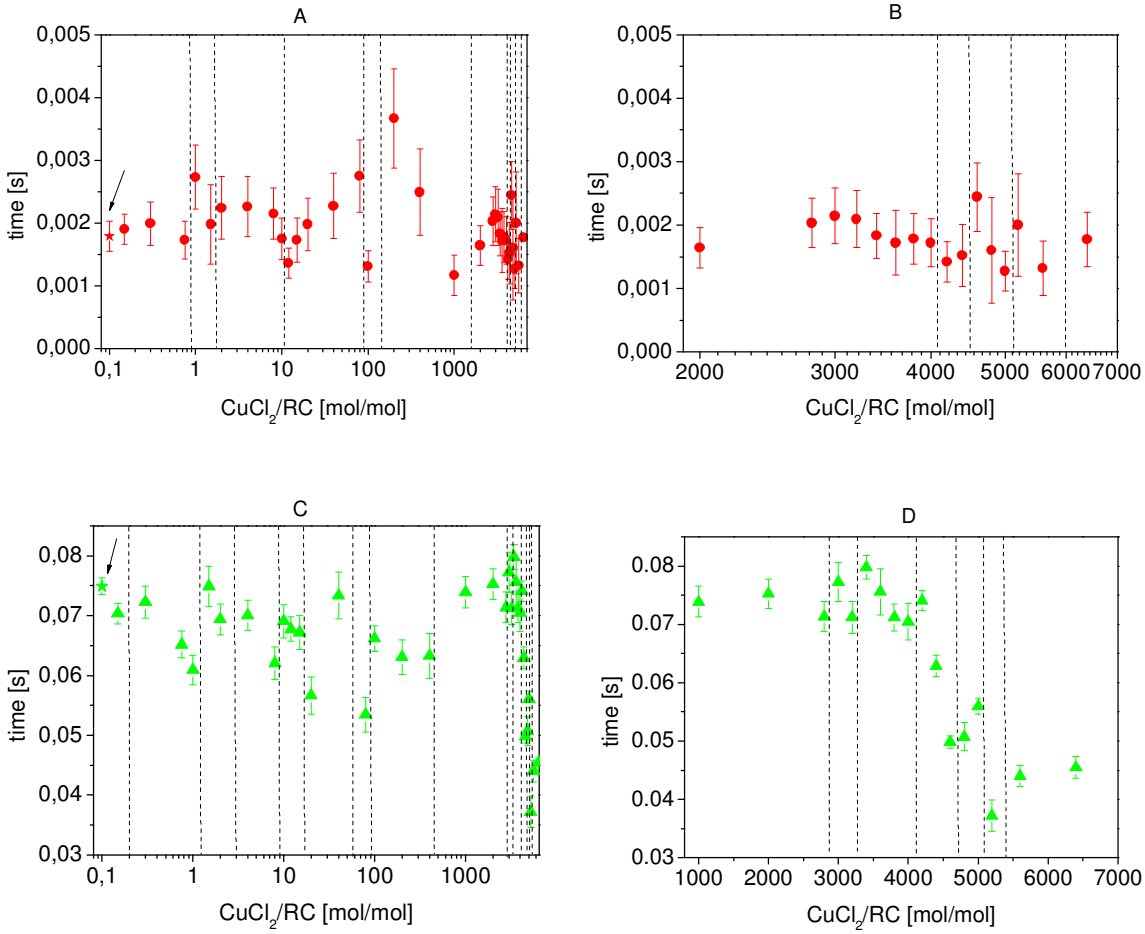

Figure 41. The semilogarithmic plots of the saturation time constants: t_2 (A and B) and t_3 (C and D) obtained from the fits of the experimental data. In (A) and (C) these paramets are presented in the whole range of the applied $CuCl_2$ concentrations, whereas in (B) and (D) in the spread scale from 1000 $CuCl_2$/RC to 7000 $CuCl_2$/RC). The values obtained for the control sample are indicated by the arrows in the figure.

There are visible characteristic variations of the t_2 and t_3 values with the increasing $CuCl_2$ concentrations. The t_2 time constant exhibits changes at the following $CuCl_2$/RC concentrations: 1, 2, 8, 10, 100, 200, 1000, 3000, 4600, 5200 and 5600 whereas the t_3 time constant for the concentrations: 0.3, 1, 2, 10, 20, 40, 100, 400, 1000, 3000, 3500,

4200, 4600, 5200 and 5600. The most striking dicontinuities of the both parameters are observed for the 1, 10, 100, 1000 and 4000 $CuCl_2$/RC concentrations . It is also worth to notice that the t_3 time constant decreases (the process is faster) about 2 times within the range of copper concentration from 3000 to 5000 $CuCl_2$/RC.

Summary.

The PEA measurements provide information on the efficiency of the photochemistry driving the electron flow within the bacterial photosystems. Because we did not use any external electron donors (if any were present in the medium they were in a minor concentration), one can expect that the changes of the variable fluorescence came from the cyclic electron flow around the bacterial reaction center and the cytochrome c_2 served mainly as the electron donor.The two subsequent saturation time constants of the variable fluorescence within the tens of microseconds and tens of miliseconds result from the kinetic equalibrations of some inner processes related to the efficiency of the energy transfer from the inner antenna to the special pair, as well as of the charge separation and electron transfer to the primary, Q_A, and secondary, Q_B, quinone acceptors. The fastest processes determine the value of initial fluorescence F_0 which is sensitive to the efficiency of the forward electron transfer from Q_A to Q_B and to the back reactions (see Figure 7, *Methods*). It is lower for more "open" reaction centers, when the forward electron transfer from Q_A is possible (the oxidized quinones are known to be efficient fluorescence quenchers). The A_1 amplitude related to the fast variable fluorescence F_{VF} reflects the equilibration of the processes occurring within the quinone-iron complex under light conditions. The A_3 amplitude (F_{VS}) is an indicator of the availability of the oxidized quinones in the medium and thus the activity of the Q_B binding in exchanging the reduced ubiquinone molecule, Q_BH_2, with the oxidized one from the external quinone pool Q_B (see Figure 7, *Methods*). The negative amplitude A_2 we assign to the quenching processes originated from the antenna complexes because in a systems depleted from the external antenna (data not shown, experiments performed on the *Rsp. rubrum* reaction centers) we did not observe this component at all. Other additional processes cannot be excluded but additional investigations are necessary to elucidade this problem.

The results show that:

(i) F_0, F_{VF} and F_{VS} as well as the negative component most probably related to the quenching of the special pair fluorescence caused by the less efficient energy transfer to P860 are sensitive to the copper action exhibiting a characteristic discontinuities within the whole range of applied $CuCl_2$ concentrations;

(ii) one observes the variation of their values and in the case of the slow variable fluorescence and of the negative component also the variations of their characteristic time constants;

(iii) the detected discontinuities of the parameters decribing the PEA fluorescence curves indicate the existence of various specific binding sites for the Cu^{2+} ions within the investigated bacterial photosystems; for us the most interesting are the sites having the highest affinity for the copper cations, of which modifications cause the transitions occurring for the concentrations of $CuCl_2$/RC lower than 200;

(iv) non-haem iron and especially the histidines being its ligands are believed to be the first target of the Cu^{2+} action within the photosynthetic systems of type Q and therefore most pronounced variations of F_0, F_{VF}, F_{VS} and of the component with the negative amplitude as well as of the time constants t_2 and t_3 are belived to be due to the binding of the copper ions within the vicinity of the iron-quinone complex.

- the most pronounced changes of these parameters are observed for the following concentrations $CuCl_2$/RC at around 1, 2, 8,10, 20, 40 and 100 and some less striking at 0.3 $CuCl_2$/RC, the exception is the t_2 time constant which increases monotously within the range of $CuCl_2$/RC concentration from 10-80;

(v) the observed transitions of all the parameters characterizing the variable fluorescence at higher concentrations can originate from the additional interactions of Cu^{2+} with other redox active components participating in the electron and energy transfer within the photosystem, for example with the chlorophylls forming the special pair. This is supported by the photobleaching experiments which show the same strong dependence on the copper concentrations > 1000 $CuCl_2$/RC and the transitions which were observed at the same Cu^{2+} concentrations: 2800 $CuCl_2$/RC, 3800 $CuCl_2$/RC, 5500 $CuCl_2$/RC 6400 $CuCl_2$/RC and 7200 $CuCl_2$/RC. Here, we could point some more characteristic regimes than in the case of the absorption measurements because of more available experimental data.

4.2.3 Thermoluminescence experiments

The charge recombination between the acceptor side of the bacterial reaction centers and the special pair depend strongly on the dimmer midpoint potential as well as the reorganization energy [65], [66]. Therefore one should expect a different stabilization energy between the reactant and product states.

Thermoluminescence measurements were performed on reaction centers isolated from *Rb. sphaeroides* (as described in *Materials,* chapter 2.2). We studied native systems and treated with the wide range of copper concentrations from 0.02 $CuCl_2$/RC to 10000 $CuCl_2$/RC. The dark adapted samples, kept in darkness for at least one hour before the measurements and transferred onto the measuring chamber under dim light conditions, were cooled down to 0^{o}C and then flashed with a single flash. The thermoluminescence spectrum of the native *Rb. sphaeroides* RC is shown in Figure 42.

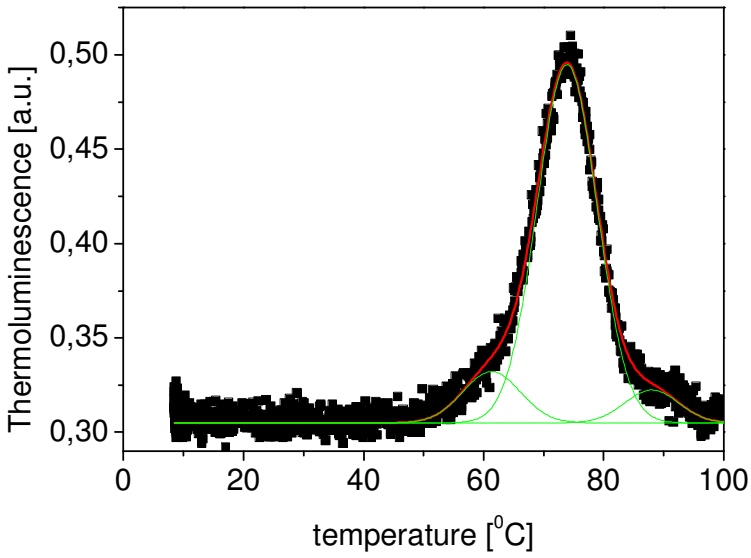

Figure 42. The thermoluminescence (TL) spectrum of the *Rb. sphaeroides* reaction centers. The solid lines represent theoretically obtained components (eq. 3.3.).

The experimental spectra for *Rb. sphaeroides* could be fitted using three Gaussian functions (see eq.3.3, chapter 3.3). The center of the dominant component appears at 74,1 ± 0.1 ^{o}C and the two others at 63,5 ± 1.0 ^{o}C and 88,8 ± 0,32 ^{o}C, which have about 8 times and 18 times lower contribution in the spectrum in comparison to the main component, respectively.

The observed TL spectra certainly originate from the charge recombination between $P860^{\bullet+}$ and $Q^{\bullet}_{A}{}^{-}(Q^{\bullet}_{B}{}^{-})$ because the peaks are quenched in the presence of *orto*-phenanthroline (*o*-phe) or DBMiB (Figure 43), which are known to be inhibitors of the iron –quinone complex [67], [68].

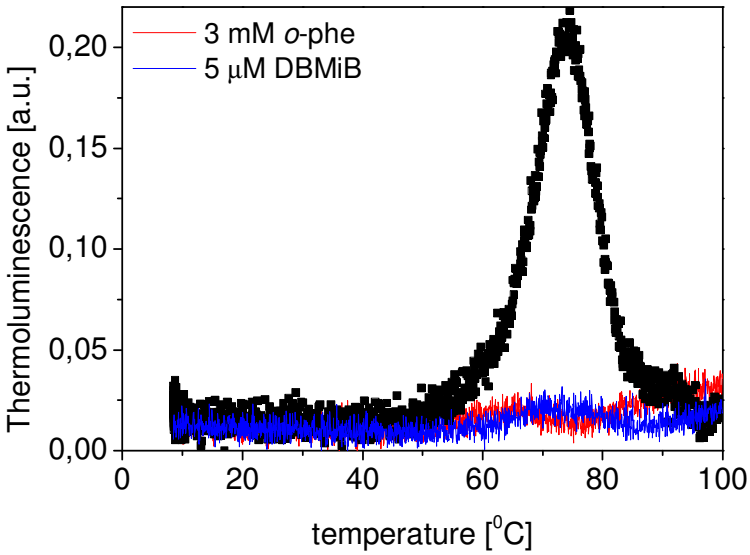

Figure 43. The thermoluminescence spectra of *Rb. sphaeroides* treated with 3 mM *o*-phe (red) and 5 µM DBMiB (blue). One can see that the peaks are quenched in the presence of the inhibitors.

An independent evidence that the thermoluminescence spectrum is related to the charge recombination processes between the acceptor side of the reaction center and its special pair P860 provide the termoluminescence measurements with various number of flashes (Figure 44). The flashes were separated 200 ms apart. For each flash experiment a new sample was taken.

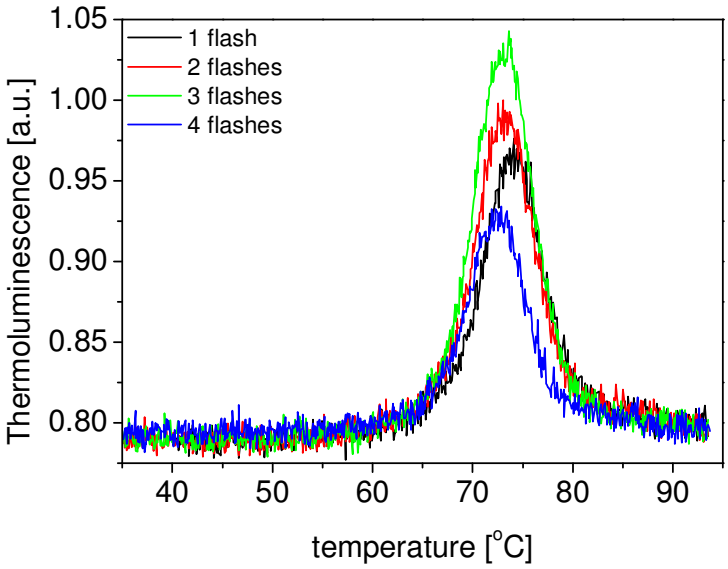

Figure 44. The thermoluminescence spectra of native *Rb. sphaeroides* recorded after one (black), two (red), three (green) and four (blue) single flashes.

One can see that the position of the maximum and the intensity of the spectrum (Figure 44) depend on the flash number. This suggests that the changes are related to the various Q_A and Q_B redox states on the acceptor side of the RCs because the different number of flashes leads to the different accumulation of the reduced forms of these two quinones.
Our earlier studies presented here (see chapter 4.1 and the further chapter 4.2.2) and the literature data [54], [55], [61], indicate that the copper ions already at as low concentrations as 1-10 Cu^{2+}/RC influence the binding site of the non-haem iron and simultaneously the redox properties of the Q_A and Q_B quinones. The thermoluminescence measurements of *Rb. sphaeroides* treated with copper chloride under different flash conditions (1, 2 3 and 4 flashes) are presented in Figure 45.

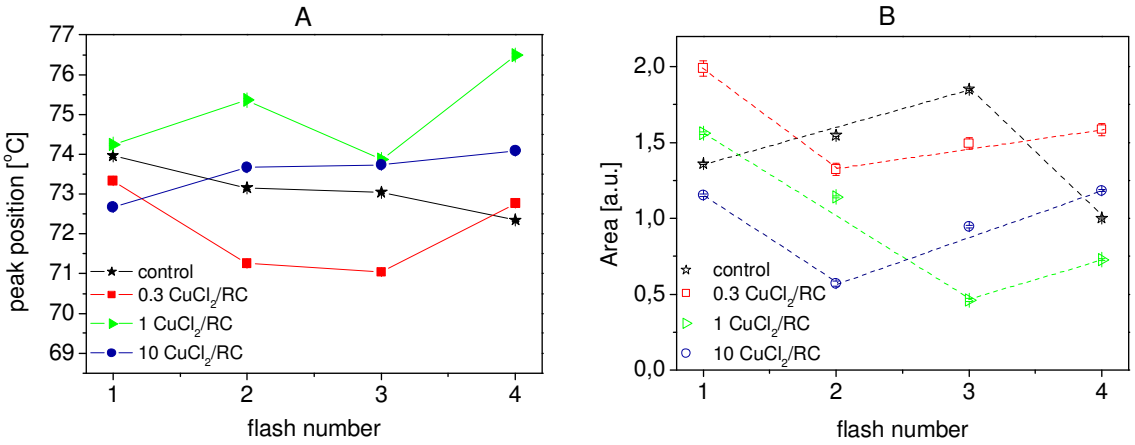

Figure 45. The dependence of the peak position (A) and the area (B) of the dominant component derived, according to the eq. 3.3, from the thermoluminescence spectra of *Rb. sphaeroides* on the flash numbers. The samples were treated with the $CuCl_2$/RC concentrations of 0.3, 1 and 10 which are indicated in the figure by different colours. The error bars are of the size of the symbols.

One can see that the increasing number of the given flashes causes changes of the position of the main component in the fluorescence spectra. In the control sample the center of the component detected at about 74 °C under 1 flash is shifted toward lower temperatures after two flashes by 1 °C. After three flashes it is still at the level of about 73 °C and after 4 flashes it is shifted to 72 °C. At the same time the intensity of the peak increases with the increasing number of flashes but after 4 flashes it decreases almost 2 times in comparison to the intensity obtained for the sample treated with three flashes. In the sample treated with 0.3 $CuCl_2$/RC the position of the peak after 1 flash is shifted to about 73.35 °C, by only 0.61 °C in comparison to the control but after 2 and 3 flashes its position is shifted by more than 2 °C toward lower temperatures. However, 4 flashes almost recover the position of the peak which occurs at around 72.8 °C. The lowest applied concentration of the Cu^{2+} ions in these experiments cause the enhancement of the intensity of the thermoluminescent component by more than 40% under 1 flash but its intensity decreases to the level of the control (under 1 flash) when 2 flashes are given. More number of flashes, 3 and 4, causes a slow increase of the intensity of the TL component. The most striking and interesting case was observed for the sample treated

with the copper concentration of 1 $CuCl_2$/RC. The main component of the spectrum obtained for a single flash has a similar position of its center and intensity as the control sample, ie. at around 74 ^oC and 1.5 a.u., respectively. However, under the increasing number of flashes its position starts to oscillate, it is shifted up to about 75.5 ^oC, then down to about 73.8 ^oC and again up to 76.6 ^oC. At the same time the intensity of the peak decreases linearly with the number of flashes by a factor of 3 but after 4 flashes it increases by about 25%. The highest applied concentration od copper chloride causes the shift of the main component position by about 1.5 ^oC in comparison to the control, to about 72,5 ^oC after 1 flash but then the subsequent flashes cause that its position is stabilized on the level of the control sample treated with 1 flash. In this case the intensity of the component treated with copper ions is lower by about 12% in comparison to the control (1 flash) but after 2 flashes it decreases by a factor of 2.5 and with the increasing number of flashes it increases linearly reaching 2 times higher intensity after 4 flashes in comparison to the situation when the sample was treated with 2 flashes. The intensity of sample treated with the highest concentration of Cu^{2+} (after fourth flash) is similar to those of the control sample treated with 4 flashes. It is interesting to notice that the peak position of the control sample and the sample treated with 10 $CuCl_2$/RC have a symmetry axis at y = 73.5 ^oC (Figure 45 A), whereas the areas of the main component for these two samples can be transferred to each other by the subsequent reflection against the symmetry axis x = 2.5 and then the symmetry axis y = 1.25 (Figure 45 B). This suggests that the stabilization energies and redox potentials of the acceptor side of the reaction centers can be reversed in the sample treated with 10 Cu^{2+}/ RC. The final interesting note is that the changes of the intensity of the main component with the number of flashes in the thermoluminescence spectrum of the samples treated with 0.3 $CuCl_2$/RC are shifted by about 1.7 a.u. toward higher values in comparison to those areas detected for the sample treated with 10 $CuCl_2$/RC.

We have also preformed thermoluminescence measurements for samples treated with a wide range of $CuCl_2$ concentrations using a single flash. The position of the centers and intensities of all components derived from the termoluminescence spectra as a function of the applied concentrations of copper salt are shown in Figure 46.

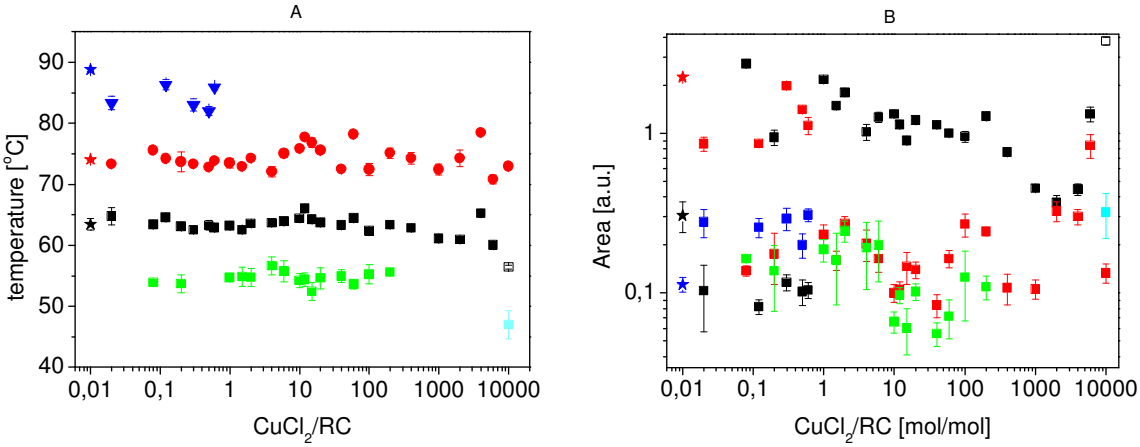

Figure 46. The semilogarithmic plots of the center position (A) and intensity (B) of the subcomponents derived from the thermoluminescence spectra for the *Rb. sphaeroides* treated with different $CuCl_2$ concentrations. The values obtained for the control sample are marked as the star symbols in the figure.

There are three components detected in the control sample as described at the beginning of this chapter and they are still present in the sample treated with 0.02 $CuCl_2$/RC, but contribution of the components in the thermoluminescence spectrum is changed, namely the intensity of the main peak decreases two times whereas the intensities of the two other components with the peak position at around 65 °C (up shifted by 2°C) and 83 °C (down shifted by 5°C) decreases 3 times and increases 2.5 times, respectively in comparison to the control sample. The most striking changes of the thermoluminescence spectrum is observed for the samples treated with the $CuCl_2$/RC concentrations up to 1. Looking more carefully at Figure 46 one can notice that the subsequent increase of the copper concentration in the sample from 0.08, 0.12, 0.2, up to 0.3 $CuCl_2$/RC results in the oscillation (occurring or disappearing) of the component with the center located at about 55°C and 85 ± 2°C. When the component positioned at 55 °C is absent the spectrum is dominated by the component localized at about 75 °C and the relative intensities of the suspectra are comparable to those detected for the sample treated with 0.02 $CuCl_2$/RC. However, in the absence of the component localized at about 85°C, the thermoluminescence spectrum is dominated by the component centered at around 63 °C and the other two subspectra have a comparable intensities but 10 times lower than the main component. The another interesting behaviour of the thermoluminecsnece spectra measured for the reaction centers treated with the copper salts is the appereance of the spectrum similar to the control sample for the $CuCl_2$/RC concentrations between 0.3 and 0.6. At the copper concentrations $1 \leq CuCl_2$ /RC ≤ 200 the spectra are comparable to those spectrum observed for the sample treated with the 0.08 $CuCl_2$/RC (or 0.2) but the intensities of the subspectra vary with the increasing concentrations of the copper ions. There are some characteristic transitions of the areas (Figure 46 B) and of the peak positions (Figure 46 A, Figure 47) observed for the following $CuCl_2$/RC concentrations: 2, 4, 10, 20, 40, 100 and 200. At the copper concentrations higher than 200 $CuCl_2$/RC

only two components are present in the thermoluminescence spectrum with the center localized at around 63 °C and 75 °C and again some discontinuities of their position and intensities are visible at 1000, 2000, 4000, 5900 $CuCl_2$/RC. Finally, at the highest applied concentration of 9600 $CuCl_2$/RC a new component appears in the spectrum with the peak positioned at about 47 ± 2 °C and 2 times higher intensity than the component with the center at around 72 °C. However, this spectrum is dominated by the component localized at around 56°C. It has the intensity 10 times higher in comparison to the intensity of the new component.

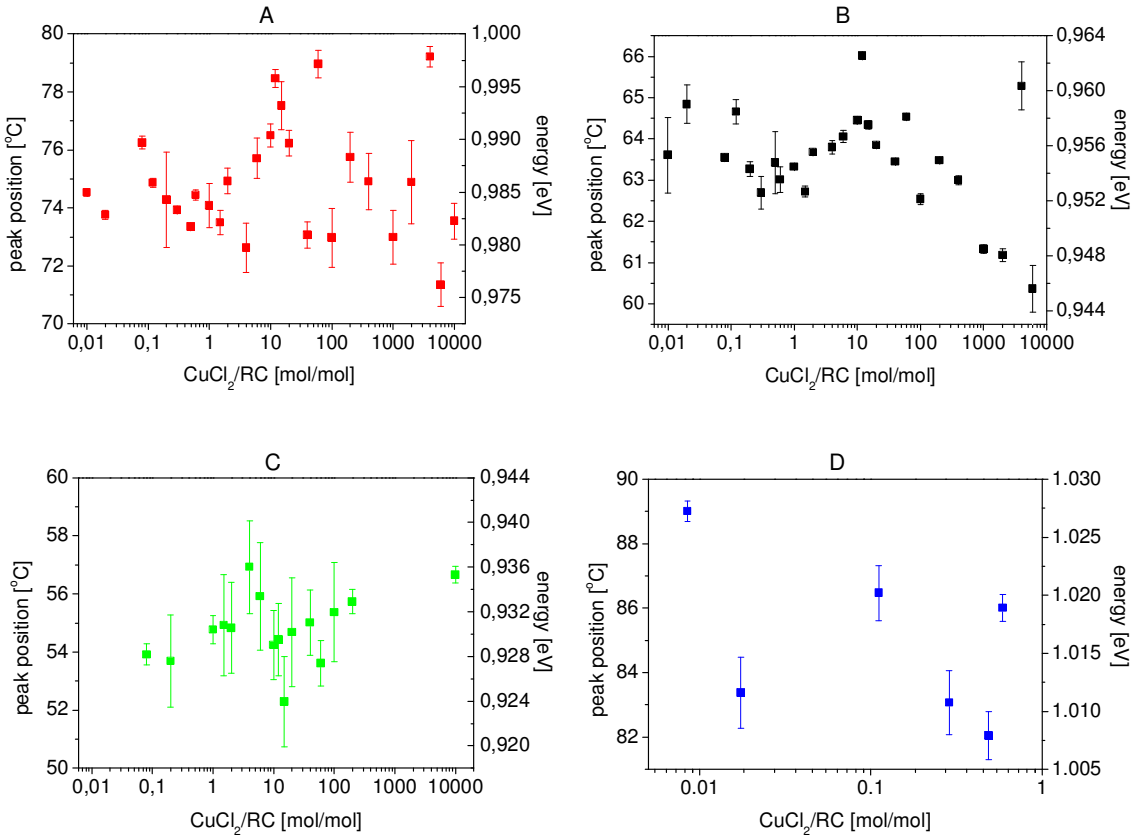

Figure 47. The semilogarithmic plots of the center position of the subcomponents derived from the thermoluminescence spectra for the *Rb. sphaeroides* treated with different $CuCl_2$ concentrations. Energies corresponding to the values of the peak positions are shown in the right side of the plot.

At the first approximation the temperature of the thermoluminescence peak position, T_m, is proportional to the total free energy and the proportionality factor is $1/(33k_B)$, where k_B is the Boltzmann constant [69], [70]. This calculation is true when one assumes that there are no steps with negative free energy proceeding the final energy detraping mechanism. According to this approach, one can estimate the free energy of the recombination processes in the photosynthetic systems. The total free energies calculated in this way from the position of the thermoluminescence peaks are presented in Figure 47.

Summary.

The thermoluminescence experiments were performed on the bacterial reaction centers isolated from *Rb. sphaeroides*, native and treated with various copper chloride concentrations. The experiments with iron-quinone inhibitors (*o*-phenanthroline, DBMiB) and flash experiements show that the observed spectrum is related to the process of the charge stabilization between $Q_A^{\bullet-}$($Q_B^{\bullet-}$) and $P860^{\bullet+}$. The spectrum of the native sample is dominated by a component centered at around 75 ^oC. Because the same sample in the photobleaching experiements has the main component characterized by the time constant of hundreds miliseconds corresponding to the process of charge recombination between $Q_A^{\bullet-} \rightarrow P860^{\bullet+}$ we assign the peak at 75 ^oC to the native Q_A site. The thermoluminescence subspectrum at around 88 ^oC in native sample may be related to the stabilization process of the Q_B site because this quinone binding site has higher free energy. This interpretation is in an accordance with the fact that DBMiB, which is known to effect the Q_B site, inhibits the transition visible in the thermoluminescence spectrum at 88 ^oC. The third component may be related to the modified Q_A site what is supported by the experiements done with *o*-phenanthroline which efficiently quenches the component positioned at around 75 ^oC but only slightly influences the component centered at around 63 ^oC . This inhibitor is acting as a chelator and therefore it is interesting to notice that higher concentrations of copper ions (> 1 $CuCl_2$/RC) have a similar effect on the thermoluminescence spectrum with the exception that they lead to the stabilization of the modified Q_A state. For these copper concentrations the thermoluminescence spectrum is dominated by the component with a center at about 63 ^oC and 10 times higher intensity than the other two components.

Copper ions can influence the structure and functioning of the iron-quinone complex in many ways as well as other structures of the photosystem but it is clear from the results obtained for the low copper concentrations that the first target of its action is the non-haem iron and especially the Fe connectivity with the two Q_A and Q_B sites. The most intriguing changes of the total free energy of the stabilization of charge separation on the acceptor side are observed for the Cu^{2+} concentrations up to 10 $CuCl_2$/RC. These transitions suggest that there are more than one high affinity binding sites within the iron-quinone complex and its vicinity. This conclusion is strongly supported by the results obtained from the measurements with a variable number of flashes which show that the periodic changes of the charge stabilization on the acceptor side of RCs are influenced differently by the low applied concentrations of Cu^{2+}. The transitions of the thermoluminescence subspectra positions and intensities are observed at the same ranges of copper concentrations as the fluorescence parameters characterizing the efficiency of forward electron transfer (see chapter 4.2.2): 0.3, 1, 2, 4, 10, 20, 40 100, 200, 1000, 2000, 3000 and 5900 $CuCl_2$/RC. So these experiments give evidence that the components important for the electron transfer within the photosystem are very sensitive targets for Cu^{2+} action.

4.2.4 Mössbauer spectroscopy measurements

The valence and spin state of the non- haem iron in the chromatophores as well as native and treated with $CuCl_2$ reaction centers, isolated from *Rb. sphaeroides,* were studied by Mössbauer spectroscopy. The absorption spectrum of reaction centers which were used in Mössbauer spectroscopy measurements is shown in Figure 48.

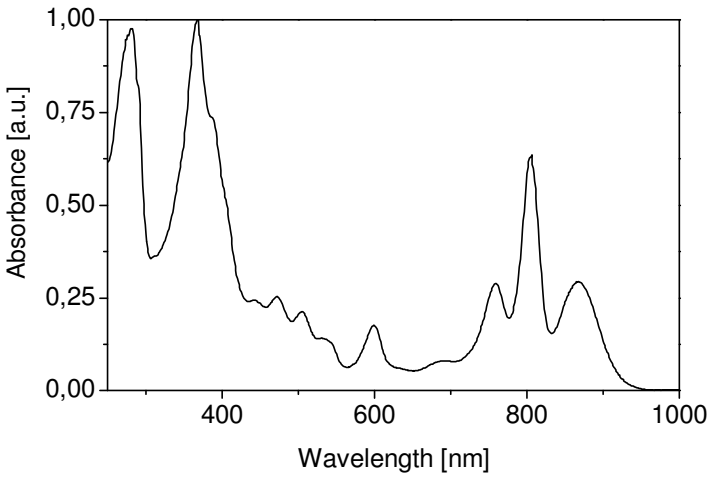

Figure 48. The normalized absorption spectrum of reaction centers isolated from *Rb. sphaeroides*.

The Mössbauer spectra of chromatophores, native and treated with Cu^{2+} reaction centers isolated from *Rb. sphaeroides* are shown in Figure 49.

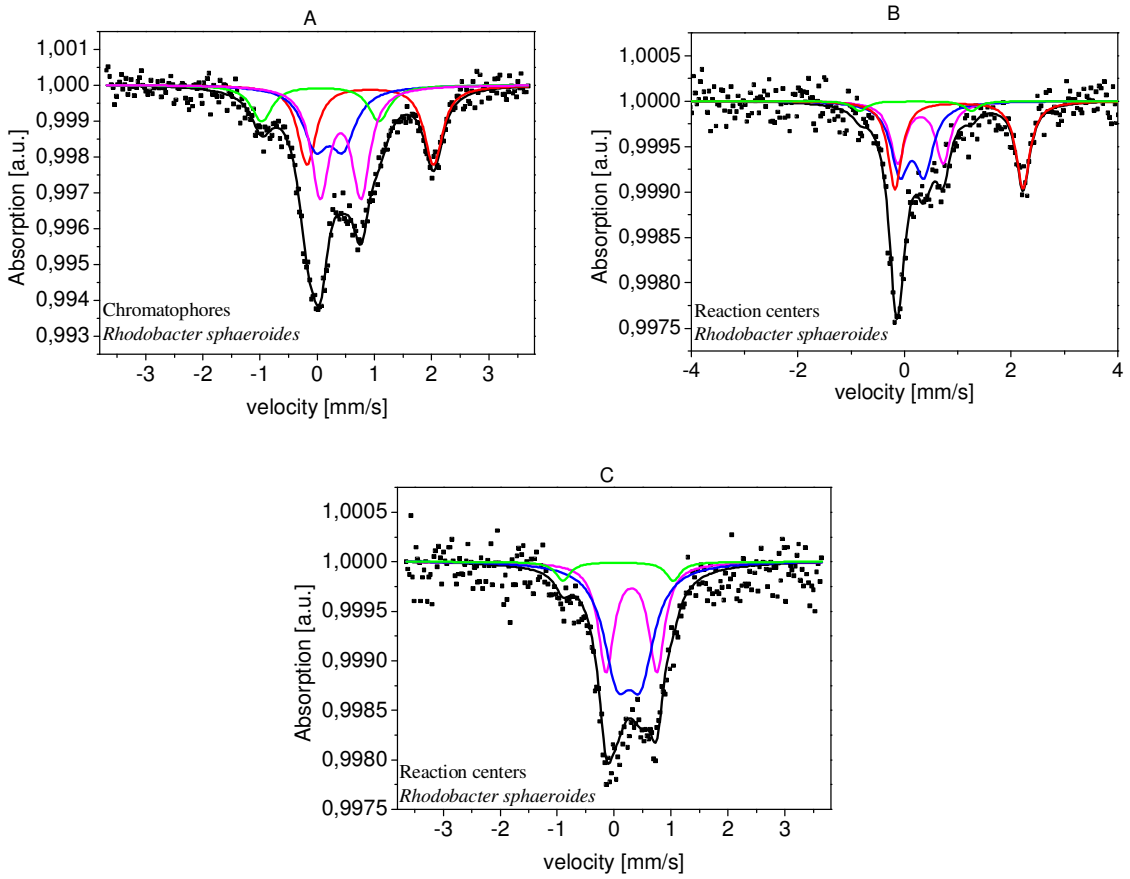

Figure 49. ^{57}Fe Mössbauer absorption spectra of chromatophores (A) native reaction centers (B) and treated with Cu^{2+} (C) isolated from *Rb. sphaeroides*. These spectra were recorded at 83 K.

The hyperfine parameters fitted to the experimental data are presented in Figure 50. The isomer shifts and quadrupole splittings of the subspectra show that in RCs of *Rb. sphaeroides* there are two different states of haem iron in cytochrome c_2, and two different spin states of non- haem iron.

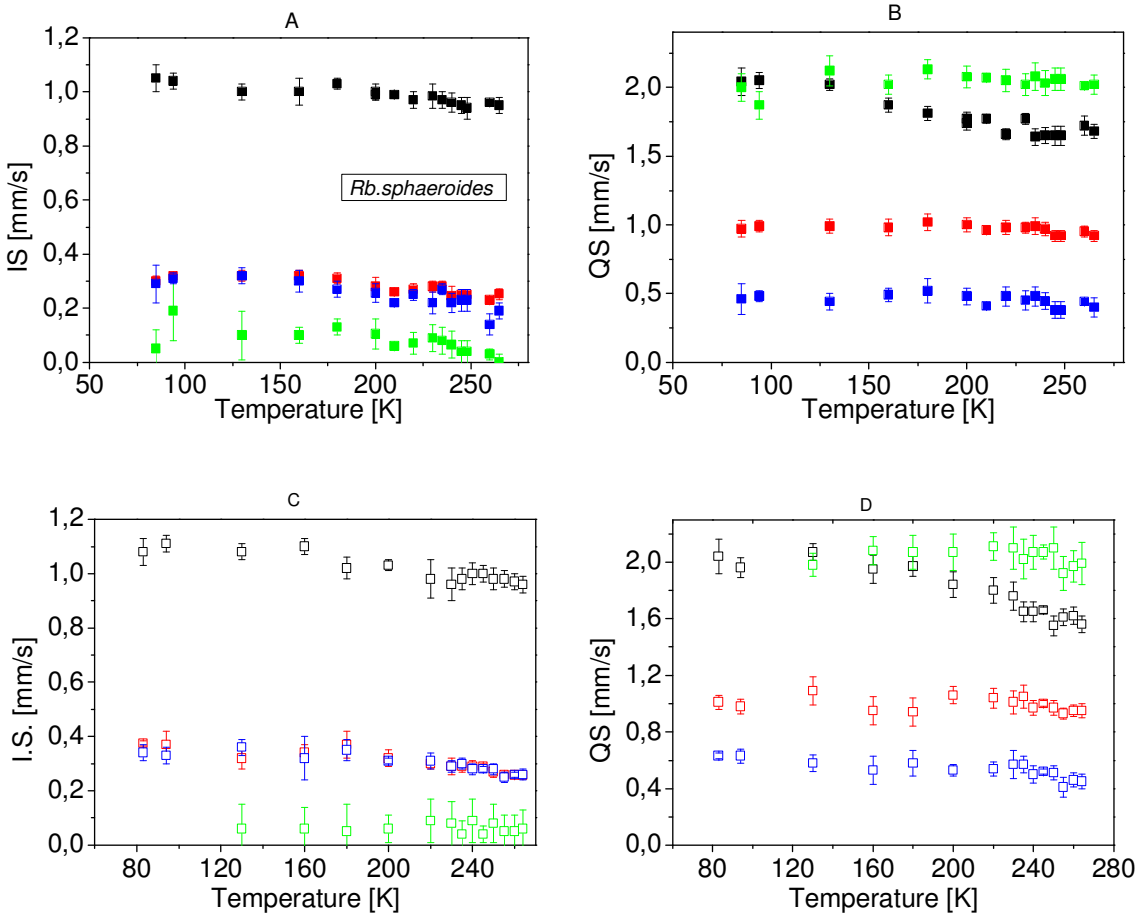

Figure 50. Temperature dependence of the hyperfine parameters fitted to the Mössbauer spectra: (A,C) isomer shifts, IS, and (B,D) quadrupole splittings, QS, of the non- haem iron (black and blue) and the haem iron of cytochrome c_2 (green and red) in untreated (A,B) and treated with $CuCl_2$ (C,D) reaction centers isolated from *Rb. sphaeroides*.

The hyperfine parameters of the component with the quadrupole splitting of about 2.0 mm/s (which has enough high contribution in the RCs modified by $CuCl_2$ only at T > 120 K when one can unambiguously fit its parameters) is an unusual ferrous low spin state which was detected for example in oxygenated hemoglobin [71]. Its hyperfine parameters suggest that an oxygen molecule can be ligated to this haem iron. For us, the most interesting result is that the non- haem iron from the Q_A-Fe-Q_B complex can exist either in high or low spin ferrous state. The low spin state of iron is formed when it is in a strong field and the strength of iron bonds increases with a simultaneous decrease of their lenghts. In addition the Fe-ligand interactions are effected by the iron coordination number and by the character of its ligands.

The Mössbauer spectra of *Rb. sphaeroides* presented here (Figure 49) show that the non-haem iron besides its well known ferrous high spin state [72], [23], [73], [74] can be stabilized also in a low spin state. It is believed that the non- haem iron should exist only in a high spin ferrous state in photosynthetic reaction centers although such a

diamagnetic state of the non- haem iron has been already observed in mutated BBY PSII isolated from algae [52]. Moreover, copper ions (~300 $CuCl_2$/RC) modified the non-haem iron binding site and transfered the iron into a new diamagnetic state [45], [52]. So far it was believed that Cu^{2+} replaces Fe^{2+} in the iron-quinone complex but the experiments on the algae mutant and on the bacterial reaction centers presented here show that the copper ions, at least at the applied concentrations, do not remove the non-haem iron from its binding site but only change the spin state of the iron atom.
The valence changes of the non- haem iron in native systems have never been observed and therefore a direct participation of the non- haem iron in the electron flow between Q_A and Q_B probably can be excluded. On the other hand EPR signal of the primary quinone acceptor is modified in the absence of iron [72], [75]. Because the two quinone molecules on the acceptor side of RCs (and PSII) are coupled via a non-haem iron, a structural role of the non-haem iron was suggested [45], [74], [76], [77]. This interpretation comes from the fact that the amino acid residues being the non-haem iron ligands, in particular His219 in the subunit M and His190 in the subunit L, may interact with the iron atom with a various force and these interactions are regulated at the same time by the hydrogen bonds between His219 and His190 with the Q_A and Q_B quinone molecules, respectively. Thus, protonation and deprotonation of the ubiquinone molecules at the Q_A and Q_B site as well as of other residues (for example Glu234 in the subunit M), which are ligated to the non-haem iron might change not only the strength of the iron atom bonds but also regulate the redox potential of the non-haem iron. Therefore, these results may indicate that the protonation and deprotonation events in the vicinity of the iron-quinone complex decide about the spin state of the non-haem iron and the stability of the charge separation between $P860^+$ and Q_A (Q_B). One can already find independent support for the importance of hydrogen bonds for the events related with the charge separation on the acceptor side of the bacterial reactions centers in the literature [78], [79], [80], [81].

The temperature dependent measurements allow to perform the analysis of the recoil- free fractions, which additionally helps to characterize the dynamic properties of the different environments of the absorbing nucleus. The decrease of the isomer shift with increasing temperature (Figure 50) is due to the second-order Doppler shift, a dynamic relativistic effect. Thus, no change of electron density at the ^{57}Fe nuclei is observed. The quadrupole splittings do not change with temperature. There is one exception, namely in the non- haem iron (high spin, Fe^{2+}). The strong decrease of the quadrupole splitting for the Fe^{2+} high spin state most probably results from the temperature stimulated fluctuations of its surrounding protein matrix. From the temperature dependence of the absorption area of the spectra, which for thin absorbers are proportional to the Lamb- Mössbauer factor (eq. 3.5.1.2, chapter 3.5.1) the mean square displacement $\langle x^2 \rangle$ of the iron states was calculated. The mean square displacement was normalized by its extrapolation to 0 for T=0 according to the classical approach. The results are presented in Figure 51.

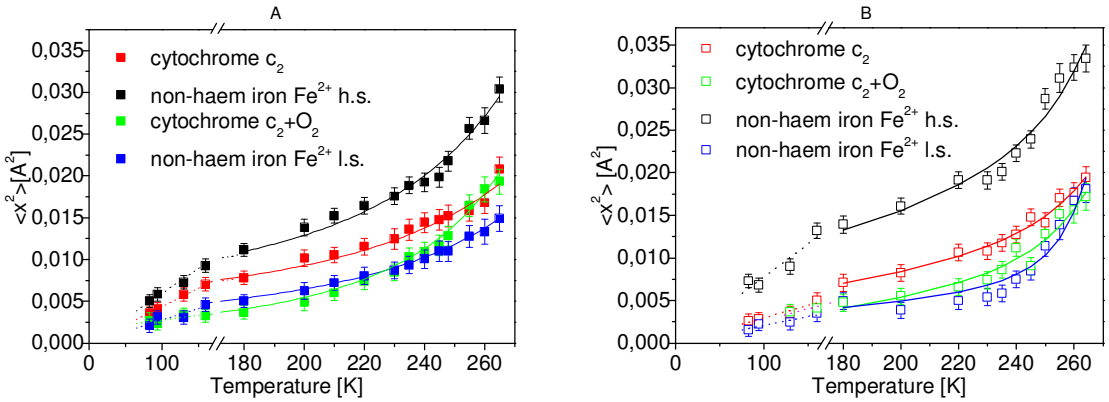

Figure 51. Temperature dependence of the mean square displacements for the non- haem and haem iron in reaction centers of *Rb. sphaeroides* native (A) and treated with $CuCl_2$ (B).

The mean square displacement $\langle x^2\rangle_t$ of iron can be approximated by a sum of three statistically independent terms [82]: $\langle x^2\rangle_t = \langle x^2\rangle_v + \langle x^2\rangle_{cf} + \langle x^2\rangle_{cs}$, where indices *v, cf, cs* are related to vibrational, collective fast and collective slow (diffusional) modes, respectively. These motions are associated with the fluidity of the protein matrix. An idependent approach describing the temperature behaviour of $\langle x^2\rangle$ is the Debye model extended for anharmonicity at higher temperatures [83]. Generally, below the Debye temperature $\langle x^2\rangle$ increases linearly with temperature and one can attribute these motions to the lattice or solid- state vibrations $\langle x_v^2\rangle$ (Figure 51). Assuming a temperature-dependent Debye temperature: $\theta_D = \theta_0(1+AT+...)$, where θ_D is the Debye temperature at the low temperature limit and A is a parameter of anharmonicity, θ_0 and A for the haem and non-haem iron were obtained. These parameters are colected in Table 4.

Table 4. Experimentally determined parameters of the Debye model extended for anharmonicity (θ_0 is the Debye temperature, A is a parameter of anharmonicity) for native and treated with copper reaction centers isolated from *Rb. sphaeroides*.

Rb. sphaeroides				
Parameter	Non- haem h.s.	Non-haem l.s.	Cytochrome c_2	Cytochrome c_2+ O_2
θ_0 [K]	168 ± 18	207 ± 12	198 ± 17	201 ± 16
A [1/K]	-0.0028 ± 0.0002	-0.0031 ± 0.0007	-0.0032 ± 0.0006	-0.0033 ± 0.0001
***Rb. sphaeroides* +Cu^{2+}**				
θ_0 [K]	164 ± 23	212 ± 17	191 ± 22	220 ± 30
A [1/K]	-0.0032 ± 0.0002	-0.0033 ± 0.0005	-0.0031 ± 0.0006	-0.0032 ± 0.0004

The uncertainty of the obtained parameters is quite high and the only significant difference is observed for the high and low spin of the non- haem iron showing much

more rigid bonds for the low spin one. On the other hand, the most flexible surrounding is detected for the high spin state of the non-haem iron. The Debye temperatures estimated for the two other iron sites in the cytochrome c_2 suggest that the haem iron is in a net which has an intermediate rigidity in comparison to the binding sites of the low and high spin states of the non-haem iron.

Summary.

Using Mössbauer spectroscopy we have shown that the non-haem iron in the chromatophores and reaction centers isolated from *Rb. sphaeroides* is stabilized either in a high spin or low spin ferrous state. The low spin state was recognized so far only in photosystem II isolated from *Chlamydomonas reinhardtii* PSI$^-$ mutant [45], [52]. It is the first time when the low spin state was detected in the native bacterial reaction centers. The occurrence of the low spin non-haem iron indicate a stronger connection of the Fe atom with its ligands. Because it shares four of its ligands with the quinone acceptors bound at the Q_A and Q_B site it can influence the coupling between these two acceptors. This was indeed observed via the studies performed at different temperatures and in the presence of copper ions, which we knew, from the PEA measurements and the thermoluminescence experiments, that they modify the electron transfer within the iron-quinone complex and the energy stabilization of the charge separation between the special pair and the acceptor site in the bacterial reaction centers (see chapter 4.2.2 and 4.2.3). We have chosen Cu^{2+} in the studies because already from the earlier studies on PSII presented in the literature [12] and the other results presented here it comes out that copper can in a highly specific way bind in the vicinity of the non-haem iron. In the literature one can find that copper can exchange the non-haem iron but it is not the case under our experimental conditions (we checked the amount of iron atoms per reaction center using atomic absorption spectroscopy). However, we have observed that copper chloride transformed the ferrous non-haem iron from its high spin state into low spin one. There were not detected any significant changes of the hyperfine parameters of the non-haem iron low spin state occurring in the modified photosystems in comparison to the native samples. Copper also does not influence the valence and spin states of the two haem irons in cytochrome c_2 which was present in our preparations. The studies of the temperature dependence of the mean square displacement of the iron atoms give evidence that the non-haem iron being in the low spin state is bound in a more rigid environment ($\theta_{D0} \approx 207 \pm 12$ K) than the iron in the high spin state ($\theta_{D0} \approx 165 \pm 18$ K). The two haem-irons in cytochrome c_2 are in surroundings of the intermediate rigidity ($\theta_{D0} \approx 199 \pm 17$ K) but their characteristic Debye temperature is not significantly different from that one evaluated for the low spin ferrous non-haem iron. The copper ions transferring the high spin state of the non-haem iron into the low spin one caused the increase of the strength of the bonds between the iron and its ligands. The estimated Debye temperature for the low spin state of the non-haem iron is higher by about 5 K than that one observed for the native photosystems but the difference is within the uncertainty of the fits.

4.2.5 Inelastic scattering of synchrotron radiation measurements

Experiments of the nuclear resonant inelastic X-ray scattering around the central elastic peak with the resonance energy of about 14.4 keV were performed in order to check how the temperature higher than 200 K and copper ions bound in the vicinity of the non-haem iron causing its transfer into the low spin state influence the rigidity of the surrounding protein matrix in bacterial reaction centers isolated from *Rb. sphaeroides*. The spectra normalized to the intensity of their elastic part for the native RCs detected at two different temperatures 60 K and 240 K and for the RCs treated with $CuCl_2$ collected at 60 K are presented in Figure 52.

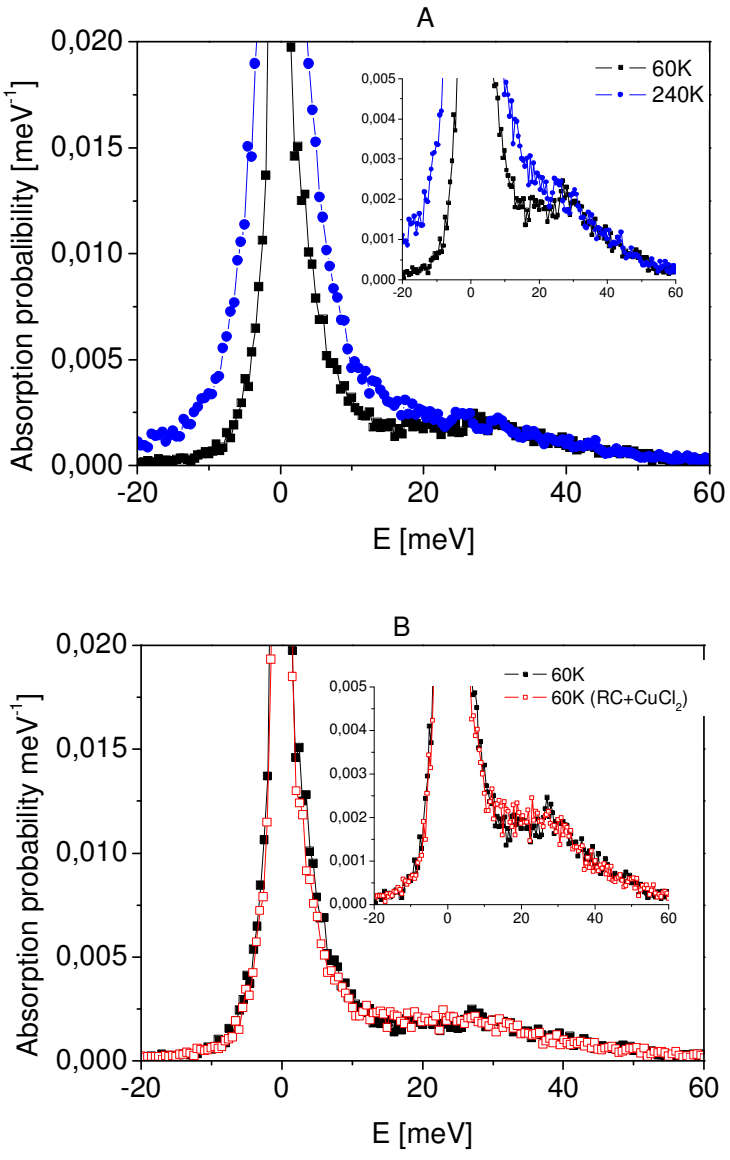

Figure 52. Spectra of the nuclear inelastic X-ray scattering around the resonance elastic peak of 14.4 keV in *Rb. sphaeroides* RCs measured at 60K (black) and 240 K (blue) applying synchrotron radiation (A). In (B) the comparison of the spectra for native (black) and incubated with Cu^{2+}(red) samples are shown. The spectra were normalized to the intensity of the elastic peak.

The main difference between the high and low temperature spectra of the native RCs is the enhanced contribution of the low energy vibrations. On the contrary, the copper ions caused lowering of the intensity of these energy vibrations. In order to get more detail information on the inelastic vibrations, the inelastic contribution was extracted from the elastic part, the central peak was substracted from the spectrum shown in Figure 52 as described in [84]. The uncertainty introduced into the *f* (Lamb- Mössbauer) factor was estimated not to be larger than 0.1%. Assuming that $g(E) \sim E^2$ for small energies ($E \leq 3$ meV), the DOS (density of vibrational states) at 60K and 240K were derived from the experimental data and are presented in Figure 53.

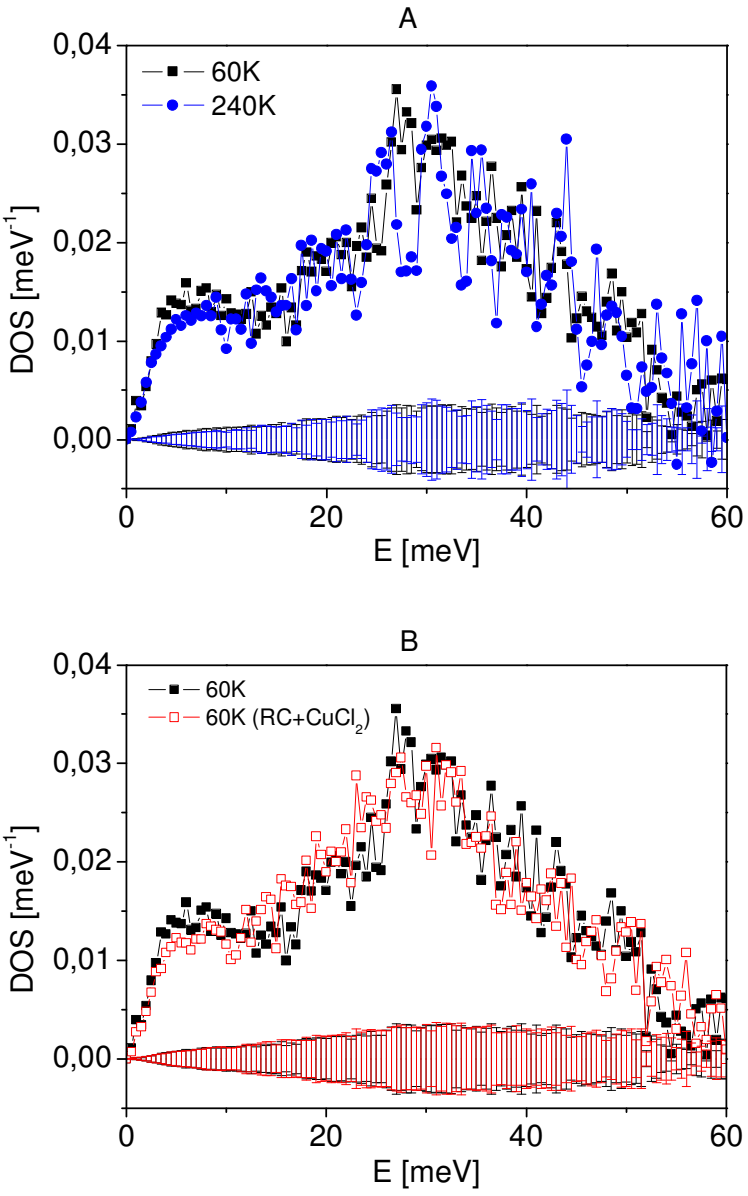

Figure 53. Density of vibrational states (DOS) in *Rb. sphaeroides* RCs measured at 60K (black) and 240 K (blue) applying synchrotron radiation (A). In (B) the comparison of the spectra for native (black) and incubated with Cu^{2+} (red) samples are shown.

There are two characteristic plateaus of DOS at low energies from around 4 meV to 17 meV and from 17 meV to 22 meV (Fig. 53 A). DOS gradually decreases with increasing energy at E> 30 meV exhibiting some small maxima observed at around 26.5-28.5 meV, a plateau between 30- 32.5 meV, and then small narrow peaks at 36.6 meV, 39.5 meV, 41meV and 46 meV, 53 meV and 57 meV and broader ones at 43-44 meV and 48- 51.5 meV. At 240K one observes an increase of the contribution of fluctuations especially for ranges from 10 meV to 23.5 meV and from 30 meV to 60 meV. In the further discussion we will concentrate only on the vibrations occurring below 30 meV because the DOS spectrum at E > 30 meV is dominated by the vibrational modes of the cytochrome c_2. The density of the vibrational states of the haem irons, for example in heamoglobin and cytochrome c determined with the same experimental method [85] shows a peak at 3.5 meV, a rather featureless and silent energy region between 8 meV and 30 meV. Therefore the lower energetic fluctuations in our spectra are related to the non-haem iron, which is directly connected to the protein matrix via all its ligands in contrary to the haem iron in the cytochrome or haemoglobin. The differences of the density of the vibrational states (g(E)) at low energies for the *Rb. sphaeroides* samples are better visualized by showing them in terms of g(E)/E (Figure 54) and $g(E)/E^2$ (Figure 55).

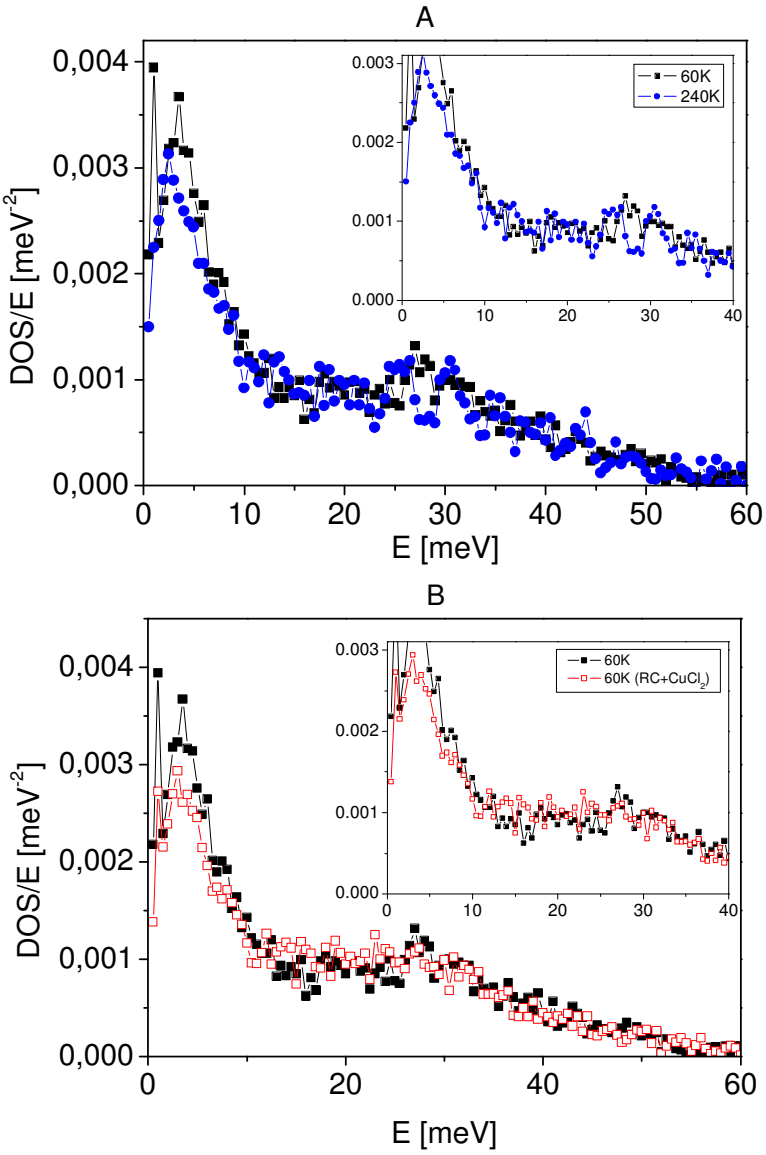

Figure 54. Density of vibrational states (DOS) devided by the corresponding energy value, E, in *Rb. sphaeroides* measured at 60 K (black) and 240 K (blue) using synchrotron radiation (A). In (B) the comparison of the spectra for native (black) and incubated with Cu^{2+} (red) samples are shown.

It is interesting to note that the spectrum at 240 K has extra vibrational modes at around 12-17 meV and 22.5 – 26.5 meV whereas the modes at 27- 28.5 meV disappear (Figure 53 A and Figure 54 A). In the case of the spectrum of RCs modified with Cu^{2+}, additional vibrations at the energies around 12-16 meV, 18 meV and 25 meV occur causing decrease of the fluctuations at energies of 26.5- 28.5 meV (Figure 53 B, Figure 54 B). The low energy part originating from the slow collective motions is the most interesting one because these collective motions affect the rate of the electron transfer between the acceptor side and $P860^{+}$ in RCs and within the iron-quinone complex, [65], [68], [75], [86],[87], [88].

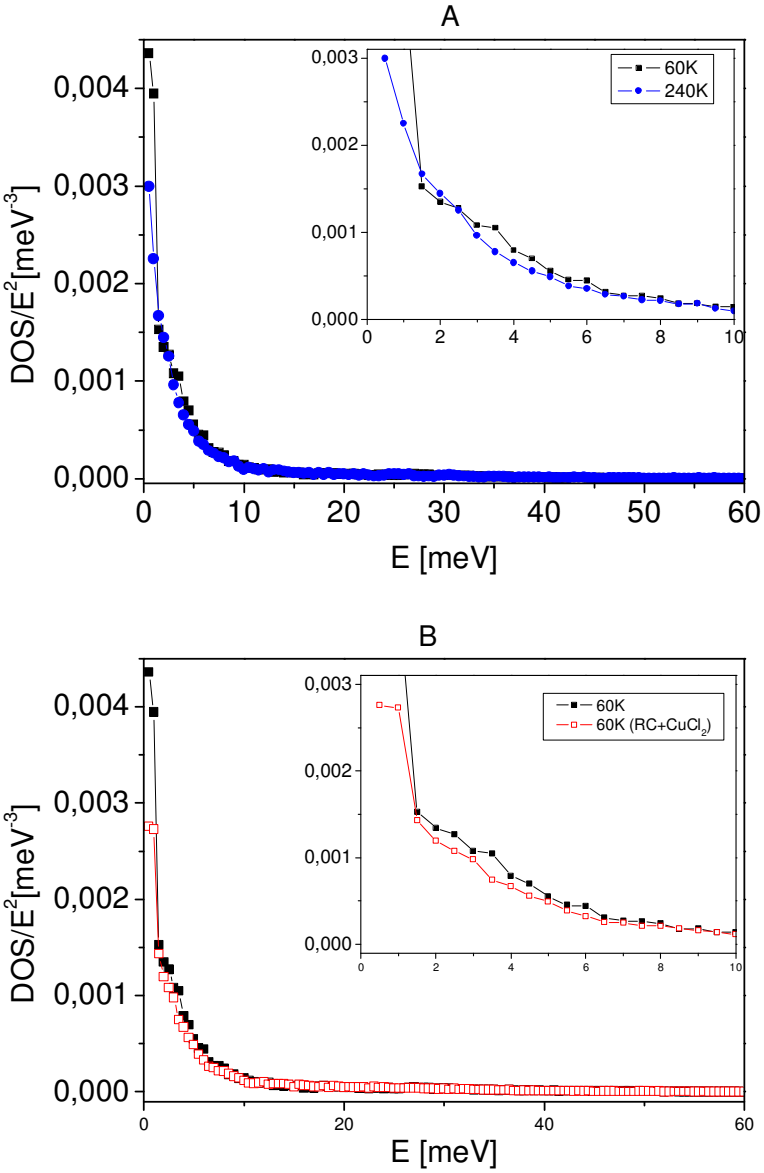

Figure 55. Density of vibrational states (DOS) devided by the corresponding E^2 in *Rb. sphaeroides* measured at 60 K (black) and 240 K (blue) using synchrotron radiation (A). In (B) the comparison of the spectra for native (black) and incubated with Cu^{2+} (red) samples are shown.

One can see also some differences for the spectra of the native RCs detected at 60K and 240K at around 2 meV and from 3-6 meV (Figure 55A) and in the case of the sample incubated with Cu^{2+} at around 2-6 meV (Figure 55B).

Summary.

Experiments of the nuclear resonant inelastic X-ray scattering using synchrotron radiation allow to study the dynamical properties of the non-haem iron and haem- iron binding sites within the reaction centers isolated from *Rb. sphaeroides*. The measurements were preformed at two temperatures 60 K and 240 K in the case of native photosystems in order to check how the temperature increase above the transition temperature (~ 200 K) influences the protein matrix vibrations in the vicinity of the non-haem iron. It is known that the electron transfer within the iron-quinone complex is possible when some collective motions of the protein net are activated, i.e. only above 200 K. The NIS (nuclear inelastic scattering) method gives the unique opportunity to follow such changes in the biological systems. It has to be emphasized that it is the first time when this technique was used to follow such changes in a complex photosynthetic systems and especially to study the non-haem iron binding site [89].

The vibrational modes characteristic for the non-haem iron were recognized in the density spectra as the vibrations occurring at the low energies below 28 meV whereas those at higher than 28 meV originate mainly from the haem-iron fluctuations. This observation is in accordance with the fact that all ligands of the non-haem iron come directly from the protein matrix and therefore this iron atom is especially sensitive to the protein net fluctuations. From our experimental data we can point the vibrations activated at around 12-17 meV and 22.5 – 26.5 meV and deactivated at 27- 28.5 meV as the most important differences in the high and low temperature DOS spectra. The additional changes of the vibrations at around 2 meV and 3-6 meV observed at 240 K in comparison to the spectrum detected at 60K indicate also changes in the diffusion motion of the whole photosynthetic complex.

It was also interesting to see how the copper ions bound in the vicinity of the non-haem iron influence its vibration modes. The measurements were performed at 60 K and we found that additional vibrations at the energies around 12-16 meV, 18 meV and 25 meV occur whereas the fluctuations at the energies of 26.5- 28.5 meV disappear in the sample treated with Cu^{2+}. In addition we see a systematic decrease of the contribution of the vibrations at around 2-6 meV in the DOS spectra. These changes we can assign to the changes of the non-haem iron spin state from its high state into low spin one. This suggest that the fluctuations at around 26-28 meV are those characteristic for the high spin state of the non-haem. These results also support the phenomenon observed in the Mössbauer experiments that the copper binding results in increasing the rigidity of the surrounding in the vicinity of the non-haem iron.

5 Conclusions

The aim of this work was to gain an insight into the function of non-haem iron, a conserved cofactor of the photosynthetic chain in photosystems of type Q, and of cytochrome b_{559}, which is a unique component of photosystem II. In our investigations we applied copper salts because copper ions are expected to interact with the other two cofactors in a highly specific way. The complementary experimental methods used in these studies allowed us to obtain information on some new mechanisms regulating electron and energy transfer within photosystems of type Q.

We used a wild type tobacco (WT) and a mutant (MT) with modified cytochrome b_{559}, in which highly conserved phenylalanine (26) on the β ubunit was replaced by serine to investigate the influence of cytochrome b_{559} on the stabilization of the acceptor and donor sides of photosystem II. The results obtained from the Kautsky effect and Q_A reoxidation as well as fast polarographic experiments provide evidence that cytochrome b_{559} regulates the Q_B binding site within the iron-quinone complex on the acceptor side and the manganese complex on the donor side of PSII.

The following arguments support these conclusions:

- The manganese cluster of the oxygen evolving complex is stabilized mainly in the S_1-state in the mutant whereas in the wild type the S_0-state is also occupied at a rate of 30%.

- The transitions between the S-states are more efficient in MT in which the average miss parameter was twice as low as that found in WT.

- In MT BBY PSII oxygen is evolved only via the fast channel whereas in WT BBY PSII this process takes place at a level of about 45% via the channel with a metastable S_4-state.

- The saturation time constant (in the order of hundreds microseconds) of the first plateau in the Kautsky effect curve is about 2 times faster and the amplitude of the plateau as well as that of the initial fluorescence (F_0) are higher in MT than in WT BBY PSII which indicates that the forward electron transfer from the reduced plastoquinone in the Q_A site is less efficient in MT than in WT; the higher F_0 in MT may also be related to the decreased efficiency of energy transfer from antenna to the PSII reaction center.

- The processes directly related to the exchange of the reduced and protonated plastoquinon Q_B with the external oxidized plastoquinone are about 4 times slower in MT than in WT, which indicates a more difficult rebinding of the quinone molecules at the Q_B site. This observation from Kautsky effect measurements is confirmed by Q_A reoxidation experiments. Simultaneously, the

contribution of this faster component in the variable fluorescence is at a level of 42% of the maximal fluorescence in MT but of about 70% in WT. The contribution of the slower component in MT is at a level of 20% but in WT it is about 8 times lower (it is only a minor component in WT).

Experiments carried out on the MT and WT thylakoids enriched in PSII and incubated in the presence of two different copper salts, $CuCl_2$ and $CuSO_4$, show that the mechanisms or cofactors regulated by cytochrome b_{559} are sensitive to the action of copper and some of the copper binding sites are especially sensitive to the activity of Cl^- anions.

These conclusions are drawn from the following experimental results:

- The dependence of the maximal fluorescence, F_M, on $CuCl_2$ differs significantly between WT and MT BBY PSII:
  - variable F_M stimulation is observed for $CuCl_2$/PSII < 40 and then there is a small decrease up to 200 $CuCl_2$/PSII by about 10% in WT whereas in MT an oscillation around the control value is detected for $CuCl_2$/PSII ≤ 10 and then a decrease, which is very sharp within 30 ≤ $CuCl_2$/PSII ≤ 80;
  - a steep F_M decrease for 200 < $CuCl_2$/PSII ≤ 400 occurs in WT whereas an increase is observed for 80 ≤ $CuCl_2$/PSII ≤ 400 in MT;
  - MT is more resistant to the inhibitory action for $CuCl_2$/PSII> 500 than WT.

- The activity of $CuSO_4$ on F_M is comparable in both tobacco types. In the case of WT BBY PSII the F_M value starts to decrease for the $CuSO_4$ concentrations >40. Such decreasing behaviour is observed for ~ 5 times higher concentrations of copper chloride. In contrary, this effect is detected for ~ 5 times lower concentrations of $CuCl_2$ in MT samples.

- At Cu^{2+}/PSII concentrations < 40 the sulfate anions stimulate the inhibitory action of copper ions in WT and MT but at ≥ 400 they have a protective role in WT and show no influence on F_M in MT.

- The changes in variable fluorescence observed in WT and MT BBY PSII are caused either by fast events with kinetics < about 1.5 ms or slow events with kinetics > 1.5 ms. The decrease in slow variable fluorescence is responsible for a strong fluorescence inhibition and specially its faster component, F_{VS1}. At the same time the fluorescence spectrum starts to be dominated by initial fluorescence. A more detailed discussion is included in the summary (chapter 4.1.1)

- The time constants describing the different mechanisms which were derivable from the Kaustky effect and Q_A reoxidation measurements show that the process of hundreds microseconds is sensitive differently in WT and MT BBY PSII but only in the presence of Cl^- ions (this time constant is the same within the bounds of uncertainity and varies in the same way in WT and MT treated with $CuSO_4$). The time constants of the order of hundreds milliseconds have discontinuities at similar copper ions for both tobacco types but they are much more sensitive to copper activity in the case of MT, and especially in the presence of Cl^- for the concentrations < 40 Cu^{2+}/PSII. For the copper concentrations >40 Cu^{2+}/PSII MT is more sensitive for sulfate anions.

- Kinetic measurements of fluorescence changes show that the energy and electron transfer processes are differently stabilized under light and dark conditions in WT and MT BBY PSII but some characteristic changes due to the activity of Cu^{2+} and Cl^- ions are always present. A more detailed discussion is presented in a summary (chapter 4.1.1) and another summary (chapter 4.1.2).

The most striking difference in fluorescence induction curves between WT and MT related to the steep decrease and increase in variable fluorescence observed in MT treated with $30 \leq CuCl_2$/PSII ≤ 400 without doubt originates from cytochrome b_{559}'s regulatory function in the cyclic electron flow around PSII and its participation in the energy dissipation process via an accessory chlorophyll Chl_Z^+.

Changes in the fluorescence induction curves in the presence of the lowest applied copper concentrations (1, 2, 4, 8, 10, 20 and 40 Cu^{2+}/PSII) are of special interest because they show that there are high affinity binding sites of copper ions and the vicinity of non- haem iron may be postulated as the most probable target.

Studies on the reaction centers isolated from *Rb. sphaeroides* both native and treated with $CuCl_2$ extended our investigations on Q- type photosystems. We investigated the kinetic changes of electron transfer (PEA and photobleaching experiments), stabilization energy of the charge separation process (thermoluminescence measurements) and the valence and spin state of non-haem iron as well as its dynamic properties (Mössbauer spectroscopy and the nuclear resonant inelastic X-ray scattering using synchrotron radiation).

The obtained results provide direct evidence that:

- Copper ions bind in the vicinity of non-haem iron change its high spin into a low spin ferrous state.

- The strength of non-haem iron bonds increases in the presence of Cu^{2+} and the iron binding site is more rigid (the Debye temperature increases by about 40 K) in comparison to the high spin state of this iron .

- A charge separation is still detected in centers treated even with such high concentrations of $CuCl_2$/RC as ~ 8000 and it shows variable kinetics depending on the copper concentrations used. However, the most interesting results come from fast induction fluorescence measurements at Cu^{2+}/RC < 1000 where we observed the most pronounced changes in the theoretically evaluated parameters characterizing the fast and slow processes of charge transfer at the following concentrations $CuCl_2$/RC at around 1, 2, 6, 10, 20, 40 and 100 and some less striking at 0.3 $CuCl_2$/RC, where usually the first changes in the parameters are observed. One has to underline that here the same copper concentrations were observed as those at which the kinetics and contributions of subsequent processes of energy and electron transfer in PSII occur.

- Thermoluminescence measurements, applied for the first time to study the acceptor side of bacterial RCs, show that the variations in the kinetics of charge transfer within the iron- quinone complex and the rereduction of P860 by reduced Q_A are related to the changes in the free energy of the charge stabilization process.

- The changes in stabilization energy originate from the different strength of coupling between the two quinone acceptors which is also regulated by the vibrational modes of the protein matrix, which was shown via nuclear resonant inelastic X-ray scattering measurements. These precursor studies of the vibrational modes of non-haem iron in both native and bacterial RCs modified by Cu^{2+} provide information on the specially activated (12- 17 meV and 22.5- 26.5 meV) and deactivated (27- 28.5 meV) fluctuation modes which also originate from the fact that non-haem iron was transferred to a low spin state.

- Temperature dependent measurements of the vibrational modes of non-haem iron in native bacterial RCs indicate that modes of 2 meV and 3- 6 meV are responsible for temperature activated electron transfer within the iron-quinone complex.

Summarizing, the results obtained from the studies described in this dissertation give direct evidence of the activity of non-haem iron in regulating the coupling of the quinone acceptors via changes of its spin state (the low spin state is observed also in the native bacterial reaction centers) and the existence of extra vibrational modes of the protein matrix in the vicinity of the iron-quinone complex at T > 200 K, which are crucial for the activation of the electron transfer between Q_A and Q_B quinones. The studies on photosystem II show that cytochrome b_{559} controls both the acceptor and donor side of PSII and it is an important factor stabilizing the Q_B binding site in an optimal configuration for the efficent exchange between the protonated reduced Q_BH_2 and the external oxidized plastoquinone pool. It is

interesting to point out that copper ions bind in a highly specific way in the vicinity of these two cofactors, and that some of these interactions are inhibited in the presence of sulfate anions or maybe stimulated by chloride anions.

These studies will provide the basis for our further investigations.

6 Literature

[1] Ke, B. (2001) Photosynthesis: Photobiochemistry and Photobiophysics, Kluwer Academic Publishers. Dordrecht.

[2] Olson, J.M. (2001). "Evolution of Photosynthesis" (1970), re-examined thirty years later. Photosyn. Res 68, 95-112.

[3] Allen, J.P., Feher, G., Yeates, T.O., Komiya, H. and Rees, D.C. (1987). Structure of the reaction center from *Rhodobacter sphaeroides* R- 26: The cofactors. Proc. Natl. Acad. Sci. USA 84, 5730- 5734.

[4] Heathcote, P., Fyfe, P.K. and Jones, M.R. (2002). Reaction centres: the structure and evolution of biological solar power. TiBS 27, 79-87.

[5] Loll, B., Kern, J., Saenger, W., Zouni, A. and Biesiadka, J. (2005). Towards complete cofactor arrangement in the 3.0 Å resolution structure of photosystem II. Nature 438, 1040-1044.

[6] Gruszecki, W.I. and Strzałka, K. (2005). Carotenoids as modulators of lipid membrane physical properties. Biochim. Biophys. Acta 1740, 108-115.

[7] Sujak, A., Gabrielska, J., Grudziński, W., Borc, W., Mazurek, P. and Gruszecki, W.I. (1999). Lutein and zeaxanthin as protectors of lipid membranes against oxidative damage: The structural aspects. Arch. Biochem. Biophys. 371, 301-307.

[8] Allen, J.P. and Williams, J.C. (1998). Photosynthetic reaction centers. FEBS Lett 438, 5-9.

[9] Thompson, L.K., Miller, A.F., Buser, C.A., De Paula, J.C. and Brudvig, G.W. (1989). Characterization of the multiple forms of cytochrome b_{559} in photosystem II. Biochemistry 28, 8048- 8056.

[10] Stewart, D.H. and Brudvig, G.W. (1998). Cytochrome b_{559} of photosystem II. Biochim. Biophys. Acta 1367, 63-87.

[11] Barber, J. and De Las Rivas, J. (1993). A functional model for the role of cytochrome b_{559} in the protection against donor and acceptor side photoinhibition. Proc. Natl. Acad. Sci. USA 90, 10942-10946.

[12] Burda, K., Kruk, J., Schmid, G.H. and Strzałka, K. (2003). Inhibition of oxygen evolution in photosystem II by Cu(II) ions is associated with oxidation of cytochrome b_{559}. Biochem. J. 371, 597-601.

[13] Annanyev, G., Renger, G., Wacker, U.and Klimov, V.V. (1994). Photoproduction of superoxide radicals and SOD activity of photosystem II. Photosyn. Res 4, 327-338.

[14] Pakrasi, H.B., De Ciechi, P. and Whitmarsh, J. (1991). Site directed mutagenesis of the heme axial ligands of cytochrome b_{559} affects the stability of the photosystem II complex. EMBO J. 10, 1619-1627.

[15] Shukla, V.K., Stabenkova, G.H., Shestakov, S.V. and Pakrasi, H.B. (1992). The D1 protein of the photosystem II reaction centre complex accumulates in the absence of the D2: analysis of a mutant of the cyanobacterium *Synechocystis sp*. PCC 6803 lacking cytochrome b_{559}. Mol. Microbiol. 6, 947-956.

[16] Diner, B.A. (2001). Amino acid residues involved in the coordination and assembly of the manganese cluster of photosystem II. Proton-coupled electron transport of the redox-active tyrosines and its relationship to water oxidation. Biochim. Biophys. Acta 1503, 147-163.

[17] Roberts, K. (2007) Handbook of Plant Science, John Wiley&Sons. Chichester.

[18] Seidler, A. (1996). The extrinsic polipeptides of Photosystem II. Biochim. Biophys. Acta 1277, 35-60.
[19] Zouni, A., Witt, H.T., Kern, J., Fromme, P., Krauss, N., Saenger, W. and Orth, P. (2001). Crystal structure of photosystem II from *Synechococcus elongatus* at 3.8 A resolution. Nature 409, 739-743.
[20] Taiz, L. and Zeiger, E. (2006) Photosynthesis: The light reactions. In Plant physiology (Tzfira, T., ed.^eds), pp. 705. Sinauer, Sunderland.
[21] Ferreira, K.N., Iverson, T.M., Maghlaoui, K., Barber, J. and Iwata, S. Architecture of the photosynthetic oxygen-evolving center. Science 303, 1831-1838.
[22] Goussias, C., Boussac, A. and Rutherford, A.W. (2002). Photosystem II and photosynthetic oxidation of water: an overview. Phil. Trans. R. Soc. Lond. B 357, 1369-1381.
[23] Debus, R.J. (1992). The manganese and calcium ions of photosynthetic oxygen evolution. Biochim. Biophys. Acta 1102, 269-352.
[24] Yachandra, V.K., DeRose, V.J., Latimer, M.J., Mukerji, I., Sauer, K. and Klein, M.P. (1993). Where plants make oxygen: a structural model for the photosynthetic oxygen- evolving manganese cluster. Science 260, 675-679.
[25] Joliot, P., Barbieri, G. and Chabaud, R. (1969). Un nouveau modèle des centres photochimiques du système II. Photochem. Photobiol. 10, 309-329.
[26] Kok, B., Forbush, B. and McGloin, M. (1970). Cooperation of charges in photosynthetic oxygen evolution. Photochem. Photobiol. 11, 457-475.
[27] Vermaas, W.F.J., Renger, G. and Dohnt, G. (1984). The reduction of the oxygen-evolving system in chloroplasts by thylakoid components. Biochim. Biophys. Acta 764, 194-202.
[28] Bock, R., Kössel, H. and Maliga, P. (1994). Introduction of a heterologous editing site into the tobacco plastid genome: the lack of RNA editing leads to a mutant phenotype. The EMBO Journal 19, 4623-4628.
[29] Berthold, D.A., Babcock, G.T. and Yocum, C.E. (1981). A highly resolved, oxygen evolving Photosystem II preparation from spinach thylakoid membranes: EPR and electron transport properties. FEBS Lett 134, 231-234.
[30] Schmid, G.H. (1971) Origin and properties of mutant plants: yellow tobacco. In Methods in enzymology (San Pietro, A., ed.^eds), pp. 171-194. Academic Press, New York.
[31] Cohen- Bazire, G., Sistrom, W.R. and Stanier, R.Y. (1957). Kinetic studies of pigment synthesis by non- sulfur purple bacteria. J. Cell. Comp. Physiol. 49, 25-58.
[32] Kautsky, H. and Hirsch, A. (1931). Neue Versuche zur Kohlensäureassimilation. Naturwissenschaften 19, 694-699.
[33] Roháček, K. (2002). Chlorophyll fluorescence parameters: the definitions, photosynthetic meaning, and mutual relationships. Photosynthetica 40, 13-29.
[34] Trtílek, M., Kramer, D.M., Kobližek, M. and Nedbal, L. (1997). Dual-modulation LED kinetic fluorometer. J. Luminesc. 72, 597-599.
[35] Stowell, M.H.B., McPhillips, T.M., Rees, D.C., Soltis, S.M., Abresch, E. and Feher, G. (1997). Light-Induced structural changes in photosynthetic reaction center: implications for mechanism of electron-proton transfer. Science 276, 812-816.

[36] Tiede, D.M., Utschig, L., Hanson, D.K. and Gallo, D.M. (1998). Resolution of electron and proton transfer events in the electrochromism associated with quinone reduction in bacterial reaction centers. Photosyn. Res 55, 267-273.
[37] Kaftan, D., Meszaros, T., Whitmarsh, J. and Nedbal, L. (1999). Characterization of Photosystem II activity and heterogeneity during the cell cycle of the green alga *Scenedesmus quadricauda*. Plant Physiol. 120, 433-441.
[38] Chen, R. and Kirsh, Y. (1981) Analysis of Thermally Stimulated Processes, Pergamon Press. Oxford.
[39] Vass, I. (2003). The history of photosynthetic thermoluminescence. Photosyn. Res 76, 303-318.
[40] Schmid, G.H. and Thibault, P. (1979). Evidence for a rapid oxygen uptake in tobacco chloroplasts. Z. Naturforsch. 34 c, 414-418.
[41] Burda, K. and Schmid, G.H. (1996). On the determination of the S- state distribution in the Kok model. Z. Naturforsch. 51 c, 329-341.
[42] Łątka, K., Gurgul, J., Kmieć, R., Pacyna, A.W. and Chajec, W. (2005). Hyperfine interactions studies by Sn- 119 Mössbauer spectroscopy in TbAuSn and TmAuSn compounds. J. All and Com. 400, 16-22.
[43] Łątka, K., Rams, M., Kmieć, R., Pacyna, A.W., Zaremba, V.I., Rodewald, U.C. and Pöttgen, R. (2007). Structure and properties of $Gd_4Pd_{10}In_{21}$. Solid St Sci. 9, 173-184.
[44] Garbers, A., Kurreck, J., Iakovleva, O., Renger, G. and Parak, F. (2001). Mössbauer study of iron centers in D1/D2/Cyt b_{559} complexes isolated from photosystem II of spinach. Eur Biophys J. 30, 485-493.
[45] Burda, K., Kruk, J., Borgstadt, R., Stanek, J., Strzałka, K., Schmid, G.H. and Kruse, O. (2003). Mössbauer studies of the non- heme iron and cytochrome b_{559} in *Chlamydomonas reinhardtii* PSI minus mutant and their interactions with α–tocopherol quinone. FEBS Lett 535, 159-165.
[46] Gütlich, P.(1975) Mössbauer spectroscopy in chemistry. In Mössbauer spectroscopy (Gonser,U.,ed.^eds), pp. 53-96. Springer Verlag, Berlin Heidelberg.
[47] McCammon, J.A., Gelin, B.R. and Karplus, M. (1977). Dynamics of folded proteins. Nature 267, 585 - 590.
[48] Chumakov, A.I., Rüffer, R., Leupold, O. and Sergueev, I. (2003). Insight to dynamics of molecules with nuclear inelastic scattering. Structural Chem. 14, 109-119.
[49] Chumakov, A.I. et al. (2000). High- energy resolution x- ray optics with refractive collimators. Appl. Phys. Lett. 77, 31-33.
[50] Baron, A.Q.R. (1995). Report on the X- ray efficiency and time response of a 1 cm^2 reach through avalanche diode. Nucl. Instrum. Meth. Phys. Res. A 352, 665-672.
[51] Hsu, B.D. and Lee, J.Y. (1988). Toxic effects of copper on photosystem II of spinach chloroplasts. Plant Physiol. 87, 116-119.
[52] Burda, K., Kruk, J., Stanek, J., Strzałka, K., Schmidt, G.H. and Kruse, O. (2006). Mössbauer studies of Cu(II) ions with the non- heme iron and cytochrome b_{559} in *Chlamydomonas reinhardtii* PSI minus mutant. Acta Phys. Polon. A 109, 237-247.
[53] Bernal, M., Roncel, M., Ortega, J.M., Picorel, R. and Yruela, I. (2004). Copper effect on cytochrome b_{559} of photosystem II under photoinhibitory conditions Physiol. Plantarum 120, 686-694.

[54] Burda, K., Kruk, J., Strzałka, K. and Schmid, G.H. (2002). Stimulation of oxygen evolution in photosystem II by copper (II) ions. Z. Naturforsch. 57c, 853-857.
[55] Yruela, I., Pueyo, J., Alonso, P. and Picorel, R. (1996). Photoinhibition of photosystem II from higher plants. JBC 271, 27408-27415.
[56] Yruela, I., Alfonso, M., Baron, M. and Picorel, R. (2008). Copper effect on the protein composition of photosystem II. Physiol. Plantarum 110, 551-557.
[57] Orzechowska, A., Bock, R., de Odrowąż Piramowicz, M., Strzałka, K. and Burda, K. (2008) Cu^{2+} binding sites in PSII. In Energy from the sun: 14th International Congress on Photosynthesis (Allen, J.P., Gantt, E., Golbeck, J. H., Osmond, B., ed.^eds), pp. 661-664. Springer
[58] de Odrowąż Piramowicz, M., Bock, R., Orzechowska, A., Strzałka, K. and Burda, K. (2008) Binding sites of cadmium ions within photosystem II. In Energy from the sun: 14th International Congress on Photosynthesis (Allen, J.P., Gantt, E., Golbeck, J. H., Osmond, B., ed.^eds), pp. 305-308. Springer
[59] Burda, K., Orzechowska, A., Kruk, J., Strzałka, K. and Bock, R. (2009). Regulatory function of cytochrome b_{559} in photosystem II. FEBS Lett; *submitted*
[60] Burda, K., Strzałka, K. and Schmid, G.H. (1995). Europium- and dysprosium-ions as probes for the study of calcium binding sites in photosystem II. Z. Naturforsch. 50c, 220-230.
[61] Yruela, I., Gatzen, G., Picorel, R. and Holzwarth, A.R. (1996). Cu(II) inhibitory effect on photosystem II from higher plants. A picosecond time- resolved fluorescence study. Biochemistry 35, 9469-9474.
[62] Okamura, M.Y., Isaacson, R.A. and Feher, G. (1975). Primary acceptor in bacterial photosynthesis: obligatory role of ubiquinone in photoactive reaction centers of *Rhodopseudomonas sphaeroides*. Proc. Natl. Acad. Sci. USA 72, 3491-3495.
[63] McPherson, P.H., Okamura, M.Y. and Feher, G. (1990). Electron transfer from the reaction center of *Rb. sphaeroides* to the quinone pool: doubly reduced Q_B leaves the reaction center. Biochim. Biophys. Acta 1016, 289-292.
[64] Allen, J.P., Williams, J.C., Graige, M.S., Paddock, M.L., Labahn, A., Feher, G. and Okamura, M.Y. (1998). Free energy dependence of the direct charge recombination from the primary and secondary quinone in reaction center from *Rhodobacter sphaeroides*. Photosyn. Res 55, 227-233.
[65] Schenck, C.C., Parson, W.W., Windsor, M.W. and Sarai, A. (1981). Temperature dependence of electron transfer between bacteriopheophytin and ubiquinone in protonated and deuterated reaction centers of *Rhodopseudomonas sphaeroides*. Biophys. J. 36, 479-489.
[66] Kriegl, J.M. and Nienhaus, G.U. (2004). Structural, dynamic, and energetic aspects of long-range electron transfer in photosynthetic reaction centers. Proc. Natl. Acad. Sci. USA 101, 123-128.
[67] Dutton, P.L., Leigh, J.S. and Wraight, C.A. (1973). Direct measurements of the midpoint potential of the primary electron acceptor in *Rhodopseudomonas sphaeroides* in situ and in the isolated state: some relationship with pH and o-phenantroline. FEBS Lett 36, 169-173.
[68] His, E.S.P. and Bolton, J.B. (1974). Flash photolysis- electrospin resonance study of the effect of o- phenanthroline and temperature on the decay time of the ESR signal B1 in reaction- center preparation and chromatophores of mutant and wild type strains of *Rhodopseudomonas sphaeroides* and *Rhodospirillum rubrum*. Biochim. Biophys. Acta 374, 126-153.

[69] DeVault, D., Govindjee and Arnold, W. (1983). Energetics of photosynthetic glow peaks. Proc. Natl. Acad. Sci. USA 80, 983-987.
[70] DeVault, D. and Govindjee. (1990). Photosynthetic glow peaks and their relationship with the free energy changes. Photosyn. Res 24, 175-181.
[71] Lang, G. and Marshall, W. (1966). Mössbauer effect in some hemoglobin compounds. Proc. Phys. Soc 87, 3-34.
[72] Wraight, C.A. (1977). Electron acceptors of photosynthetic bacterial reaction centers. Direct observation of oscillatory behaviour suggesting two closely equivalent ubiquinones. Biochim. Biophys. Acta 459, 525-531.
[73] Boso, B., Debrunner, P., Okamura, M.Y. and Feher, G. (1981). Mössbauer spectroscopy studies of photosynthetic reaction centers from *Rhodopseudomonas sphaeroides* R- 26. Biochim. Biophys. Acta 638, 173-177.
[74] Parak, F., Frolov, E.N., Kolonenko, A.A., Mössbauer, R.L., Goldanskii, V.I. and Rubin, A.B. (1980). Evidence for a correlation between the photoinduced electron transfer and dynamic properties of the chromatophore membranes from *Rhodospirillum rubrum*. FEBS Lett 117, 368-372.
[75] Kleinfeld, D., Okamura, M.Y. and Feher, G. (1984). Electron transfer kinetics in photosynthetic reaction centers cooled to cryogenic temperatures in the charge-separated state: evidence for light-induced structural changes. Biochemistry 23, 5780-5786.
[76] Diner, B.A. and Petrouleas, V. (1988). Q400, the non- heme iron of the photosystem II iron- quinone complex. A spectroscopic probe of quinone and inhibitor of binding to the reaction cente. Biochim. Biophys. Acta 895, 107-125.
[77] Burda, K. (2007). Dynamics of electron transfer in photosystem II. Cell Biochem. Biophys. 47, 271-284.
[78] Brudler, R. (1994). Asymmetric binding at the 1- and 4-C=O groups of Q_A in *Rhodobacter sphaeroides R26* reaction centers monitored by Fourier transform infrared spectroscopy using site- specific isotopically labeled ubiquinone- 10. EMBO J. 13, 5523-5530.
[79] Remy, A. and Gerwert, K. (2003). Coupling of light- induced electron transfer to proton uptake in photosynthesis. Nature Struct. Biol. 10, 637-644.
[80] Breton, J., Boullais, C., Burie, J.R., Nabedryk, E. and Mioskowski, C. (1994). Binding sites of quinones in photosynthetic bacterial reaction centers investigated by light-induced FTIR difference spectroscopy: assignment of the interactions of each carbonyl of Q_A in *Rhodobacter sphaeroides* using site-specific ^{13}C-labeled ubiquinone. Biochemistry 33, 14378-14386.
[81] Brudler, R., de Groot, H.J., van Liemt, W.B., Gast, P., Hoff, A.J., Lugtenburg, J. and Gerwert, K. (1995). FTIR spectroscopy shows weak symmetric hydrogen bonding of the Q_B carbonyl groups in *Rhodobacter sphaeroides* R26 reaction centres. FEBS Lett 370, 88-92.
[82] Frauenfelder, H., Petsko, G.A. and Tsernoglou, T.(1979). Temperature-dependent X-ray diffraction as a probe of protein structural dynamics Nature 280, 558-563.
[83] Burda, K., Hrynkiewicz, A., Kołoczek, H., Stanek, J. and Strzałka, K. (1994). Molecular dynamics and local electronic states of Sn and Fe in metallocytochrome and metalloporphyrin. Hyp. Int. 91, 891-897.
[84] Chumakov, A.I., Rüffer, R., Baron, A.Q.R., Grünsteudel, H. and Grünsteudel, H.F. (1996). Temperature dependence of nuclear inelastic absorption of synchrotron radiation in α- ^{57}Fe. Phys. Rev. B 54, 9596-9599.

[85] Leu, B.M., Zhang, Y., Bu, L., Straub, J.E., Zhao, J., Sturhahn, W., Alp, E. and Sage, J.T. (2008). Resilence of the iron environment in heme proteins. Biophys. J. 95, 5874-5889.

[86] Sarai, A. (1979). Energy gap and temperature dependences of electron transfer and excitation transfer in biological system. Chem. Phys. Lett. 63, 360-366.

[87] Kakitani, T. and Kakitani, H. (1981). A possible new mechanism of temperature dependence of electron transfer in photosynthetic systems. Biochim. Biophys. Acta 635, 498-514.

[88] Starley, S.C., Parson, W.W., Mauzerall, D.C. and Clayton, R.K. (1973). Pigment content and molar excitation coefficients of photochemical reaction centers from *Rhodopseudomonas sphaeroides*. Biochim. Biophys. Acta 305, 597-609.

[89] Orzechowska, A. M.Lipińska, A.Chumakov, J.Fiedor, M.Zając, T.Ślęzak, K. Matlak, J.Korecki, M.Trtilek, L.Fiedor, K.Strzałka, R.Rüffer and K.Burda (2009). Spin state of the non- haem iron influences electron transfer rates in bacterial reaction centers via modification of local motions of the protein matrix. Proc. Natl. Acad. Sci. USA; *submitted*